

SINGLE-MOLECULE MICROSCOPY TO STUDY PLASMA MEMBRANE RECEPTOR DYNAMICS

THÈSE N° 6917 (2016)

PRÉSENTÉE LE 11 MARS 2016

À LA FACULTÉ DES SCIENCES DE BASE

LABORATOIRE DE CHIMIE PHYSIQUE DES POLYMÈRES ET MEMBRANES

PROGRAMME DOCTORAL EN CHIMIE ET GÉNIE CHIMIQUE

ÉCOLE POLYTECHNIQUE FÉDÉRALE DE LAUSANNE

POUR L'OBTENTION DU GRADE DE DOCTEUR ÈS SCIENCES

PAR

Luc VEYA

acceptée sur proposition du jury:

Prof. S. Gerber, présidente du jury
Prof. H. Vogel, Prof. K. Johnsson, directeurs de thèse
Prof. J. Widengren, rapporteur
Dr J. Le Coutre, rapporteur
Dr G. Turcatti, rapporteur



ÉCOLE POLYTECHNIQUE
FÉDÉRALE DE LAUSANNE

Suisse
2016

The present thesis has been performed in the Laboratory of Physical Chemistry of Polymers and Membranes (LCPPM) at the Swiss Federal Institute of Technology in Lausanne (EPFL, Switzerland), under the supervision of Prof. Horst Vogel, between May 2011 and November 2015.

Part of the work accomplished during the thesis has been published in peer-reviewed journals and presented at international conferences:

► Journal papers

- ◇ **Veya, L.**, J. Piguet, and H. Vogel. Single-molecule imaging deciphers the relation between mobility and signaling of a prototypical G protein-coupled receptor in living cells. *Journal of Biological Chemistry*, 290(46):27723-27735, 2015.
- ◇ Baud, O., S. Yuan, **L. Veya**, S. Filipek, H. Vogel, and H. Pick. Exchanging ligand-binding specificity between a pair of mouse olfactory receptor paralogs reveals odorant recognition principles. *Scientific Reports*, 5:14948, 2015.

► Conference posters

- ◇ **Veya, L.**, J. Piguet, and H. Vogel. Single-molecule microscopy deciphers the relation between trafficking and signaling of the NK1 receptor in living cells. 58th Annual Meeting of the Biophysical-Society in San Francisco(CA), USA, 15-19 February 2014.
- ◇ **Veya, L.**, J. Piguet, and H. Vogel. Tracking NK1 receptor diffusion in the membrane of living cells - Part 1: Effects of receptor activation. 9th European Biophysics Congress in Lisbon, Portugal, 13-17 July 2013.
- ◇ Piguet, J., **L. Veya**, and H. Vogel. Tracking NK1 receptor diffusion in the membrane of living cells - Part 2: Roles of clathrin and cytoskeleton. 9th European Biophysics Congress in Lisbon, Portugal, 13-17 July 2013.

► Conference talks

- ◇ **Veya, L.** Single-molecule microscopy deciphers the relation between trafficking and signaling of the NK1 receptor in living cells. GLISTEN (GPCR-Ligand Interactions, Structures, and Transmembrane Signaling) Conference in Budapest, Hungary, 2-4 October 2014.

Abstract

Cell surface receptors allow the cell to sense and respond to external signals. Receptor malfunctions are associated with many diseases. The diffusional behavior of receptors is of particular interest to understand how the cell modulates receptor function in the complex, heterogeneous plasma membrane. Unlike traditional ensemble methods, single-molecule techniques give access to events taking place at the nanometer scale and millisecond time regime, providing unprecedented means to correlate biological functions of the cell membrane with the spatio-temporal organization of its individual components.

In this work, advanced fluorescence microscopy techniques were used to track the motion of individual receptors in the plasma membrane of living cells to elucidate principles regulating their function. Two very different neurotransmitter receptors were investigated: the G protein coupled neurokinin-1 receptor (NK1R), and the ionotropic serotonin type 3 receptor (5-HT₃R). The first important step towards tracking single receptor molecules is the specific labeling of a small fraction of these receptors with a photostable fluorescent probe. The choice of a suitable labeling strategy is of paramount importance, as it will largely determine the success of the experiment. Single-molecule tracking requires extremely specific, long-lasting, stoichiometric and bright fluorescent labels that do not interfere with the function and diffusion of the receptor.

For the NK1R, a two-step labeling strategy based on the strong biotin-streptavidin interaction yielded the best labeling specificity. Enzymatic biotinylation of the receptor followed by binding streptavidin-coated quantum dot (QDot) enabled a straightforward and precise adjustment of the label density to a few QDots per cell. The combination of high brightness and photostability of semi-conductor QDots allowed us to record receptor trajectories with high spatial resolution over long time periods. The investigation of thousands of single NK1R trajectories revealed a very heterogeneous mobility pattern with two major, broadly distributed receptor populations, one showing high mobility and low lateral restriction, the other low mobility and high restriction. We found that 40% of the receptors in the basal state are already confined in membrane domains. After agonist stimulation, an additional 30% of receptors became further confined. Using inhibitors of clathrin-mediated endocytosis, we showed that the fraction of confined receptors at the basal state depends on the quantity of membrane-associated clathrin and is correlated to a significant decrease of the receptors' canonical pathway activity. These findings add further insights to the plasticity of receptor signaling.

There is a risk that one streptavidin-coated QDot could bind several biotinylated receptors and

thereby alter the receptor's mobility. The generation of monovalent StrepTactin-conjugated QDots allowed us to exclude any cross-linking artifacts in our previous measurements of NK1R diffusion.

In the case of the 5-HT₃R, the diffusion of individual receptors was followed using a fluorescent nanobody (VHH15-CF640R). This novel high-affinity label which is small, monovalent and highly photostable enabled us to track native 5-HT₃Rs over long time regimes, revealing a surprising and intriguing diffusional behavior of some receptors.

Key words: Fluorescence microscopy, single-molecule tracking, plasma membrane, protein labeling, membrane protein diffusion, G protein-coupled receptors, neurokinin-1 receptor, ligand-gated ion channels, 5-HT₃ receptor, quantum dots, monovalent StrepTactin, single-domain antibodies.

Résumé

Les récepteurs présents à la surface des cellules permettent à ces dernières de percevoir des signaux extérieurs et d'y répondre. Leur dysfonctionnement est à l'origine de nombreuses maladies. L'étude de la diffusion des récepteurs est d'un intérêt particulier pour comprendre comment la cellule module leur fonction au niveau de la membrane plasmique. L'hétérogénéité de cette dernière rend l'utilisation de techniques permettant la détection de molécules individuelles particulièrement adaptée. En effet, contrairement aux mesures d'ensemble, ces techniques permettent d'accéder à des événements prenant place à l'échelle du nanomètre et de la milliseconde, et offrent ainsi la possibilité de corrélérer les fonctions biologiques de la membrane avec l'organisation spatio-temporelle de ses composants individuels.

Dans ce travail, des techniques avancées de microscopie de fluorescence ont été utilisées pour suivre le mouvement de récepteurs individuels dans la membrane de cellules vivantes afin d'élucider les principes régulant leur fonction. Deux neurorécepteurs très différents ont été investigués : le récepteur de la neurokinine 1 (NK1) couplé aux protéines G et le récepteur ionotrope de la sérotonine (5-HT₃).

La première étape pour pouvoir suivre des molécules uniques est le marquage spécifique d'une petite fraction des récepteurs avec une sonde fluorescente. Pour que l'expérience soit un succès, la sonde en question doit se lier de manière spécifique, stœchiométrique et durable au récepteur, être brillante et photostable, et ne pas interférer avec la fonction ou la diffusion du récepteur.

Pour le récepteur NK1, une stratégie de marquage en deux étapes s'est avérée supérieure en terme de spécificité. La biotinylation enzymatique du récepteur, suivie par la liaison de boîtes quantiques (QDots) liées à la streptavidine a permis d'ajuster aisément la densité du marquage à quelques QDots par cellule. Grâce à l'exceptionnelle brillance et photostabilité des QDots, nous avons été capable de reconstituer les mouvements du récepteur avec une très grande précision spatiale sur de longues périodes. L'investigation de milliers de trajectoires a révélé une diffusion très hétérogène avec deux populations majeures de récepteurs, l'une exhibant une grande mobilité et une faible restriction latérale, l'autre une faible mobilité et une grande restriction latérale. Nous avons découvert que 40% des récepteurs étaient déjà confinés dans des domaines à l'état basal. Après stimulation avec un agoniste, 30% supplémentaires sont devenus confinés. En utilisant des inhibiteurs de l'endocytose dépendante de la clathrine, nous avons montré que la fraction de récepteurs confinés à l'état basal dépend de la quantité de clathrine associée à la membrane et est corrélée avec une inhibition de l'activité de la voie de signalisation canonique. Ces résultats offrent un nouvel aperçu de la plasticité de la

signalisation du récepteur NK1.

Il y a un risque qu'un QDot lié à la streptavidine puisse se lier à plusieurs récepteurs biotinylés et, de ce fait, en altérer la mobilité. La génération de QDots liés à une StrepTactin monovalente nous a permis d'exclure tout artefact de ce type dans nos précédentes mesures.

Dans le cas du récepteur 5-HT₃, la diffusion de récepteurs individuels a été investiguée en utilisant un nanobody fluorescent (VHH15-CF640R). Ce nouveau marqueur qui est à la fois petit, monovalent et photostable, nous a permis de suivre des récepteurs natifs pendant de longues périodes et ainsi de révéler le comportement surprenant et intrigant de certains d'entre eux.

Mots clefs : Microscopie de fluorescence, suivi de molécules uniques, membrane plasmique, marquage de protéines, diffusion de protéines membranaires, récepteurs couplés aux protéines G, récepteur neurokinine 1, canaux ioniques ligand-dépendants, récepteur 5-HT₃, boîtes quantiques, StrepTactin monovalente, anticorps à domaine unique.

Contents

Abstract (English/Français)	i
Aim and scope of this thesis	1
General introduction	3
The plasma membrane	3
Lipids and proteins	3
Membrane organization and lateral diffusion	4
Cell-surface receptors	8
G protein-coupled receptors	9
Pentameric ligand-gated ion channels	15
Relationship between NK1R and 5-HT ₃ R	17
Membrane receptor labeling strategies	18
Fluorescent probes	19
Measuring protein diffusion using fluorescence microscopy	21
General aspects of single-molecule imaging	22
Single-molecule tracking	24
1 Labeling of NK1 receptor for single-particle tracking in living cells	31
1.1 ACP labeling	31
1.2 Labeling of NK1 receptor with quantum dots	32
1.2.1 Experimental procedures	32
1.2.2 Results and discussion	35
1.2.3 Conclusion	37
2 Single-molecule microscopy deciphers the relation between mobility and signaling of the NK1 receptor in living cells	39
2.1 Abstract	39
2.2 Introduction	40
2.3 Experimental procedures	42
2.3.1 Cell culture	42
2.3.2 Addition of chemicals to cells	42
2.3.3 siRNA knockdown of clathrin	42
2.3.4 Receptor function assay	43

Contents

2.3.5	Receptor labeling	43
2.3.6	Microscopy	43
2.3.7	Single-molecule tracking	44
2.3.8	Analysis of individual trajectories	44
2.3.9	Population analysis	44
2.3.10	Classification of individual trajectories	45
2.3.11	Dimension of confined regions	45
2.4	Results	45
2.4.1	Heterogeneous mobility of the NK1R in the plasma membrane of 293T cells	45
2.4.2	Receptor immobilization after activation	48
2.4.3	Temporal classification of trajectory segments	48
2.4.4	Contribution of the Rho/ROCK pathway	50
2.4.5	Role of the cytoskeleton on NK1R confinement	51
2.4.6	Decrease of receptor mobility after cholesterol depletion	53
2.4.7	NK1R interaction with clathrin	53
2.4.8	Impairment of NK1R-mediated Ca ²⁺ signaling	56
2.5	Discussion	56
2.6	Conclusion	61
3	A monovalent StrepTactin for cross-linking-free labeling of membrane receptors	63
3.1	Abstract	63
3.2	Introduction	63
3.3	Experimental procedures	64
3.3.1	mST expression and purification	64
3.3.2	Conjugation of Atto635 to mST	66
3.3.3	Functionalization of QDots with mST	66
3.3.4	Fluorescence Correlation Spectroscopy (FCS)	66
3.3.5	Surface Plasmon Resonance (SPR)	68
3.3.6	Cell culture	68
3.3.7	Labeling of Strep-tagged receptors	68
3.3.8	Labeling of biotinylated receptors	69
3.3.9	Microscopy	69
3.4	Results and discussion	69
3.4.1	Production of monovalent StrepTactin	69
3.4.2	Verification of tetramer subunit composition	70
3.4.3	Binding to biotin	70
3.4.4	Binding to Strep-Tag II	72
3.4.5	Organic dye-mST conjugate for labeling membrane receptors in living cells	73
3.4.6	mST-QDot conjugate for tracking individual receptors in living cells . . .	73
3.4.7	SA-QDots vs. mST-QDots to track membrane receptor dynamics	74
3.5	Conclusion	76

4 Tracking 5-HT₃ receptor dynamics using a fluorescent nanobody	79
4.1 Abstract	79
4.2 Introduction	79
4.3 Materials and methods	81
4.3.1 Materials	81
4.3.2 Cell culture	81
4.3.3 Synthesis of VHH15-CF640R	81
4.3.4 5-HT ₃ R labeling	82
4.3.5 Drug treatments	82
4.3.6 Confocal microscopy	82
4.3.7 SMT experiments	82
4.3.8 Data analysis	83
4.4 Results	83
4.4.1 Direct labeling of the 5-HT ₃ R using a fluorescently labeled VHH	83
4.4.2 VHH15-CF640: a perfect probe for tracking individual 5-HT ₃ Rs	84
4.4.3 Comparison of the lateral mobility of heterologously and endogenously expressed receptors	84
4.4.4 A particular diffusional behavior of 5-HT ₃ R in NG108-15 cells	86
4.4.5 Effect of cytoskeleton-disrupting agents on receptor mobility	86
4.5 Discussion	90
4.6 Conclusion	91
 General conclusion and outlook	 93
 Appendix	 95
A Single-molecule microscopy setups (Wide-field/TIRF)	95
 Bibliography	 97
 List of abbreviations	 119
 Acknowledgments	 123
 Curriculum vitae	 125

Aim and scope of this thesis

The central goal of this PhD project was the study of the lateral mobility of membrane receptors at the single-molecule level in living cells. The lateral diffusion of membrane proteins is a surprisingly complex phenomenon which plays a central role in the regulation of many cellular signaling processes. Revealing how the plasma membrane laterally organizes and controls the mobility of its constituents at the nanoscopic level is essential to understand central functional processes of a cell. In order to do so, methods enabling detection of single-molecules with high spatial and temporal resolution are needed. In this context, single-molecule tracking (SPT) of receptors labeled with quantum dots (QDots) as fluorescent probes is particularly well suited and is therefore at the center of this PhD project.

The thesis starts with a general introduction. It provides an overview of the scientific topics treated in the following chapters, including the biological background and the experimental methods concerned.

Chapter 1 (p. 31) presents different labeling strategies that have been assessed in order to attach QDots to the neurokinin-1 (NK1) receptor which has been chosen as a prototypical representative of a G protein-coupled receptor. The objective was to establish a protocol providing maximum labeling specificity and stability for studying the diffusion of single receptors in the plasma membrane of living cells.

In chapter 2 (p. 39), the labeling strategy established in the previous chapter is applied to track trajectories of individual NK1 receptors over long time periods with high lateral precision in order to solve important biological questions, such as what are the underlying causes of the restricted mobility of the receptor, and how does the receptor's spatio-temporal distribution influence the transmembrane signaling network. The results of this study have been published in an article entitled "*Single-molecule imaging deciphers the relation between mobility and signaling of a prototypical G protein-coupled receptor in living cells*" in the *Journal of Biological Chemistry*.

Chapter 3 (p. 63) presents a new approach based on an engineered StrepTactin protein to label membrane receptors without risk of cross-linking. The aim was to produce a StrepTactin tetramer (a genetically modified form of streptavidin) with only one functional binding site that retained the intrinsic affinity of the wild-type protein towards biotin and strep-tagged proteins.

Aim and Scope of this Thesis

The final purpose was to use this monovalent StrepTactin to specifically label biotinylated or Strep-tagged receptors with QDots for SPT experiments.

Chapter 4 (p. 79) focuses on the 5-HT₃ receptor, an important member of the superfamily of Cys-loop ligand-gated ion channels. Here the goal was to use the nanobody VHH15 (recently developed to improve crystallization for structure determination of the 5-HT₃ receptor) to label and track individual 5-HT₃ receptors in primary neurons endogenously expressing the receptor.

General introduction

The plasma membrane

The cellular plasma membrane is a 5 nm-thin flexible layer with fascinating and intriguing functions separating the interior of the cell from the outside environment and thereby defining the cell's dimension. The plasma membrane is far more than a simple barrier; it is a very complex and highly dynamic structure, composed of many different lipid and protein species, involved in fundamental cellular processes such as the transmission of matter and information between the outside and the inside of the cell. Tools for exploring the structural and dynamic organization of the plasma membrane on relevant spatial and temporal scales are still emerging, and our comprehension of this extraordinary biological entity at the basis of our existence is far from complete.

Lipids and proteins

The plasma membrane is primarily composed of amphiphilic lipids which are made up of polar head groups and hydrophobic tails (acyl chains). In an aqueous environment, lipids spontaneously self-assemble into membrane structures such as bilayers, vesicles or micelles as illustrated in Figure 1. This process, primarily driven by entropy, is commonly referred to as the hydrophobic effect and causes the lipid acyl chains and head groups to arrange in such a manner that the hydrophobic surface area exposed to the aqueous phase is minimized.

In the cell membrane, the lipids form a bilayer in which all the acyl chains point toward its center, while the polar head groups are oriented toward the aqueous phase. The lipid membrane is thus only two lipid molecules thick, i.e. about 5 nm. Despite being extremely thin, the plasma membrane functions as an efficient barrier. In absence of transmembrane proteins, a lipid bilayer is virtually impermeable to ions and to most water-soluble molecules, such as glucose or amino acids. This property is essential for fundamental cellular processes such as maintenance of ionic concentration gradients which are of critical importance for generation and propagation of action potentials that underlie the functioning of the nervous system [1].

Eukaryotic cell membranes are composed of a large variety of different lipid species [2],

General introduction

including glycerophospholipids, sphingolipids, and cholesterol. Lipids have multiple functions; they are of particular importance for energy storage, signaling and regulating membrane fluidity.

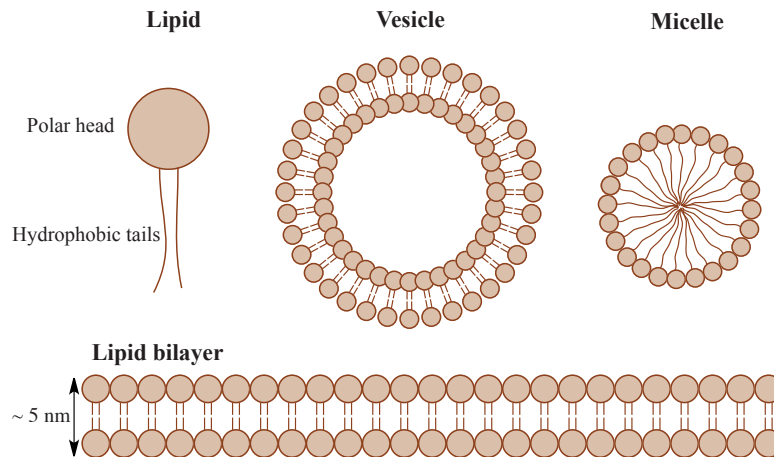


Figure 1: **Lipid structures.** Lipids are amphiphilic molecules with a polar head group and a non-polar tail (acyl chains). They can self-assemble into different structures such as a spherical vesicle, a micelle or a planar lipid bilayer.

The plasma membrane also contains proteins. Integral membrane proteins form transmembrane domains with amino acid residues with hydrophobic side chains that interact with the hydrophobic inner region of the bilayer. They represent about 1/3 of the total human proteome [3]. The protein content in the plasma membrane varies between 20-80% between different cell types according to the cells' function [4]. An important part of these membrane proteins are receptors that transmit extracellular signals across the membrane. The different receptor types in a mammalian plasma membrane are described below (p.8).

Membrane organization and lateral diffusion

In 1935, Danielli and Davson postulated that a cell membrane is composed of a lipid bilayer covered on both sides by globular proteins [5]. This model persisted until Singer and Nicholson proposed the *fluid-mosaic model* [6], which describes the membrane as a two-dimensional *fluid* with phospholipids and embedded proteins moving freely laterally. The term *mosaic* refers to the heterogeneous plasma membrane composition both in time and space. This model is still considered as correct to describe the general structural features of biological membranes although it has been largely refined. The development of high resolution microscopy techniques in the past 20 years led to a better understanding of plasma membrane organization on a nanometer scale [7].

According to the *fluid-mosaic model*, membrane proteins are randomly distributed and diffuse freely and uniformly in a two-dimensional plane. Saffman and Delbrück derived a theoretical relation for the lateral diffusion of molecules in a Singer-Nicholson membrane, where

$D \propto \ln(1/r)$, with r the radius of the molecule and D , the diffusion coefficient within the membrane plane [8]. However, experimental evidences have accumulated suggesting a locally restricted mobility of proteins in the plasma membrane of living cells. It has been shown that the diffusion of membrane proteins and lipids is slower by a factor 5-50 in plasma membranes than in artificial reconstituted membranes or liposomes [9, 10]. Such a reduction cannot be explained by lipid composition, e.g. addition of cholesterol [11]. This suggests significant barriers and obstacles for protein diffusion [9, 12, 13]. Furthermore, several research groups have shown, especially using single molecule tracking (SMT), that "big" molecular complexes (e.g. clusters of membrane proteins) diffuse much slower than predicted by the Saffman and Delbrück equation, even leading to total immobilization of the proteins [10, 14, 15, 16, 17]. Elucidating the mechanisms for such slowing effects is of utmost importance for understanding the signal transduction mechanisms taking place at, in and across the cell membrane [18]. Present models assume that membranes are composed of dynamic spatially segregated domains [7]. Two prevailing models of small-scale organization of the cell membrane allow to explain the two conflicts with the Singer-Nicholson model described above: *the cytoskeleton fence* [19] and *lipid micro-domains* [13], also known as *lipid rafts* [20]. These structures may influence the mobility of membrane-associated and -integrated molecules.

Cytoskeleton compartments

The shape and internal organization of a cell is maintained by the cytoskeleton, an intracellular scaffold, extensively and intimately interacting with the plasma membrane [21]. The cytoskeleton of eukaryotic cells is made up of three major kinds of filamentous proteins: actin microfilaments, microtubules which are polymeric tubulin, and intermediate filaments which are composed of different proteins. The cytoskeleton is a highly dynamic network capable of changing its dimension and shape very rapidly according to the cell's requirements. Its dynamic re-organization is essential for controlling cell polarity, cellular division or synapse formation [21]. A variety of cytoskeletal drugs that stabilize or destabilize actin filaments or microtubules have been discovered, and are extensively used to study the cytoskeletal influence on cellular functions [22].

The cytoskeleton plays an important role on the organization of the components of the plasma membrane [23]. The hypothesis that the actin cytoskeleton forms a boundary network on the membrane [24], which may be responsible for temporary confinement of membrane proteins and lipids has been proposed by Akihiro Kusumi [9, 10, 24, 25, 26, 27]. Kusumi's group was the first to highlight a possible correlation between the cytoskeleton and the mobility of membrane particles by investigating the mobility of *band 3* protein (an erythrocyte anion channel) in erythrocyte ghost membranes using fluorescence recovery after photobleaching (FRAP) microscopy. They observed that the fraction of immobile *band 3* protein in the membrane decreased upon diminution of spectrin polymers (a cytoskeleton-associated protein) [28]. Later they performed many SMT experiments on diverse membrane-associated molecules demonstrating that membrane proteins can be spatially confined within 30-700 nm compartments

and undergo non-Brownian diffusion in the plasma membrane, for example short-term confined diffusion in a compartment and long-term hop diffusion over the compartments [29] [30] [31]. This led to the proposal of the *membrane-skeleton fence model* (Figure 2A). An important consequence of this model is that the rate of diffusion cannot be described by a single diffusion coefficient [32].

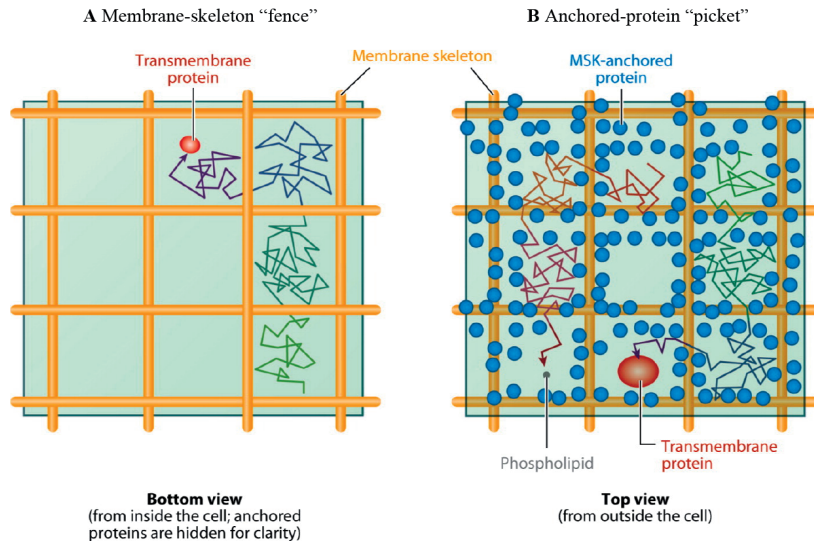


Figure 2: **Schematic illustration of Kusumi's anchored-picket-fence model.** The plasma membrane is compartmentalized by (A) the actin-based membrane-skeleton (MSK) "fences" and (B) the transmembrane proteins anchored to and aligned along the MSK ("pickets"). In the short term, barriers formed by the cortical MSK (i.e. the portion of the cytoskeleton that lies just beneath the plasma membrane) and the associated anchored proteins compartmentalized the diffusion of transmembrane proteins and lipids. However, on longer timescales, the molecule may escape and move to a neighboring compartment (hop diffusion) when a space allowing the passage of the molecule is formed as a consequence of the thermal fluctuations. Taken from [27].

An unexpected observation arose from the tracking of the lipid DOPE (1,2-dioleoyl-*sn*-glycero-3-phosphoethanolamine): in the outer leaflet of the plasma membrane this lipid also undergoes hop-diffusion, despite the fact that it does not span the membrane and is therefore not in direct contact with the cytoskeleton [11]. To explain this observation, the authors proposed the *anchored membrane-protein picket model* (Figure 2B) in which the transmembrane proteins anchored and aligned along the actin-based membrane-skeleton may act as rows of pickets, temporally confining the phospholipids [11]. According to this model, the barrier effect against the free diffusion of lipids and proteins may be due to steric hinderance and circumferential slowing (hydrodynamic-like friction effect near the anchored membrane proteins which slows down the diffusion) [11].

The only cloud on the horizon for these models based on hop-diffusion is that experimental validation from other research groups and with complementary methods is relatively limited. Nevertheless, the picket-fence model remains very attractive, as it explains convincingly why

the diffusion of both lipids and proteins is reduced by an order of magnitude compared to synthetic membranes.

Lipid raft domains

The raft hypothesis postulates that the membrane is able to laterally segregate its constituents (dynamic liquid-liquid immiscibility of regions enriched in cholesterol and sphingolipids [33]) creating nanometer-sized domains which over time can change size, composition and lateral position. These membrane domains are supposed to act as platforms for membrane signaling and trafficking [20]. Although thousands of papers on lipid rafts have been published, there is still controversy about their existence in the cellular plasma membrane, their size, and function [34].

Originally, lipid rafts were defined as detergent resistant membrane (DRM) fractions, insoluble in non-ionic detergents such as *Triton X-100* at low temperatures (e.g., 4°C). If we add such a detergent to the cells, the fluid membrane will dissolve while the DRM fractions may remain intact and could be isolated by sucrose gradient ultracentrifugation. This extraction method has received much criticism, because it has been shown that it induces a substantial reorganization of the plasma membrane leading to variable, and sometimes inconsistent results.

In model membranes, cholesterol and sphingomyelin, the two major "raft molecules", often form large micrometer-sized domains. However, despite the variety of experimental techniques available [35], such domains have never been observed in live cells.

This has led to the postulations that lipid rafts are small, smaller than the resolving power of a conventional optical microscope (i.e. ca. 200 nm) and that they are highly dynamic and short-lived (milliseconds or less) structures. This complicates considerably the question and requires the use of cutting-edge super-resolution microscopy techniques, such as STED-FCS (Stimulated Emission Depletion-Fluorescence Correlation Spectroscopy) microscopy [36]. But to date, rafts have still not been directly observed in a living cell. On the contrary, recent papers would seem rather to indicate that nanodomains based on lipid-mediated phase separation do not exist [37] [38]. Sevcski and coworkers rearranged a fluorescent glycosylphosphatidylinositol(*GPI*)-anchored protein (a typical raft-associated molecule), in the plasma membrane of living cells using protein micropatterning and then measured the effect on the local membrane environment using super-resolution single-molecule tracking. Their results showed that "*GPI-anchored proteins do not influence their membrane environment over distances beyond their actual physical size by stabilizing ordered membrane domains*" [38]. By demonstrating that GPI-anchored proteins do not reside in ordered domain, the raft hypothesis might be questioned. If phase partitioning could no longer be considered as a cornerstone of protein organization in the plasma membrane, then the role of the actin meshwork in close proximity to the plasma membrane would be further strengthened in this context.

Cell-surface receptors

The ability of organisms, or individual cells to sense and react to different physical (e.g. light, temperature, pressure) or chemical (e.g. odorant molecules, hormones, neurotransmitters, peptides, lipids) stimuli is crucial for their survival. In most cases, these various external signals are sensed by cell-surface receptors which transduce that information across the plasma membrane and alter intracellular molecules leading to a cellular response. According to the transduction mechanism used, three major classes of cell-surface receptors can be defined [39]:

- **G protein-coupled receptors (GPCRs)** (Figure 3A) regulate the activity of separate effector proteins bound to the plasma membrane which can be either an enzyme or an ion channel. The interaction between the receptor and the effector is generally mediated by a trimeric guanosine triphosphate (GTP)-binding protein (G protein).
- **Ion channel-linked receptors (ICLRs)** (Figure 3B) are involved in particular in rapid synaptic signaling between electrical excitable cells. Neurotransmitters released from the presynaptic cell control the opening of the channel which changes the ionic permeability of the postsynaptic membrane, triggering an action potential.
- Activation of **enzyme-linked receptors** (Figure 3C) causes enzymatic activity in their intracellular domain. They can function directly as enzymes or be associated with enzymes that they activate; the great majority of these receptors are protein kinases, or associate with protein kinases. Receptor tyrosine kinases (RTKs) are particularly important type of enzyme-linked receptors which recognize many polypeptide growth factors, cytokines, and hormones (e.g. insulin) and play important roles in growth, proliferation, differentiation, making them essential for the cell survival [39].

There are some cell-surface receptors that do not fit into any of the above classes, in particular receptors that activate signaling pathways that depend on proteolysis such as the *notch* receptors [40, 41].

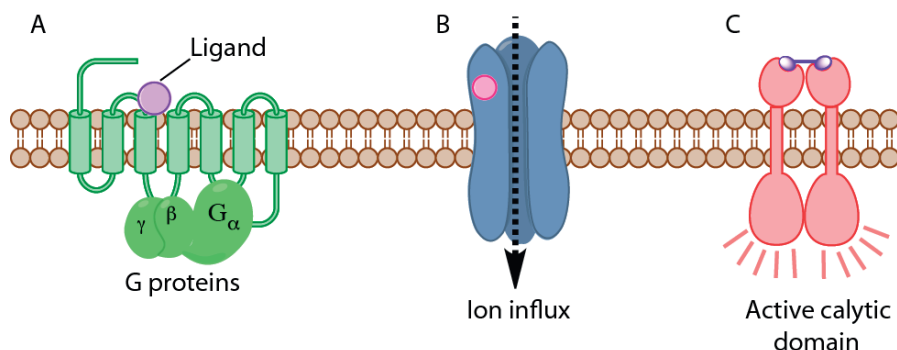


Figure 3: **Cell-surface receptors superfamilies.** (A) G protein-linked receptors, (B) ion channel-linked receptors, and (C) enzyme-linked receptors.

In the present thesis, a GPCR, the neurokinin-1 receptor (NK1R), and a ICLR, the serotonin 5-HT₃ receptor (5-HT₃R) will be in the spotlight. A general description of these two cell-surface receptors is given below.

G protein-coupled receptors

GPCRs represent the largest family of membrane proteins in the human genome, with almost 1000 members [42]. Members of this family exhibits a common structural motif consisting of seven membrane-spanning regions — explaining why they are sometimes called seven-transmembrane domain (7TM) receptors (for a review of the structural aspects of GPCR signaling, see [43]). These receptors can be activated by a tremendous variety of stimuli such as neurotransmitters, hormones, pheromones, growth factors, drugs, odors, and even photons [44]. GPCRs are involved in an incredible array of functions in the human body and play a role in many diseases. In fact, they represent the richest source of targets for the pharmaceutical industry [45]. We estimate that between one-third and one half of all marketed drugs act by binding GPCRs [46]. The 2012 Nobel Prize in Chemistry was awarded to Brian Kobilka and Robert Lefkowitz for their work crucial for understanding how GPCRs function [47].

GPCR activation and canonical signal transduction pathways

In the classical view of GPCR signalling, when a ligand binds to a GPCR, the latter undergoes a conformational change that activates heterotrimeric G proteins present inside the cell. These signaling proteins are composed of three different subunits (α , β and γ) and can bind guanyl nucleotides. The α and γ subunits are usually anchored to the membrane via aliphatic chains [48]. In the G protein's inactive state, a GDP (guanosine diphosphate) molecule is bound to the α subunit (referred to as G_α) which is a P-loop NTPase, where the motif *Gly-X-X-X-Gly-Lys* interacts with phosphoryl groups on the bound nucleotide. After activation, G_α releases GDP and binds GTP. This leads to the dissociation of G_α from the $\beta\gamma$ -associated subunits ($G_{\beta\gamma}$). It is important to note that a single activated-receptor can stimulate nucleotide exchange in many G-protein heterotrimers resulting in an amplified response [49]. Both G_α -GTP and $G_{\beta\gamma}$ can then activate different intracellular second messenger signaling cascades and effector proteins.

There are three main transduction pathways involved in GPCR signaling depending on the α subunit type (G_{α_s} , $G_{\alpha_{i/o}}$, $G_{\alpha_q/11}$, $G_{\alpha_{12/13}}$) [50]:

cAMP signal pathway The GTP-bound form of G_{α_s} activates, and of $G_{\alpha_{i/o}}$ inhibits adenylate cyclase (AC), an enzyme that catalyzes formation of cyclic adenosine monophosphate (cAMP) from ATP (adenosine triphosphate). In the first case, each activated AC can catalyze the formation of many cAMP molecule (second level of amplification). The resulting cAMP concentration increase regulates the activity of several ion channels as well as protein kinase A (PKA),

General introduction

thereby influencing diverse cellular processes (Figure 4A).

Phosphatidylinositol signal pathway The phosphatidylinositol pathway is mediated by $G_{\alpha q/11}$ which activates phospholipase C (PLC). The latter catalyzes the cleavage of a membrane lipid (phosphatidylinositol 4,5-biphosphate, PIP₂) to produce two secondary messengers: inositol 1,4,5-triphosphate (IP₃) and diacylglycerol (DAG). Soluble IP₃ diffuses away from the membrane and binds to IP₃ sensitive calcium channels found in the endoplasmic reticulum (ER) membrane leading to Ca²⁺ release (Figure 4B). Plasma membrane embedded DAG activates protein kinase C (PKC), a kinase targeting serine and threonine residues. DAG binding domain of PKC requires calcium ions to bind DAG. Thus, DAG and IP₃ work in tandem: IP₃ increases the Ca²⁺ concentration, which in turn, facilitates PKC activation (Figure 4B).

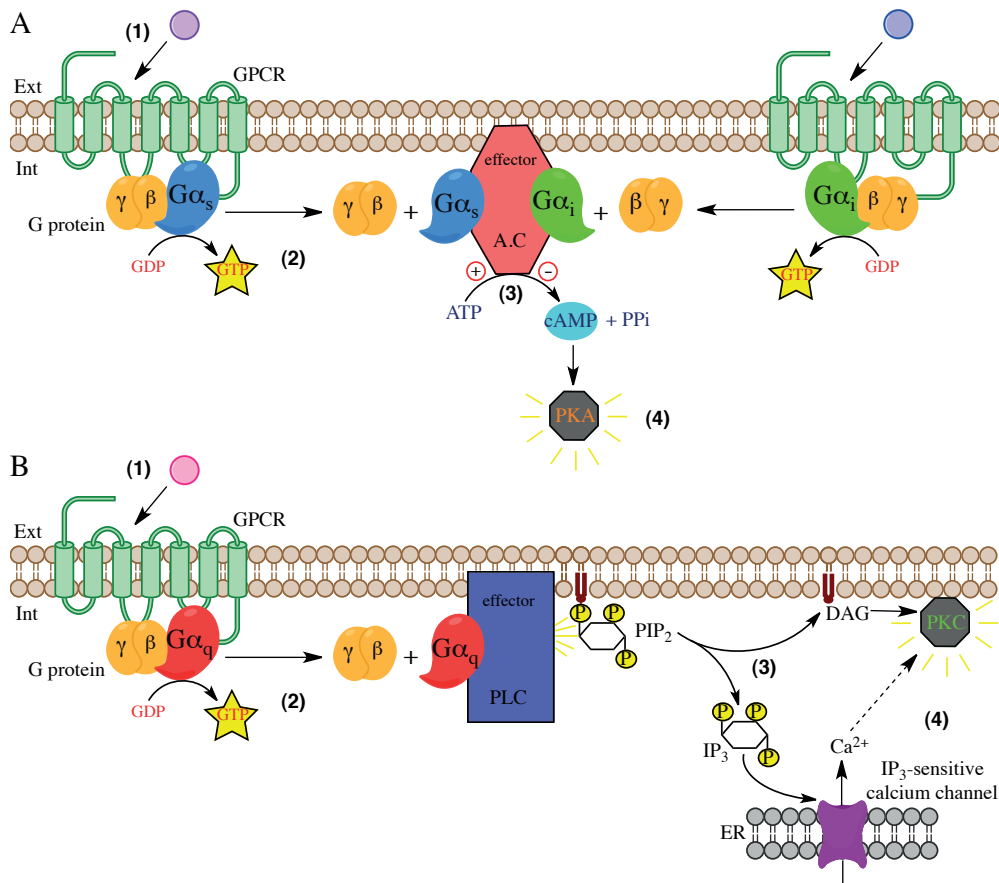


Figure 4: **GPCR signaling pathways.** (A) cAMP signal pathway. (1) Receptor activation by an external stimulus. (2) G_{α_s} or $G_{\alpha i/o}$ activation. (3) Activation via G_{α_s} or inhibition via $G_{\alpha i/o}$ of cAMP production from adenylate cyclase (AC). (4) Activation of protein kinase A (PKA). (B) Phosphatidylinositol signal pathway. (1) Receptor activation by an external stimuli. (2) G_{α_q} activation. (3) Hydrolysis of phosphatidylinositol 4,5-biphosphate (PIP₂) into inositol triphosphate (IP₃) and diacylglycerol (DAG). (4) Opening of endoplasmic reticulum IP₃ gated calcium channels and PKC activation by DAG.

$G_{\alpha 12/13}$ -RhoGEF-mediated pathway GPCRs coupling to $G_{\alpha 12/13}$ activate RhoGTPase nucleotide exchange factors (Rho-GEFs), leading to the activation of members of the Rho family of small GTPases, and other downstream effectors [51]. For instance, the small monomeric GTPase RhoA, once bound to GTP can activate various proteins controlling cell cytoskeleton remodeling, including the rho-associated protein kinase (ROCK) [52]. The latter promotes actin-myosin contractility and consequent membrane blebbing as will be seen with activation of the NK1 receptor. All known GPCRs that couple to $G_{\alpha 12/13}$ also signal through other types of G proteins, often $G_{\alpha q/11}$ [51].

Following its liberation from the heterotrimeric G protein complex, the $G_{\beta\gamma}$ subunit can also play an important role in GPCR signaling by regulating various ion channels or PLC isoforms [53].

G-protein signaling is terminated by the hydrolysis of the bound GTP to GDP. The inactive heterotrimeric G protein returns in its inactive state by re-association of $G_{\beta\gamma}$ with the GDP-bound form of G_{α} [49].

The question of whether the heterotrimeric G protein physically dissociate or not upon GTP binding is a subject of long-running disputes. Dissociation has initially been proposed based on in vitro experiments with purified proteins [54], but its relevance in vivo has been questioned [55]. Bünemann *et al.* have shown using fluorescence resonance energy transfer (FRET) that G_i protein activation in intact cells involves subunit rearrangement rather than dissociation [56]. It has subsequently been suggested that some G protein subunits physically dissociate in living cells, whereas other heterotrimers may signal without physically dissociating [57]. These contradictory results led to the proposition of a combined model that defends an equilibrium between dissociated and intact heterotrimers in the active state [58] [59]. More recently, Bondar *et al.* have shown that the presence and localization of the fluorescent label may have a great influence on the molecular mechanism of heterotrimeric G protein activation [60]. Their results revealed that non-modified G_i proteins dissociate upon activation, whereas fluorescently labeled heterotrimers dissociate or rearrange depending on fluorescent protein localization, further feeding the debate on the nature of the activated form of heterotrimeric G proteins.

GPCR desensitization

Desensitization is the loss of response induced by a prolonged or repeated exposure of the receptor to an agonist. Desensitization can be: (i) homologous, when the loss of response of the receptor results only from activation by an agonist of the same receptor; (ii) heterologous, when activation of a GPCR can lead to the desensitization of another type of GPCR even in the absence of agonist binding.

This process includes a combination of different mechanisms: uncoupling of the receptor from heterotrimeric G proteins in response to receptor phosphorylation, internalization of cell

General introduction

surface receptors to intracellular compartments, and down-regulation of protein expression, as well as both the lysosomal and plasma membrane degradation of pre-existing receptors [61]. The time frames over which these processes occur range from seconds (phosphorylation) to minutes (endocytosis) and hours (down-regulation) [61]. Phosphorylation of specific residues within the intracellular loops and C-terminus of the receptor is the first step of the desensitization process. Receptor phosphorylation is mediated by second messenger-dependent protein kinases, or by a distinct family of GPCR kinases (GRKs) [62]. Second-messenger dependent kinases, such as PKA or PKC, are activated by signals resulting from G protein activation such as increases in the second messengers concentration (Ca^{2+} , cAMP, and DAG). Thus, activation of PKA or PKC directly uncouples receptors from their respective G proteins. However, they can also induce heterologous desensitization in receptors other than those activated [63]. GRKs phosphorylate only activated or agonist occupied conformation of the receptor (homologous desensitization), thereby promoting binding of a β -arrestin molecule, which sterically uncouples the receptor from the G protein and leads to receptor desensitization, internalization, dephosphorylation and recycling of the GPCR. These processes are illustrated in Figure 5.

β -arresting-dependent signaling

While arrestins were initially named for their ability to shut down (“arrest”) receptor signaling via G proteins, it is now becoming evident that β -arrestins also function to activate signaling cascades independently of G protein activation [65, 66]. β -arrestins may act as multi-protein scaffolds, bringing elements of specific signaling pathways into close proximity, including in particular many mitogen-activated protein (MAP) kinases [67]. In addition, nuclear functions of β -arrestins in transcriptional regulation have been highlighted [68]. Classical and new roles of β -arrestins in cell signaling have been reviewed by Lefkowitz and coworkers [65, 69].

Interestingly, recent evidences suggest that signaling by internalized GPCRs is not only restricted to mechanisms independent of G protein activation, such as the previously cited scaffolding by β -arrestins, but that canonical GPCR signaling may also occur from endosomes [70, 71]. Using a conformation-sensitive biosensor based on a fluorescently labeled nanobody, Irannejad *et al.* were able to directly and specifically visualize β 2-adrenergic receptors (β 2ARs) which are in the active state [70]. The biosensor translocated to the plasma membrane upon β 2AR activation and then again to endosomes after ligand-induced internalization of the receptor, thus revealing a “second wave” of G protein activation.

The NK1 receptor

In this thesis, particular attention will be paid to the *neurokinin-1* receptor (NK1R) also known as tachykinin receptor 1 (TACR1) or substance P receptor. It is a prototypical neuropeptide GPCR belonging to the rhodopsin-like family (class A) and to the tachykinin receptor subfamily. The human NK1R consists of 407 amino acid residues, and has a molecular mass of 46 kD [72].

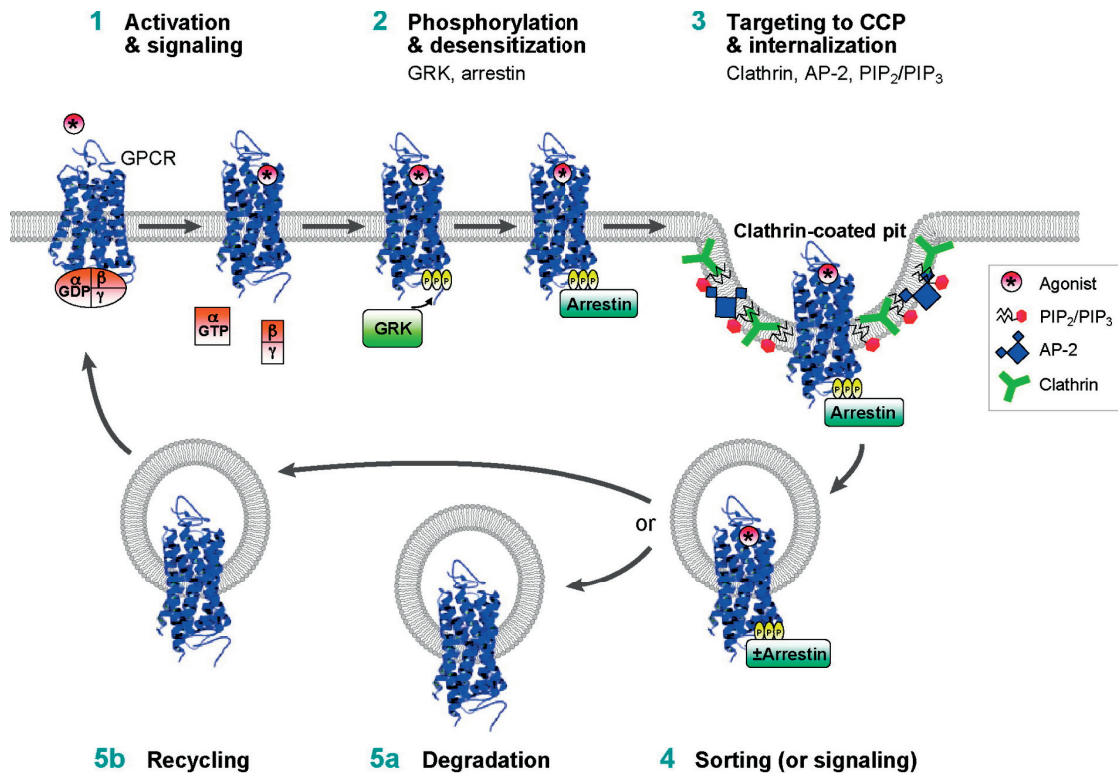


Figure 5: **Regulation of GPCR trafficking by GRKs and arrestins.** Agonist (*) binding leads to receptor activation, G protein coupling, and signal transduction (step 1). GRKs then phosphorylate the agonist-activated GPCR on intracellular domains, initiating arrestin recruitment. Arrestin binding to the receptor inhibits G protein coupling and terminates signaling, a process termed desensitization (step 2). Receptor/arrestin complexes are then targeted to clathrin-coated pits, where arrestin forms a multicomponent complex with clathrin, AP-2, and phosphoinositides, resulting in receptor internalization (step 3). Internalized GPCRs are sorted (step 4) to either degradation (step 5a) or recycling (step 5b) compartments. Taken from [64].

It is present in the central nervous system (CNS) and peripheral nervous system (PNS) [73] where it is involved in a wide variety of different process, e.g. neural signal transmission, regulation of the intestine, hematopoiesis, nociception and neurogenic inflammation [74]. NK1R is therefore an important target for pharmaceutical agents [75, 76]. It is easily expressed in heterologous systems and several fluorophore labeled agonists and antagonists which bind with high affinity are known. Therefore, NK1R is particularly well-suited as a model for GPCR studies.

One of the most potent NK1R natural agonist is an undecapeptide called substance P (SP) (insert figure 6) [77]. Binding of SP to NK1R mainly activates $G_{\alpha q/11}$, which stimulates the production of IP₃ via PLC, leading to the release of calcium ions from the intracellular stores [78] as illustrated in figure 6.

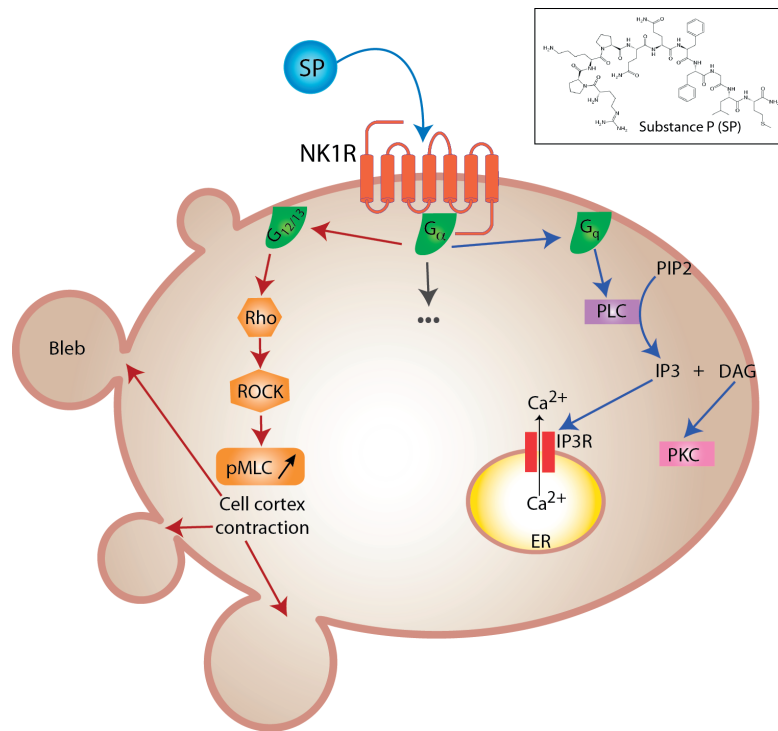


Figure 6: **Main G protein signaling pathways of the NK1 receptor.** Upon SP binding, NK1R couples mainly to $G_{\alpha q/11}$, resulting in a transient increase in intracellular calcium concentration. See legend of figure 4 for a more detailed description of this pathway. In parallel SP induces changes in cellular morphology that are G_q -independent. These changes are triggered by activation of the Rho, Rho-associated coiled-coil kinase (ROCK) signaling pathway, probably via $G_{12/13}$ proteins. ROCK activates myosin light chain kinase (MLCK) (not shown) [79], which phosphorylates the MLC. Phosphorylation of this protein activates the actin-myosin machinery responsible for the formation at the membrane of small spherical outgrowths known as blebs. The insert in the right upper corner shows the primary structure of SP (Arg-Pro-Lys-Pro-Gln-Gln-Phe-Phe-Gly-Leu-Met-NH₂).

The NK1R may also signal through other pathways depending on the nature of the G proteins (for a detailed review, see [80]), including activation or inhibition of cAMP production by G_s [81] and G_i [82] proteins, respectively. Nevertheless, the stimulation of cAMP formation by NK1R agonists is much less efficient than that of IP₃ formation and intracellular calcium increase [81].

Besides the classical $G_{\alpha q/11}$ mediated signaling cascade, SP induces cell membrane blebbing through Rho-ROCK pathway by contraction of the actomyosin cell cortex. This blebbing phenomenon is not related to apoptosis and is independent of PLC activation, cytosolic calcium ion increase or PKC activation, but rather induced by the coupling with $G_{12/13}$ protein [83]. Cell-derived vesicles originating from membrane blebbing are believed to participate in communication between distant cells [84], cell movement, cell spreading, and cancer cell invasion [52].

Chen *et al.* have shown that NK1R is present in vesicles derived from membrane blebbing of HEK293 cells expressing NK1R [84]. In order to prove this, cells expressing a NK1R-GFP fusion protein or the corresponding non-fluorescent receptor were stimulated with SP and the resulting microparticles were analyzed by flow cytometry. As expected, microparticles generated from HEK293-NK1R-GFP cells displayed increased levels of fluorescence, as compared to those coming from non-fluorescent HEK293-NK1R cells, demonstrating that the NK1R is present on microparticles [84]. The release of these microparticles may be a form of intercellular communication, with a preponderant role in cancer progression, in particular through the development of metastasis [85] [86]. This is very interesting, since NK1R antagonists that effectively block cellular blebbing are known [87, 83]. In fact, it has been shown that L-733,060, a non-peptide selective NK1R antagonist, reduces SP-mediated migration and invasion of gastric cancer cells through inhibition of SP binding [88].

Therefore, the NK1R could be a promising new target in cancer treatment. In this regard, antagonists against the NK1R are of particular interest as they exert three harmonizing actions as explained by Rosso *et al.* [85]: “First, they have an antiproliferative action due to the inhibition of tumor cell growth and induction of apoptosis; second, they inhibit angiogenesis in the tumor mass; third, they block the migration of tumor cells and thereby inhibit invasion and metastasis.”. For more details see also [86].

Additional information about the NK1R are presented in chapter 2 (p. 39).

Pentameric ligand-gated ion channels

Ion channels are macromolecular proteins that control the passage of ions across the plasma membrane. In contrast to simple aqueous pores, gated ion channels are (i) ion selective, allowing only ions of particular size and charge to pass through and (ii) gated, i.e. they are not continuously open, but they open and shut transiently. These ion channels may be classified by the nature of the stimulus required for their gating.

Ligand-gated ion channels (LGICs), also known as ionotropic receptors, are regulated by the binding of specific ligand molecules to the extracellular domain of the channel. Ligand binding triggers conformational changes in the transmembrane domain, leading to gate opening and thus allowing the selective passage of specific ions down their electrochemical gradient. LGICs diverge from voltage-gated ion channels (which open and close in response to the voltage across the membrane), metabotropic receptors (which act through second messengers or G proteins-activated ion channels), or mechanosensitive ion channels (which opens in response to mechanical deformation of the membrane) [89].

In mammals, LGICs can be classified into three different superfamilies: the pentameric ligand-gated ion channels (pLGICs), the tetrameric glutamate receptors, and the trimeric P2X receptors (ATP-gated channels). Here we will focus on pLGICs, also known as cys-loop receptors because they contain a characteristic extracellular loop with a pair of disulphide-

General introduction

bound cysteines. These receptors are of particular importance for fast signal transduction in synapses. pLGICs are further subdivided into cation- and anion-selective channels, including, respectively, excitatory receptors activated by acetylcholine or serotonin, and inhibitory receptors activated by γ -aminobutyric acid (GABA) or glycine. These receptors, composed of five subunits surrounding a central transmembrane pore, can assemble from five copies of a single type of subunit, or more commonly from several different types of subunits. Due to the numerous subunit types, formation of such hetero-pentamers provides an increased functional and regulatory diversity, probably to meet the diverse needs for proper synaptic transmission [90].

Each subunit is composed of a large N-terminal extracellular domain, four transmembrane alpha helices (M1-M4) and a cytoplasmic loop of variable length between M3 and M4. The ligand binding sites are located at the extracellular side at the interface between two subunits [91]. The pair of the disulfide-linked cysteines present in the N-terminal extracellular domain of each alpha subunit is essential for ligand binding [92]. The channel pore is formed primarily by M2, which dictates ion-selectivity and conductance [91]. The large intracellular linker between M3 and M4 is believed to be involved in protein-protein interactions modulating pLGIC activity, assembly and trafficking [93]. The M3-M4 loop is also thought to play important role in receptor anchoring to the cytoskeleton and to the postsynaptic membrane [94] [95].

In recent years, the X-ray crystal-structure of several eukaryotic pLGICs have been solved [96] [97] [98], greatly extending our knowledge of the structure-function relationship of the family.

The 5-HT₃ receptor

The 5-hydroxytryptamine type 3 receptor (5-HT₃R) is a member of the pLGIC receptor superfamily [99]. It is expressed throughout the central and peripheral nervous systems and is involved in a wide variety of physiological processes. Binding of the neurotransmitter 5-hydroxytryptamine (serotonin) to 5-HT₃R opens the channel, letting Na⁺ and Ca²⁺ ions enter into the cell, which leads to depolarization of the plasma membrane. The 5-HT₃R differs clearly in a structural and mechanistic point of view from the other 5-HT subtypes. Indeed 5-HT type 1, 2, 4, 5, 6 and 7 receptors are all GPCRs [100]. To date, five different subunits, named A to E, have been isolated in humans, whereas only A and B subunits are present in rodents. The A subunit is the only that can form a functional homopentameric receptor. All the others have to be expressed in combination with the A subunits to form a functional heteropentamer [101].

Recently, the atomic structure of the mouse 5-HT₃R has been solved by X-ray crystallography (Figure 7), giving new insights for understanding the operating mechanism of receptors of the pLGIC superfamily [96]. It is the first high resolution structure of a mammalian LGIC that includes the intracellular loop (absent in prokaryotic receptors).

In the CNS, 5-HT₃Rs can be localized either on pre- or post-synaptic cells. Post-synaptic

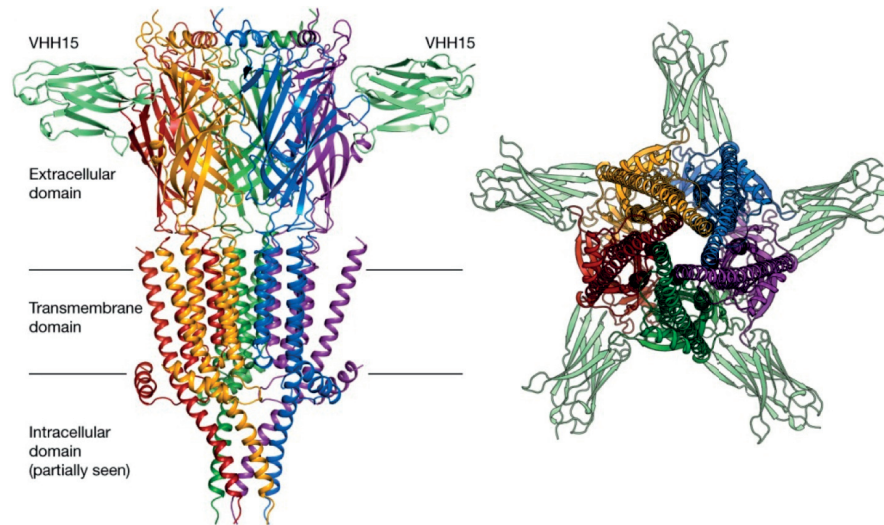


Figure 7: **X-ray structure of the mouse serotonin 5-HT₃ receptor.** 5-HT₃R in complex with VHH15 viewed parallel to the plasma membrane. Only two out of five nanobodies are shown (left). View of the complex from the intracellular side perpendicular to the membrane (right). Taken from [96].

5-HT₃Rs have been shown to be present in GABAergic interneurons where they mediate fast excitatory synaptic transmission [102]. In pre-synaptic nerve terminals 5-HT₃Rs are thought to be involved in modulation of neurotransmitter release [103]. On a molecular level, activation of pre-synaptic 5-HT₃Rs induce robust increase in presynaptic Ca²⁺ which, in turn, trigger the release of neurotransmitters by promoting fusion of synaptic vesicles with the plasma membrane. In particular, evidence has been provided that 5-HT₃R activation facilitate release of SP in the rat spinal cord [104].

The 5-HT₃R, like all receptors having an important role in cell signaling, is involved in many diseases and disorders and is therefore an important pharmacological target [105, 106]. The most well established roles of the 5-HT₃R are the regulation of gastrointestinal mobility and the control of emesis. Currently marketed 5-HT₃R antagonists are used for the treatment of chemotherapy-induced and post-operative nausea and irritable bowel syndrome [107]. Promising other therapeutic uses have been reported for treatment of complex psychiatric disorders such as anxiety and depression, schizophrenia, cognitive dysfunction and substance abuse and addiction [108, 109]. 5-HT₃R antagonists may also be beneficial in rheumatic diseases as anti-inflammatory drugs [110].

Relationship between NK1 and 5-HT₃ receptors

In 1983, Coates *et al.* conducted a survey to identify and rank side-effects perceived by patients receiving chemotherapy [111]. Nausea and vomiting were classified as the first and second most severe side effects, respectively. In those days, up to 20% of cancer patients were

General introduction

reluctant to take emetogenic but potentially curable chemotherapeutic agents [112]. Since then, significant progress has occurred in antiemetic drug development [113]. Nevertheless the situation of cancer patients regarding nausea and vomiting is far from comfortable and improved antiemetic treatments are needed.

Chemotherapy-induced nausea and vomiting (CINV) has been historically categorized as acute, delayed, or anticipatory depending upon the time period of vomiting. The acute phase occurs in the first 24 hours of administering chemotherapy, the delayed phase persists for 6-7 days after therapy and the anticipatory emesis precedes drug administration (conditioned response from a previous negative experience with chemotherapy) [114].

According to the established dogma, 5-HT is considered as one of the major actors inducing the acute vomiting phase after administration of chemotherapy drugs such as cisplatin, while activation of NK1R by SP is assumed to trigger the delayed CINV phase [115]. It is therefore not surprising that 5-HT₃R and NK1R antagonists are the two major classes of antiemetics prescribed to prevent CINV [116].

Interestingly, crosstalk between NK1 and 5-HT₃ receptor signaling pathways has been reported by different laboratories [116]. In vitro and in vivo experiments have shown that palonosetron, a second generation 5-HT₃R antagonist with demonstrated efficacy in preventing both acute and delayed emesis, can inhibit SP-induced calcium release. Because palonosetron does not bind to the NK1R [117], it is thought that it inhibits the SP response uniquely by its interaction with the 5-HT₃R. Inhibition of these interactions among the crossroads of acute and delayed emesis may offer new perspectives in the treatment of CINV [116].

In line with this synergistic relationship, SP has been shown to potentiate serotonin-induced 5-HT₃R-mediated currents in rat ganglion neurons, presumably through activation of PKC by the NK1R [118]. Note that this PKC-mediated up-regulation of 5-HT₃R is thought to be caused by a trafficking mechanism, instead of direct phosphorylation of the receptor protein [119]. Such NK1R-5-HT₃R cross-talk may be of particular importance for regulation of peripheral pain caused by tissue damage or inflammation [118], and might be considered for development of new therapeutic approaches [120].

Membrane receptor labeling strategies

In order to specifically detect and identify a membrane protein, e.g. the NK1R or the 5-HT₃R, the latter has to be labeled, generally with a fluorescent probe. Numerous labeling strategies have been published, including the involvement of antibodies, agonists, antagonists, toxins, affinity tags, or genetically encoded fluorescent proteins. Together with the choice of the fluorophore, the choice of the labeling method is of fundamental importance for a successful observation of the protein of interest. This is particularly true for single-molecule experiments which require a highly specific labeling method and very bright and photostable probes that do not induce protein cross-linking.

In this thesis, an enzyme-mediated labeling strategy based on a genetically encoded short peptide tag (chapter 2) and an nanobody-based labeling strategy (chapter 4) have been used to mark and track individual NK1 and 5-HT₃ receptors, respectively. Fluorescent ligands (agonist or antagonist) binding specifically these two receptors have also been used.

Fluorescent probes

Numerous different types of probes can be used in combination with the labeling strategies mentioned above. Initially, micro-sized latex beads and gold-nanoparticles (40-100 nm in diameter), which could be detected by differential interference contrast microscopy, were employed to investigate the diffusion of single molecules in the plasma membrane of living cells [121]. Since 1990, and the demonstration that single fluorophores could be detected under biologically relevant conditions [122], single-molecule fluorescence-based imaging has become an indispensable tool in experimental biophysics and new fluorophores with increasingly better properties such as fluorescent proteins (FPs), organic dyes and quantum dots (QDots) have been developed. All these probes have distinct characteristics, which should be considered to select the most appropriate probe for a given application or experimental system.

Fluorescent proteins

The discovery and development of the green fluorescent protein (GFP) from the jellyfish *Aequorea victoria* [123], in parallel with advances in fluorescence imaging methods and microscope systems provided unprecedented insights into protein localization, dynamics and interactions in living cells [124].

Fusion of a FP to the protein of interest is probably the most convenient and non-invasive way to visualize the latter in a living cell. Because the fusion is achieved at the genetic level, the labeling is highly specific and a 1:1 FP/protein stoichiometry is guaranteed. However FPs suffer of serious disadvantages, particularly a strong photobleaching which limits the total imaging time of single-molecules to a few seconds. Moreover the signal to noise ratio is in general relatively low, inducing a localization accuracy well below that of the other fluorescent probes discussed below [125].

Quantum dots

QDots are fluorescent semiconductor nanocrystals with an extraordinary potential in biological detection and imaging [126, 127]. These nanocrystals demonstrate unique optical properties allowing measurements at the single-molecule level with high signal-to-noise ratio. Unlike organic fluorophores and fluorescent proteins, QDots do not rapidly photobleach, thereby allowing to record much longer trajectories. Furthermore QDots have been estimated to be up to 20 times brighter and almost indestructible as compared to traditional fluores-

General introduction

cent reporters [128], enabling a better localization accuracy, and allowing imaging on fast time-scales [129].

Their nanometric size induces a quantum confinement that provokes a discretization of the energy levels, giving them a unique physical property: the color of the emitted light depends on the size of the QDot; the larger the QDot, the more is the emitted light shifted to the red/infrared (Figure 8B) [130]. Combined with a broad absorption spectrum, this make QDots particularly well suited for multi-color observations [131, 132].

QDots are generally composed of a core and a shell of semi-conductor material (e.g. a core of CdSe and a shell of ZnS). Biocompatibility of QDots is crucial for biological applications. In this sense, different coatings with amphiphilic polymers, phospholipids and small molecules have been developed and tested successfully on living cells [128]. Coated QDots can be further functionalized with antibodies, proteins (e.g. streptavidin) or targeting ligands, allowing specific labeling of proteins of interest (Figure 8A) [133].

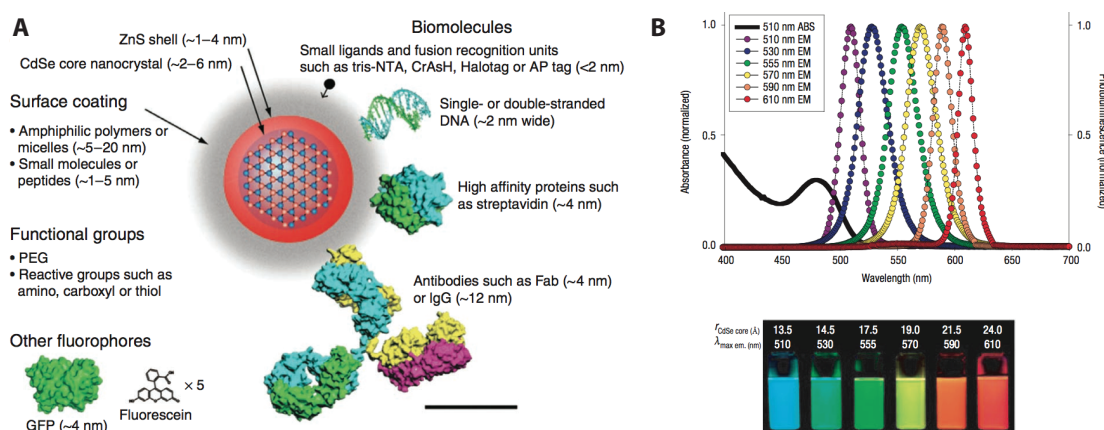


Figure 8: Structure and properties of QDot probes. (A) Schematic representation of a QDot. The inorganic cadmium selenide (CdSe) core nanocrystal and zinc sulfide (ZnS) shell (in red) can be coated with different organic molecules (in gray) such as peptides, amphiphilic micelles or polymers, providing colloidal stability in biological buffers. Key features of the surface coating include PEG to reduce nonspecific interactions and reactive groups to enable conjugation of biomolecules such as DNA, streptavidin or antibodies. GFP and fluorescein dye are shown for size comparison. Scale bar, 5 nm. Taken from [129]. (B) Size-tunable fluorescence properties and spectral range of QDots. Absorption and emission spectra of different QDots (upper panel). Photo of QDot dispersions plotted above, excited at 365 nm with a UV source (lower panel). Taken from [134].

Despite their relative large size (6-60 nm), the influence of QDots on the diffusion coefficient of the targeted membrane proteins is negligible because the viscosity of the plasma membrane is much higher (100- to 1000-fold) than that of the extracellular medium, thus the membrane is dominating the receptor diffusion. However this is not necessarily the case in a restricted environment, like the synaptic cleft [135].

The most commonly cited disadvantage of QDots in the literature after the size, is their blinking behavior, or fluorescence intermittency [136]. This phenomenon of random switching between ON (bright) and OFF (dark) states may cause difficulties in monitoring protein dynamics at the single-molecule level, especially in establishing correspondence between consecutive frames in tracking experiments [137]. Specific tracking algorithms are required [138, 139, 140]. However, there is some hope that blinking can be suppressed by improved surface chemistries or addition of reducing agents [127]. Wang and coworkers reported a new generation of gradient-based QDots that exhibits continuous, non-blinking photoluminescence and that can be produced in smaller sizes (5-7 nm) [141]. These novel non-blinking nanocrystals may enable substantial advances in single-molecule imaging and tracking. On the other hand, blinking can be seen as an advantage as it provides a criterion for distinguishing single QDots from aggregates. Furthermore, the blinking behavior of QDots can be exploited to achieve super-resolution. For example, SOFI (super-resolution optical fluctuation imaging), a technique based on the temporal and spatial cross-correlation analyses of fluorescence fluctuation, take advantage of the blinking mechanism to achieve background free, contrast enhanced 3D super-resolution imaging [142].

For an extensive review about QDots see [143].

Organic dyes

The principal advantage of organic dyes is their small size (~0.5 nm) and their highly controlled stoichiometry in the complex with the receptor, thereby lowering the risk of interference with the proper biological function of the protein of interest. They also provide a higher photostability and brightness than FPs [144]. For a review, see [145].

The development of new organic dyes with improved photostability and brightness which could potentially rival with QDots is ongoing [146].

Measuring protein diffusion using fluorescence microscopy

The plasma membrane has a fundamental role in many essential cell functions. All these functions are performed by an extremely complex network of interacting proteins and lipids present on or near the cell surface. The direct study of surface molecules association is often not possible. However, important information about their interactions may be obtained via their mobility behavior over time and space. Interestingly, the lateral mobility of membrane molecules can influence the location and the manner these associations occur. Therefore, studying mobility is essential for the membrane function and organization comprehension.

Fluorescence-microscope-based methods to investigate both membrane organization and dynamics include FRAP, FRET, fluorescence correlation spectroscopy (FCS) [147] and single-molecule/particle tracking techniques. In the following, focus will be on single-molecule

imaging and tracking.

General aspects of single-molecule fluorescence imaging

The saga of single-molecule experiments is relatively recent. One of the first breakthroughs in this field was achieved by Moerner in 1989 with the optical detection of a single fluorophore molecule in a solid at cryogenic temperature [148]. Before that, direct observation of single molecules was thought to be impossible. In the 90s, considerable advances in experimental instrumentation and in particular in the sensitivity of detectors allowed the detection and tracking of single fluorophores in the plasma membrane of living cells [121]. This resulted in the appearance of new concepts accounting for the dynamic organization of biological systems, a good example being the picket-fence model proposed by Kusumi and discussed in the first part of this introduction (p. 5).

The diffusion coefficient is the most common and accessible parameter to account for the mobility of molecules in membranes. Its determination does not necessarily require single-molecule resolution. Techniques such as FRAP and FCS have been extensively used to measure dynamic molecular behavior both in purified systems and in cells [149, 150]. However the diffusion coefficients obtained provide diffraction-limited information and reflect only the average diffusive behavior of an ensemble of molecules. In single-molecule experiments the properties of individual molecules are investigated, offering more valuable and precise information for the comprehension of the biological system. This is particularly true in a complex and heterogenous system like the plasma membrane where individual proteins can behave very differently and are not synchronized. In this case, ensemble measurements are only providing average properties and only experiments at the single-molecule level are able to reveal the presence of sub-ensembles. This can be of critical importance for the elucidation of the dynamic organizing principles of the plasma membrane underlying the molecular mechanism that regulate signal transduction [27].

A key challenge in single-molecule experiments is to distinguish photons coming from a single fluorescent probe from those coming from the noise. This requires well prepared samples combined with a high-end measurement setup. A schematic view of the experimental setups used in this thesis for imaging and tracking single molecules can be found in Appendix A.

Spatial resolution and localization precision

In conventional light microscopy the spatial resolution is limited by diffraction [151]. The lateral resolution limit (Δr) corresponds to the minimum distance that two point-source objects have to be in order to discriminate (resolve) the two sources from each other. The Abbe's criterion stipulates that light with wavelength λ , traveling through a lens with numerical

aperture NA , will make a spot with radius:

$$\Delta r = 0.5 \cdot \frac{\lambda}{NA_{\text{obj}}} \quad (1)$$

Later this criterion was refined by Rayleigh (Eq. 2). This is illustrated in figure 9B.

$$\Delta r = 0.61 \cdot \frac{\lambda}{NA_{\text{obj}}} \quad (2)$$

For visible light microscopy the resolution limit is therefore on the order of 200-250 nm. However this limit is not a drawback for single-molecule imaging and tracking. It only requires that the molecules we observed must be separated by a distance larger than the resolution. This can be easily achieved by adjusting the concentration of the labeled species. Because single molecules can be localized with a precision better than the diffraction-limited resolution, single-molecule microscopy can be considered as subdiffraction imaging technique, even if the measurement is performed with a standard optical microscope.

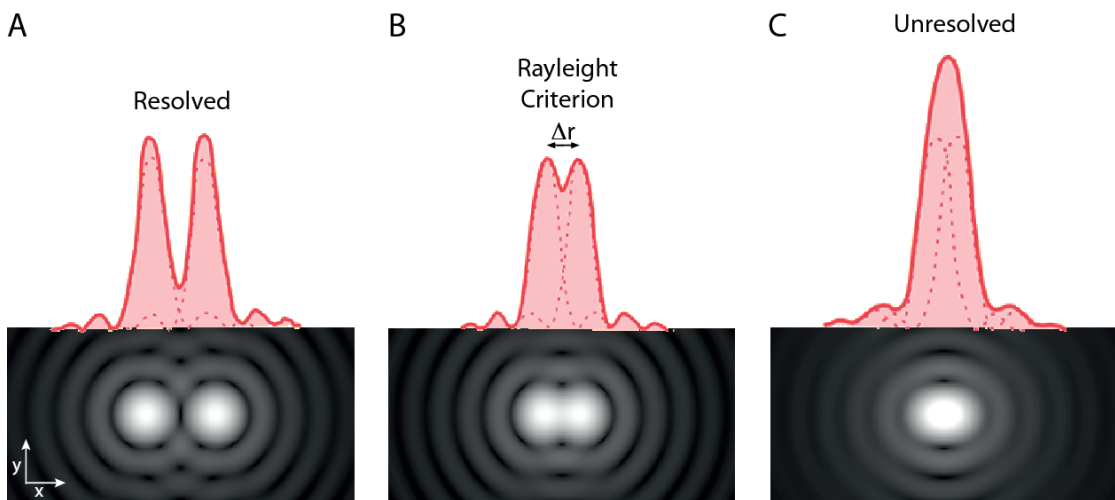


Figure 9: **Airy diffraction pattern and the limit of resolution.** Airy patterns in the xy plane (bottom) and intensity distribution plot along x -axis (top) for various angular separation of two point sources. (A) The points are far apart, the patterns are well resolved. (B) The points are at an angular separation just satisfying the Rayleigh criterion (the maximum of one diffraction pattern coincide with the first minimum of the other), the patterns are just resolved. (C) The points are closer than in the Rayleigh criterion, the patterns are not resolved. Adapted from a personal work of Spencer Bliven published on *commons.wikimedia.org*

A 2D-Gaussian is usually used to approximate the intensity profile of the diffraction-limited spot (the point spread function or PSF). For a perfect optical system, based on circular ele-

General introduction

ments, the PSF forms a so-called Airy pattern (Figure 9). The central Airy disc contains 84% of the total energy in the pattern. Hence, the position of a single molecule can be determined with high accuracy by the maximum of the Gaussian profile approximating the Airy disc. As the PSF describes the probability distribution of the emitted photons, the localization accuracy (σ_r) will increase as the number of detected photons (N) increases (equation 3). Hence, the choice of the probe is of paramount importance (see *Fluorescent probes*, p. 19).

$$\sigma_r \approx \frac{\lambda/2}{\sqrt{N}} \quad (3)$$

The typical localization accuracy in a SMT experiment is 5-50 nm depending on the choice of label [152].

Single-molecule tracking (SMT)

SMT allows the direct observation of the movement of individual single-molecules over time with subdiffraction-limited spatial resolution. To achieve this, a limited number of molecules of interest are specifically labeled with e.g. gold nanoparticles, QDots, or organic dyes. In this way, trajectories of individual proteins diffusing in the plasma membrane of living cells can be reconstructed with nanometer accuracy and millisecond temporal resolution. Thereby substantial information on relevant biological questions such as signal transduction or synaptic regulation can be elicited [25, 135, 147].

Tracking process

In a SMT experiment, a low density of labeled molecules of interest is essential for the Airy disks do not overlap. After recording a time-lapse image sequence of the single moving particles, the latter are localized in each successive frames based on their the local fluorescence intensity maxima. Reconstruction of the molecular trajectories is achieved by connecting the positions of the localized particles (Figure 10).

For the tracking procedure to be successful and not too time consuming, relatively complex mathematical algorithms are required. A home-written software running on Igor Pro (Wave-metrics) and developed by my colleague J. Piguet was used to extract the diffusional behaviors of the molecules. A detailed description of this software can be found in reference [153].

Membrane diffusion models

As a result of thermal agitation, plasma membrane components constantly undergo random collisions which result in stochastic movements. In a two-dimensional system such as the plasma membrane, the position (r) of a molecule performing Brownian motion as a function

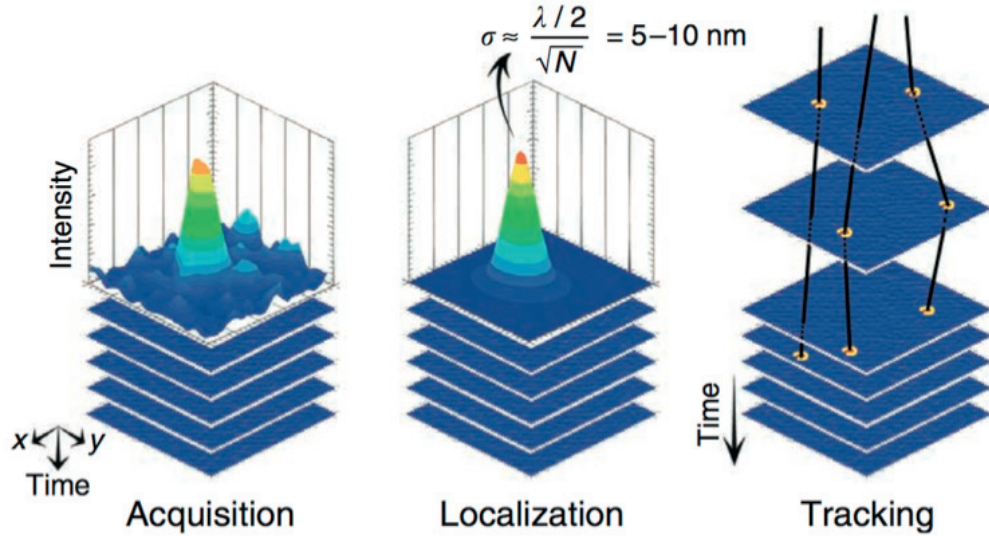


Figure 10: **Processing of SMT data.** Reconstitution of diffusing QDots trajectories is made in three distinct steps. **(i) Acquisition:** raw data collected by the detector are exported as a 2D-series of images encoding fluorescence intensity and position. **(ii) Localization:** on each frame, the center of each diffraction-limited spot which correspond to an individual QDot is located by Gaussian fitting of the fluorescence intensity profile. The localization accuracy, σ , depends according to eq. 3 strongly of the total number of detected photons, N , during the measurement. **(iii) Tracking:** Trajectories are formed by linking fluorescent spot positions in successive frames. Taken from [129].

of time (t) can be described by the following probability distribution function:

$$p(r, t)dr = \frac{1}{4\pi Dt} \cdot \exp\left(-\frac{r^2}{4Dt}\right) \cdot 2\pi r dr \quad (4)$$

where D is the diffusion coefficient (units $\mu\text{m}^2/\text{s}$).

The average position of the molecule is obviously zero, the maximum of the Gaussian profile being time independent and remaining at the origin, $\langle r \rangle = 0$. The most common and trivial way to analyze SMT data is by calculating the mean square displacement (MSD), which corresponds to the average area that a particle may cover in a given time t_{lag} . In case of two-dimensional free diffusion, the particle explore an increasingly larger area with time and the MSD increases linearly with time according to:

$$\langle r^2 \rangle = MSD = 4Dt_{\text{lag}} \quad (5)$$

General introduction

In living cells, however, the diffusion of plasma membrane molecules is rarely totally free because of transient transport, molecular crowding, transient confinement, and other barriers or obstacles that make the apparent diffusion constant time-dependent. In the general case where nothing is assumed about the nature of the constraints, the diffusion is termed anomalous and is characterized by a power law of exponent α in equation (6) [154].

$$MSD = 4D t_{lag}^{\alpha} \quad (6)$$

The exponent α can be considered as the reflection of the deviation from free Brownian diffusion ($\alpha = 1$ for Brownian motion). A negative curvature of the MSD ($\alpha < 1$) arises from obstacles or transient interactions that hinder the diffusion, whereas a positive curvature ($\alpha > 1$) results generally from active cellular transport processes.

The anisotropic nature of the cell plasma membrane makes the anomalous diffusion dependent on the time-scale. At short times, anomalous diffusion matches free diffusion, while at larger time-scales the diffusion appears slower.

In the case of confined diffusion, the MSD plot tends towards a horizontal asymptote, whose level is proportional to the confinement size. Equation (7) is a simplified function for confined diffusion in a square region of size L_c with impermeable barriers:

$$MSD_{\text{confined}} = \frac{L_c^2}{3} \cdot \left(1 - \exp\left(\frac{-12 \cdot D \cdot t_{lag}}{L_c^2}\right) \right) \quad (7)$$

Directed motion is observed for particles diffusing in a flow or undergoing active transport, for example due to the action of molecular motors [155]. It is described by a quadratic dependence of the MSD on t_{lag} :

$$MSD_{\text{directed}} = 4D t_{lag} + v^2 t_{lag}^2 \quad (8)$$

where the added term characterizes the directed motion, with v as the mean velocity of the transport.

Analysis of single-molecule trajectories

As already mentioned, the most common way to analyze a single-molecule trajectory is by plotting the mean square displacement (MSD) for each time interval (t_{lag}). The MSD for a

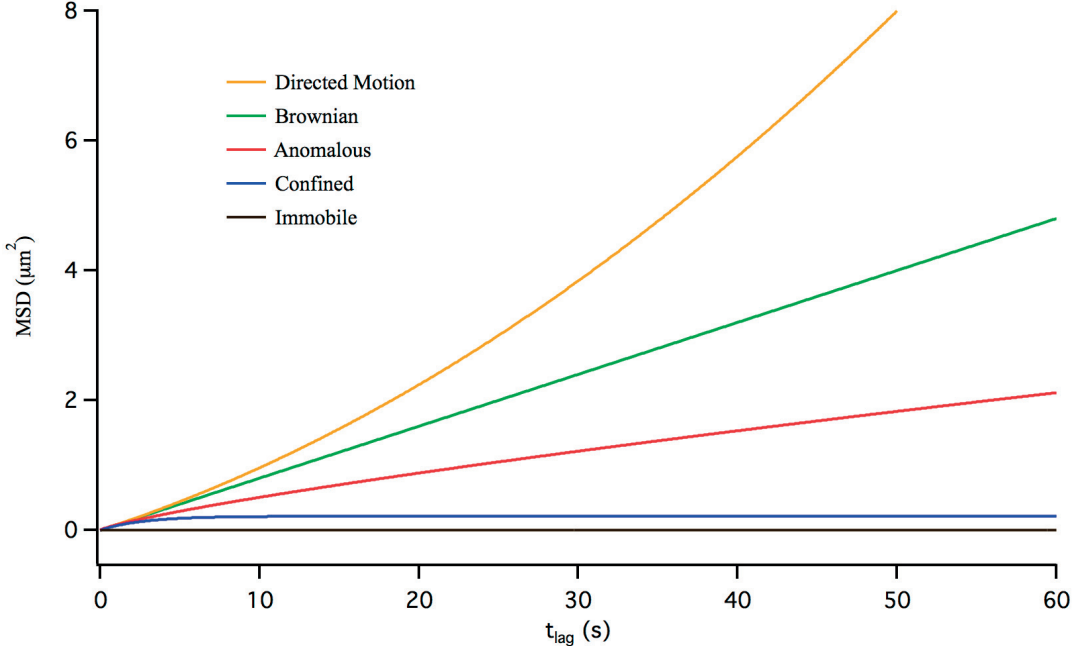


Figure 11: Plot of mean square displacement (MSD) versus time for the different modes of motion that can be observed in the cell plasma membrane. A diffusion coefficient D of $0.002 \mu\text{m}^2/\text{s}$, a confinement length L_c of 800 nm , an anomalous coefficient α of 0.8 , and a velocity v of $0.04 \mu\text{m}/\text{s}$ were used for the generation of the different MSD curves based on equations (5) to (8).

trajectory of N frames is calculated using equation (9) [137], where r is the position of the particle.

$$MSD(n t_{lag}) = \frac{1}{N-n} \sum_{i=1}^{N-n} \left[(r((i+n)t_{lag}) - r(i t_{lag}))^2 \right] \quad (9)$$

Looking at the shape of the MSD curve may give us information about the mode of motion (Figure 11) in order to classify the trajectories. However, analysis of single trajectories by using MSD vs t_{lag} is only valid for single molecules moving with constant diffusion parameters, which is almost never the case in reality.

A method frequently used for fitting SMT experimental data is to assume that the particles are free to diffuse at very short times. By fitting only the first few MSD data points, an initial diffusion coefficient (e.g. D_{1-10}), which is independent of the influence of diffusion barriers or obstacles in the plasma membrane, is obtained.

Moment scaling spectrum In spatially complex systems such the plasma membrane of living cells, the MSD often does not increase linearly in time and in this case Brownian motion will be better described by anomalous diffusion. In equation (6), the measure of the nonlinearity of the MSD with time is introduced by the parameter α [154]. Ferrari *et al.* [156] extended this measurement by introducing a non-negative integer, ν , as an extra parameter (Eq. 10). The MSD corresponds to the particular case where only the second order moment is analyzed ($\nu=2$ and $\gamma^\nu=\alpha$). A plot of γ^ν vs ν is called moment scaling spectrum (MSS) [156]. The MSS method is particularly well suited to categorize the single-molecule trajectories according to their mode of motion: the MSS slope (S_{MSS}), also called Hurst parameter, represents a value that can be directly associated with the mode of motion experienced by the molecule of interest. A S_{MSS} value of 0.5 defines a Brownian diffusion, whereas confined and directed motions are characterized by values below and above 0.5, respectively. Values equal or close to zero describes immobility.

$$\langle r^\nu \rangle \sim t^{\gamma^\nu} \quad (10)$$

The MSS method offers two major benefits over the classification with the MSD: (i) a smaller error due to the better linearity of the MSS and (ii) a clearer distinction between the different modes of motions [156, 157].

Trajectory segmentation An additional difficulty in single-molecule trajectory analysis arises when the tracked particle change its mode of motion during the acquisition process. This is particularly true for long-term measurements, with e.g. quantum dots.

The changes of diffusion mode within single trajectories can be taken into consideration using a segmentation procedure, in which the original trajectories are sequentially cut into shorter sub-trajectories. The segmentation algorithm used in the present thesis (developed by my colleague Dr. Joachim Piguet) uses a sliding window of 100-frames moving along the trajectory in steps of one frame and cutting at each step to obtain segments. In this way, a 1000-frames trajectory will results in 901 segments, the first ranging from 0 to 100, the second from 2 to 101, and so on until the last frame of the trajectory is reached. Each segmented sub-trajectories thus obtained are then analyzed as independent trajectories. This allows to drastically increase the amount of information that can be extracted from a single trajectory and in particular, to follow the temporal evolution of the diffusion and to take into account transitions between diffusion modes.

Mobility pattern To visually represent the diffusion data collected during this work, the two central mobility parameters D_{1-10} and S_{MSS} , calculated for each individual segment, were displayed as a two-dimensional probability density function (Figure 12). This novel high-

content graphical representation of single-molecule mobility was termed “mobility pattern”. It allows to visualize and analyze the complex information contained in a particular SMT experiment, by resolving highly heterogeneous receptor populations as well as following their evolution over time. This method of analysis enables to easily define and classify the diffusing molecules into different types according to their mobility regime, facilitating substantially comparison of results obtained under different experimental conditions.

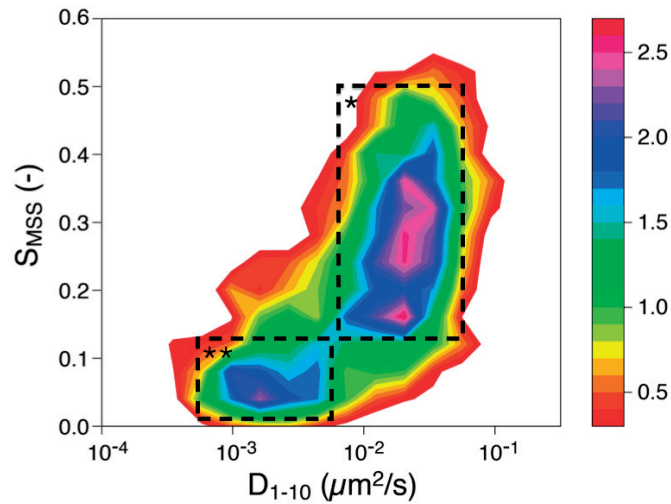


Figure 12: **Mobility pattern.** By displaying the Hurst parameter (S_{MSS}) against the diffusion coefficient (D_{1-10}) using a continuous probability density function, highly heterogeneous NK1R populations can be resolved: (*) receptors freely diffusing in the membrane, (**) receptors confined in domains. The color code scales with the indicated frequency (a.u.) of states.

1 Labeling of NK1 receptor for single-particle tracking in living cells

The general goal of this thesis is to study the dynamics of membrane receptors at the nanometer scale and on the single-molecule level in the plasma membrane of living cells. In this respect labeling of the receptor of interest with a suitable fluorescent probe is the first step towards this goal. In this first chapter focus will be on the NK1R (see *Introduction*, p.12), and more precisely on its labeling with quantum dots with a view to tracking individual receptors.

1.1 ACP labeling

Numerous methods for post-translational labeling of proteins exist [158]. Among them enzymatic labeling reactions are especially attractive because they can afford covalent labeling with high specificity. In this work a method based on the acyl carrier protein (ACP) and described by George *et al.* [159] has been extensively used. The method consists of the enzymatic modification of the ACP by phosphopantetheine transferase (PPTase), leading to the transfer of 4'-phosphopantetheine from co-enzyme A (CoA) to a serine residue of ACP, which is genetically fused to the protein of interest [159]. A large variety of chemical compounds such as fluorophores, affinity ligands but also quantum dots can be attached to CoA and subsequently covalently transferred to fusion proteins on cell surfaces [160] [161].

The ACP labeling method offers numerous advantages, including [159, 161]:

- High specificity of the reaction.
- Only the proteins correctly incorporated into the plasma membrane are labeled (this prevents background fluorescence arising from non-correctly folded receptors inside the cell).
- Straightforward control of the labeling density (critical for single-molecule experiments).
- Small and covalent attachment linker.

Chapter 1. Labeling of NK1 receptor for single-particle tracking in living cells

Furthermore it has been shown that the ACP-NK1R fusion protein was activated by binding its natural agonist, substance P (SP), at a similar effective concentration (EC_{50}) as the wild type receptor [162]

1.2 Labeling of NK1 receptor with quantum dots

As discussed in the introduction, the labeling of the protein of interest is one of the most critical step in determining the success and quality of a single particle tracking (SPT) experiment. Interaction of QDots with biological samples on a glass surface often implies nonspecific binding, which can ruin the experiment. Although there is no universal solution to this problem, several measures such as PEGylation of the QDot surface as well as correct choice of buffer conditions have proven to be effective to reduce nonspecific interactions [129]; addition of 1-2% of bovin serum albumin (BSA) to the labeling medium may greatly improve the labeling specificity [137] but also significantly enhance stability and photoluminescence quantum yield of QDots [163].

Another difficulty in single-molecule labeling is to obtain an appropriate density of specifically labeled molecules under relevant experimental conditions. SPT experiments need a very low concentration of labeled molecules (i.e. a few molecules per cell) to allow resolution of single peaks and to minimize crossing trajectories, which make the subsequent analysis more complex and time-consuming. Optimal labeling conditions have to be found by adjusting concentration, incubation time, temperature or media composition [129]. Other important parameters to consider are the QDot conjugate affinity and the expression level of the target. Therefore, finding a proper labeling procedure can be laborious.

While labeling methods are well-established for standard organic dyes, it is quite different for QDots. In order to find the best way to attach a QDot to the NK1R, three different strategies (illustrated in figure 1.1), have been explored.

1.2.1 Experimental procedures

All the preliminary experiments described below were accomplished in Shimon Weiss' Laboratory at UCLA with the help of Dr. Xavier Michalet and Dr. Jianmin Xu. CoA-biotin and PPTase were obtained from Dr. Ruud Hovius (LCPPM, EPFL).

Cell culture

Labeling experiments were performed on adherent human embryonic kidney (HEK) 293 cells stably expressing ACP-NK1R fusion protein. This stable cell line was established by Dr. Bruno Meyer [164]. Wild type HEK293 cells were used as negative control (NK1R not endogenously expressed). Cells were cultured in Dulbecco's modified Eagle's medium (DMEM)/F12 with GlutaMAX-I (Invitrogen) supplemented with 10% newborn calf serum (NBCS) (Sigma-Aldrich)

1.2. Labeling of NK1 receptor with quantum dots

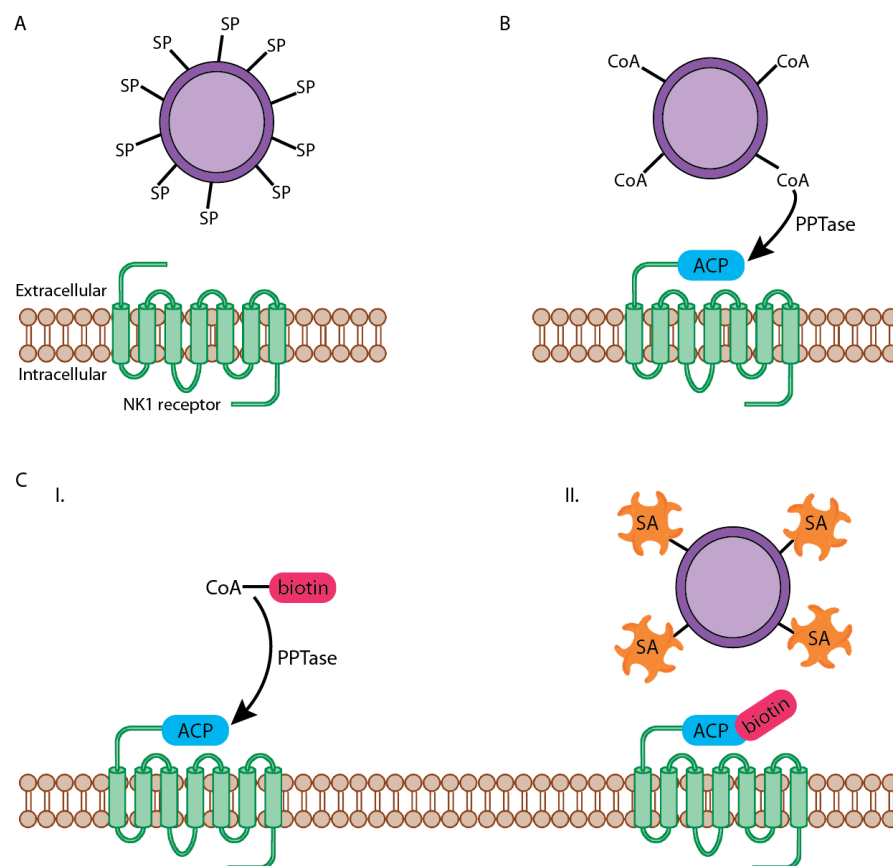


Figure 1.1: **Strategies for NK1R labeling with QDots.** (A) SP-conjugated QDots were applied on cells stably expressing NK1R. (B) CoA-functionalized QDot was transferred to the ACP tag fused to the N terminus of the receptor. The reaction is catalyzed by phosphopantetheine transferase (PPTase). (C) In a first step (i) biotinylated CoA was transferred to the ACP tag. In a second step (ii) SA-coated QDot was bound to the receptor's biotin.

at 37°C in a humidified 5% CO₂ atmosphere. ACP-NK1R expressing cells were maintained in presence of 200 µg/ml hygromycin B (Calbiochem). Cell cultures were split at regular time intervals and plated in antibiotic-free complete medium in LabTek 8-well chambered coverglass (Nunc) at a density of ~250'000 cells/ml. Labeling and single-molecule imaging experiments were performed in phosphate buffered saline (PBS) buffer (pH 7.4) supplemented with 1% (wt/vol) BSA (Sigma) 24 to 48h after plating.

SP-conjugated QDots

Commercial QDots (QDot 625 antibody conjugation kit from Invitrogen) were conjugated to SP via BS³ (bissulfosuccinimidyl suberate) as crosslinker. This homobifunctional crosslinker has two identical reactive groups (NHS ester) at each end which react with primary amines to form an amide bond. SP-conjugated QDots were prepared by a two-step reaction (Figure 1.2): (i) BS³ linker was attached to the QDot via an amine group present at the surface of

Chapter 1. Labeling of NK1 receptor for single-particle tracking in living cells

the QDot; (ii) The other end of the BS³ linker was reacted with one of the primary amine of SP. The reaction was quenched using hydroxylamine. This results in QDots comprising several SP molecules. However we can assume that there is only one QDot per SP molecule; the two reactable primary amines of SP are too close to each other (see insert Figure 6, p.14) for accommodating two QDots. Cells were incubated in PBS-BSA with SP-QDots at room temperature. Different concentrations of SP-QDots and incubation times have been tested.

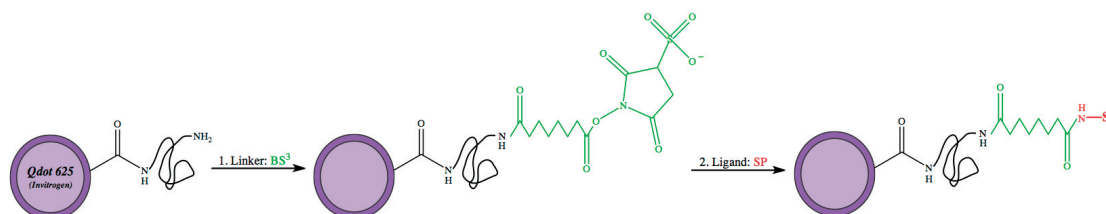


Figure 1.2: **Functionalization of QDots with SP** using bis[sulfosuccinimidyl] suberate (BS³), a crosslinker containing an amine-reactive NHS-ester at each end that can react with the primary amines present on the QDots and SP molecules.

ACP labeling with CoA-QDots

Preparation of QDot-CoA is shown in Figure 1.3. Briefly, the amines on the surface of the QDot were functionalized with a bifunctional linker (sulfo-SMCC). Then CoA was directly linked to the QDot via a maleimide-thiol reaction. Unreacted maleimide groups were capped with β -mercaptoethanol. Two different CoA:QDot ratios (3:1 and 30:1) have been tested. Labeling was performed by incubating the cells in PBS-BSA with 10 mM MgCl₂, 1 μ M PPTase and 0.2 nM CoA-QDots for 20 minutes at 37°C.

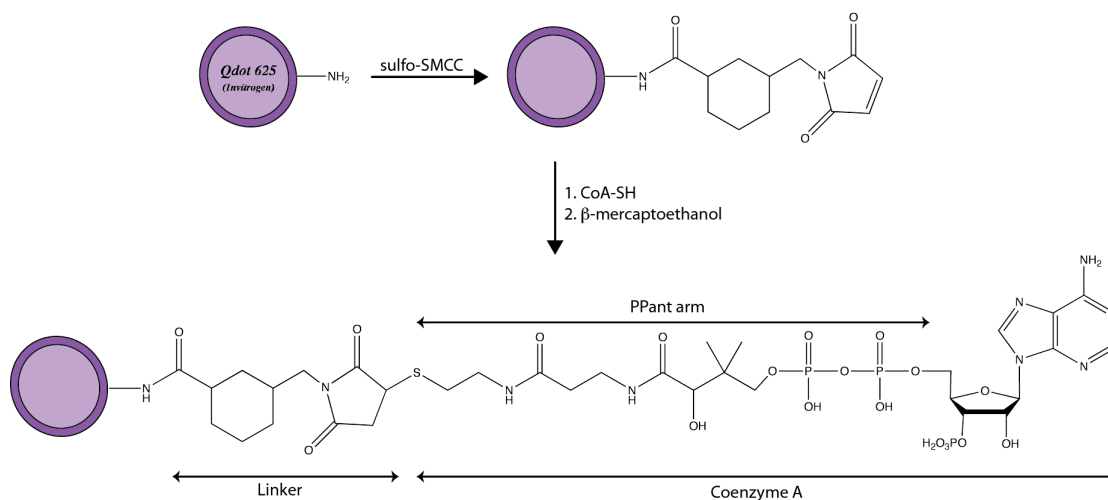


Figure 1.3: **Synthesis of CoA-conjugated QDots.** After functionalization of amines on the QDot surface with a bifunctional linker (sulfosuccinimidyl-4-(N-maleimidomethyl)cyclohexane-1-carboxylate), CoA is directly linked to the QDot via a maleimide-thiol reaction. Unreacted maleimide groups are capped with β -mercaptoethanol.

ACP labeling with CoA-biotin and streptavidin-coated QDots

The last labeling strategy which was tested was a two-step post-translational labeling procedure based on the strong interaction between biotin and streptavidin [165]. In the first step, the transfer of the phosphopantetheine moiety of a biotinylated CoA (CoA-biotin, 5 μ M) to the ACP tag fused to NK1R was catalyzed by PPTase (20 min, 37°C). The cells were washed three times with PBS-BSA. In a second step QDot 625 streptavidin conjugate (SA-QDot) (Invitrogen) was bound to the receptor's biotin (5 min, RT). Different concentrations of SA-QDot (picomolar to nanomolar) have been tested.

Single-particle imaging and tracking

A custom-built TIRF microscope based on a Zeiss Axiovert 100 inverted microscope equipped with a front-illuminated EMCCD was used to perform single-molecule imaging of QDot-labeled NK1Rs. A detailed description of the setup can be found in [166]. The ventral plasma membrane of the cells was imaged at room temperature (\sim 27°C). Diffusion trajectories (30 s) of individual receptors were recorded at a rate of 33 Hz. For measurements on activated receptors, SP was added to the sample at a final concentration of 100 nM. Single-molecule QDot-NK1R trajectories were extracted using a homemade software (named "AsteriX") developed in Labview by Dr. Xavier Michalet (UCLA).

1.2.2 Results and discussion

In order to evaluate the specificity of the different strategies for NK1R labeling (Figure 1.1), HEK293 cells not expressing the receptor were used as negative control.

For SP-QDots (Figure 1.1A) no significant differences were observed between NK1R-expressing cells and the control. In both cases, many visually immobile QDots were present. This labeling strategy would have been potentially less interesting than the two others because it would have allowed to track only activated receptors.

For CoA-QDots (Figure 1.1B), non-specific labeling was also extremely high. Yet the suitability of this technique have been successfully demonstrated on different ACP fusions of receptor proteins in living cells [161]. However in our case, despite numerous trials with different CoA:QDot ratios, the specificity of the reaction has proved to be insufficient for reliable tracking of single receptors. The reasons of this failure remain unclear. This labeling method would have been particularly attractive due to the small size of the QDot-receptor linker and to the possibility to study the dynamic of receptors before and after activation.

The use of SA-QDots (Figure 1.1 C) requires first to attach a biotin molecule to the protein of interest. Here ACP labeling with CoA-biotin was used. Subsequently different concentrations of SA-QDots have been tested. At nanomolar concentration, the receptor-bound fraction is too high for SPT (Figure 1.4 A). Picomolar concentration of SA-QDot resulted in the presence

Chapter 1. Labeling of NK1 receptor for single-particle tracking in living cells

of about ten visible QDots on a single-cell surface, allowing the tracking of individual receptors (Figure 1.4 B). As a control, cells stably expressing ACP-NK1R but not labeled with CoA-biotin were incubated with SA-QDots. At nanomolar concentration only very few immobile QDots were observed (Figure 1.4 C), whereas no QDot was present at the cell surface when using picomolar concentration (Figure 1.4 D). Similar results were obtained with HEK293 cells devoid of expressed ACP-NK1R but treated with CoA-Biotin and PPTase and incubated with SA-QDots. The ideal labeling concentration of SA-QDots for the tracking of individual NK1R is picomolar concentration range; under these conditions, unspecific labeling is negligible.

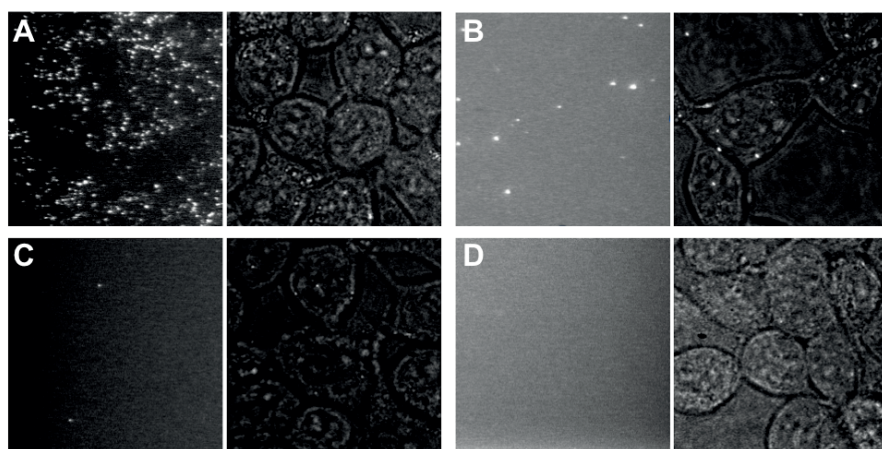


Figure 1.4: **Post-translational labeling of NK1R with QDots in living HEK293 cells.** Each panel shows TIRF microscope images on the left, and the corresponding transmission images (wide-field) on the right. **(A)** Cells stably expressing ACP-NK1R labeled with CoA-biotin and incubated with ~ 0.5 nM streptavidin-coated QDot (SA-QDot). **(B)** Cells stably expressing ACP-NK1R, labeled with CoA-biotin and incubated with ~ 5 pM SA-QDot. **(C)** Cells stably expressing ACP-NK1R, not labeled with biotin (control experiment) and incubated with ~ 0.5 nM SA-QDot. **(D)** Cells stably expressing ACP-NK1R, not labeled with biotin (control experiment) and incubated with ~ 5 pM SA-QDot.

This method offers the possibility to investigate the influence of agonist binding on receptor's mobility. A quick visual comparison of the traces recorded before and after agonist-induced receptor activation, of which an arbitrary but nonetheless representative selection is shown in figure 1.5, clearly indicates an increased confinement of activated NK1Rs.

Fitcher *et al.* showed that QDots are suitable probes for monitoring and quantifying GPCR endocytosis at the single-receptor level in live cells [167]. The fact that QDots do not impact to the internalization process has been confirmed for the NK1R as shown in figure 1.6.

The major drawback of SA-QDots is that they could potentially induce receptor cross-linking (i.e. one QDot binds to several receptors). This issue is discussed in chapter 3 (p. 63).

1.2. Labeling of NK1 receptor with quantum dots



Figure 1.5: Representative trajectories for single QDot-labeled ACP-NK1Rs in the plasma membrane of living HEK293 cells, in the absence (top line) and presence (bottom line) of the agonist SP.

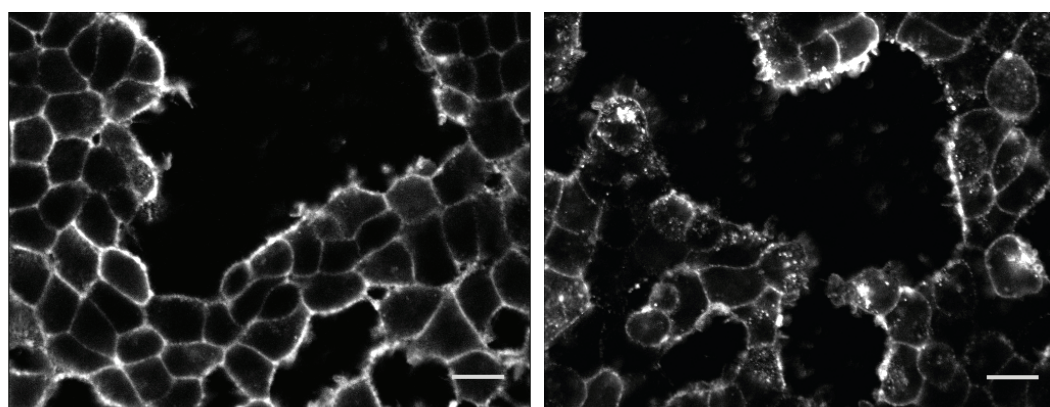


Figure 1.6: Confocal fluorescence micrographs showing HEK293 cells stably expressing ACP-NK1R labeled with CoA-biotin and incubated with 1 nM of SA-QDot 655 before (left) or after addition of 100 nM SP (right). Scale bars: 20 μm .

1.2.3 Conclusion

Among the different strategies that have been assessed for NK1R labeling with QDots, the two-step labeling procedure based on the biotin-streptavidin couple has proved to be the best by far in term of labeling specificity. The high specificity and efficiency of the ACP labeling reaction, combined with the very strong biotin-streptavidin interaction and the high photostability and brightness of QDot probes allow to precisely control the amount of labeled receptors and to record long single-molecule trajectories with very high accuracy. This provides a good starting point for a more quantitative analysis of the immobilization effect observed upon stimulation of the NK1R with SP and for the identification of the interactions that cause the latter (chapter 2).

2 Single-molecule microscopy deciphers the relation between mobility and signaling of the NK1 receptor in living cells

2.1 Abstract

Lateral diffusion enables efficient interactions between membrane proteins, leading to signal transmission across the plasma membrane. An open question is how the spatio-temporal distribution of cell surface receptors influences the transmembrane signaling network. Here we addressed this issue by studying the mobility of a prototypical G protein-coupled receptor, the neurokinin-1 receptor, during its different phases of cellular signaling. Attaching a single quantum dot to individual neurokinin-1 receptors enabled us to follow with high spatial and temporal resolution over long time regimes the fate of individual receptors at the plasma membrane. Single receptor trajectories revealed a very heterogeneous mobility distribution pattern with diffusion constants ranging from 0.0005 to 0.1 $\mu\text{m}^2/\text{s}$ comprising receptors freely diffusing and others confined in 100–600 nm sized membrane domains, as well as immobile receptors. A two-dimensional representation of mobility and confinement resolved two major, broadly distributed receptor populations, one showing high mobility and low lateral restriction, the other low mobility and high restriction. We found that about 40% of the receptors in the basal state are already confined in membrane domains and are associated with clathrin. After stimulation with an agonist, an additional 30% of receptors became further confined. Using inhibitors of clathrin-mediated endocytosis, we found that the fraction of confined receptors at the basal state depends on the quantity of membrane-associated clathrin and is correlated to a significant decrease of the canonical pathway activity of the receptors. This shows that the high plasticity of receptor mobility is of central importance for receptor homeostasis and fine regulation of receptor activity.

2.2 Introduction

Membrane receptors are of utmost importance for cellular signaling, transferring the information of extracellular stimuli into intracellular responses. In this context, their lateral distribution and mobility in the plasma membrane play a critical role as random or directed movements in the membrane plane bring signaling partners efficiently into transient or stable contact [6, 8, 168, 169]. A fundamental issue of modern quantitative cell biology is to understand how the complex, highly dynamic spatial distribution of components of the plasma membrane influences central cellular signaling processes [170, 171, 20]. Single-molecule optical imaging, more specifically single-particle tracking (SPT), is ideally suited to establish a tomogram of the distribution of individual plasma membrane components over time and space, revealing the full complexity of individual signaling reactions that would be hidden in ensemble measurements [172].

Here we concentrate on seven-transmembrane domain (7TM) receptors, also known as G protein-coupled receptors (GPCRs). GPCRs establish the largest family of cell-surface receptors converting extracellular signals into intracellular responses. As they are involved in many central physiological processes they are also among the most important targets for drug development [46, 173, 174, 175]. After activation by extracellular stimuli, GPCRs are typically desensitized, internalized and recycled. These processes occur from seconds (phosphorylation) over minutes (endocytosis) to hours (down-regulation) [61]. In this context the clathrin-mediated endocytosis (CME) machinery is essential for maintaining proper function of GPCRs on the cell surface [176]. All this yields an amazing diverse network of intracellular signaling reactions and in turn a complex receptor pharmacology.

Here we used the human neurokinin-1 receptor (NK1R) as a prototypical GPCR to investigate its lateral distribution in living cells at different states before and after activation. The NK1R is activated by tachykinin neuropeptides and belongs structurally to the rhodopsin-like GPCR family [72]. It mediates a wide variety of neuronal and metabolic processes, and is an important drug target for treating diseases such as depression or cancer [80].

The NK1R mediates classical membrane signaling reactions, summarized in Figure 2.1: After binding its natural agonist, the undecapeptide substance P (SP), the NK1R activates its G protein $G_{\alpha q}$, which in turn activates phospholipase C, leading to Ca^{2+} release from the endoplasmic reticulum [77, 78]. Thereafter, the NK1R is phosphorylated and binds β -arrestin to target the receptor to clathrin-coated pits (CCPs) and activating the CME machinery [177, 178, 179, 180, 181]. Endocytosis of the β -arrestin-NK1R complex occurs within the first minute of agonist exposition [72, 182]. Internalization of the NK1 receptor is finalized about 10 minutes later [73, 183, 184]. NK1R trafficking is influenced by SP; high SP concentration induces receptor internalization to perinuclear sorting endosomes, whereas low SP concentration induces receptor translocation to early endosomes followed by rapid recycling coinciding with the recovery of SP binding sites at the cell surface [80, 185]. Furthermore, a NK1R subpopulation can be desensitized and resensitized without leaving the vicinity of the

plasma membrane [186].

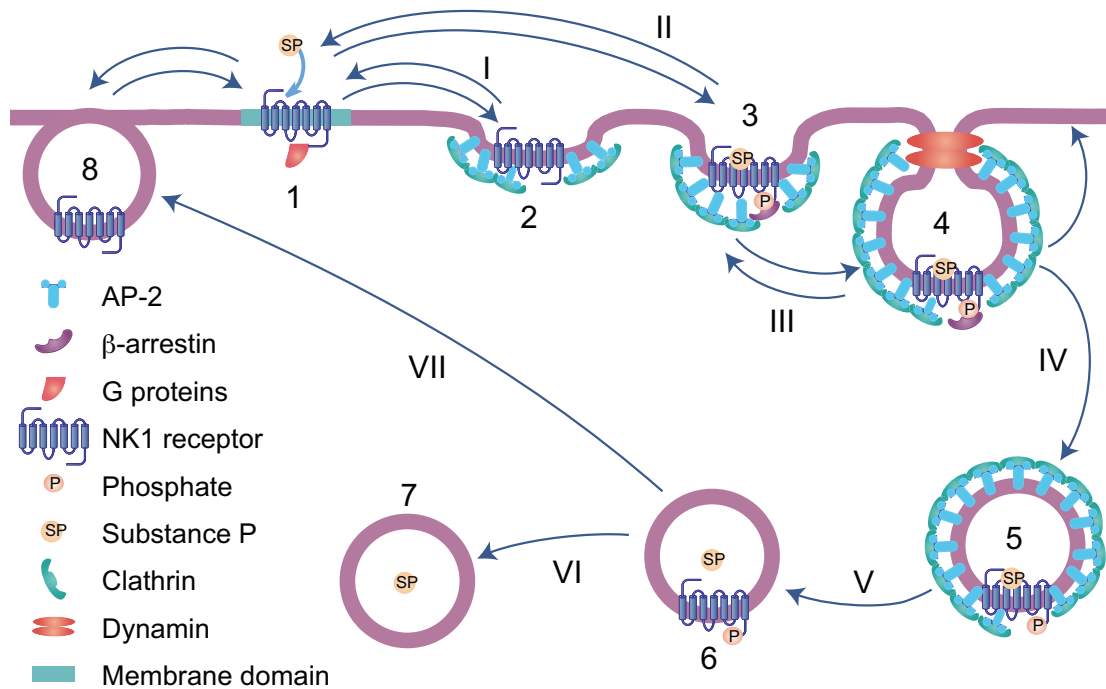


Figure 2.1: **Internalization and recycling of NK1R at the cell plasma membrane.** The NK1R can be located in different regions of the plasma membrane and in intracellular endosomes: 1. Nanometer-sized membrane domains. 2. Clathrin-related region 3. Clathrin pre-pits. 4. Clathrin-coated pits closed by dynamin. 5. Clathrin-coated vesicles. 6. Early, late, or perinuclear endosomes. 7. Lysosomes. 8. Recycling vesicles. NK1R can be recruited in the different regions described above: I. Receptor exchanges between clathrin-related region and free membrane. II. After agonist binding, receptor is phosphorylated leading to the recruitment of β -arrestin. The receptor is targeted to clathrin pre-pits. III. Receptor-clathrin complex is bound to dynamin dependent invaginating regions. IV. Receptor is internalized in clathrin-coated vesicles, which are then transformed to early endosomes. V. SP is removed from NK1R in late endosomes, where either, in step VI, SP and a fraction of the receptors is degraded in lysosomes or, in step VII, a fraction of the receptors is recycled to the cell membrane.

In living 293T cells, individual NK1Rs show highly heterogeneous diffusion properties [187]. In general, the median diffusion coefficient of a NK1R population rapidly decreases after stimulation with SP [188]. Immobile or confined receptors are already present in the basal state, i.e. in absence of activating ligands, suggesting that SP influences the equilibrium between different receptor states [187], which in turn would modulate the interaction between particular signaling proteins concentrated in membrane nano- or micro-domains [162].

The spatial organization and the mobility of GPCRs in the cell membrane are of utmost importance to ensure correct signal transduction, fast desensitization and endocytosis of the receptor. Here, we addressed these issues by attaching a single quantum dot (QDot)

Chapter 2. Mobility of individual NK1 receptors

to individual NK1Rs, which enabled us to follow with high spatial and temporal resolution over long time regimes the fate of individual receptors at the cell's plasma membrane. By characterizing simultaneously the mobility and confinement of each individual receptor it was possible to detect and distinguish different, highly dynamic receptor populations in the plasma membrane and correlate them with distinct steps of the GPCR mediated transmembrane signaling cascade.

2.3 Experimental procedures

2.3.1 Cell culture

Adherent 293T cells, stably expressing the NK1R genetically fused with an acyl-carrier protein at the extracellular N-terminus (ACP-NK1R) [162], were grown at 37°C in DMEM/F12 (Life Technologies) supplemented with 10% v/v newborn calf serum (NBCS) (Sigma-Aldrich) and 200 $\mu\text{g}/\text{ml}$ hygromycin B (Sigma-Aldrich) in a humidified atmosphere with 5% CO_2 . Cells were seeded 24-48h before microscopy experiments in 8-well plates (Lab-Tek Nunc, Naperville, IL) in growth medium without antibiotics. Single receptors were imaged in colorless DMEM supplemented with 15 mM HEPES (Life Technologies) without antibiotics or serum.

2.3.2 Addition of chemicals to cells

NK1Rs were activated adding freshly prepared SP to the extracellular medium (Tocris, Bristol, UK). Nocodazole (AppliChem, Darmstadt, Germany) was used at 1 μM and cytochalasin B (Sigma-Aldrich) at 20 μM . Dyngo-4a and PitStop 2 (Abcam, Cambridge, UK) were applied at 30 μM and Dynasore (Sigma-Aldrich) at 80 μM . Methyl- β -cyclodextrin ($\text{m}\beta\text{CD}$, Sigma-Aldrich) was used at 10 mM, and Y-27632 (Tocris) at 10 μM . All chemicals, except SP were added to the extracellular medium 20–30 minutes before SPT measurements.

2.3.3 siRNA knockdown of clathrin

Clathrin depletion was achieved using ON-TARGETplus SMARTpool siRNAs (Dharmacon/GE Healthcare, Amersham, UK) against the human clathrin heavy chain 1 (CLTC) with the following target sequences: (i) 5'-GAG AAU GGC UGU ACG UAA U-3', (ii) 5'-UGA GAA AUG UAA UGC GAA U-3', (iii) 5'-GCA GAA GAA UCA ACG UUA U-3', and (iv) 5'-CGU AAG AAG GCU CGA GAG U-3'. Transfection of siRNAs (15 pmol/well) was performed with lipofectamine 2000 (Invitrogen, Carlsbad, USA) according to the manufacturer's instruction. SPT measurements were performed 60 h after transfection.

2.3.4 Receptor function assay

The NK1R mediated activation of the $G_{\alpha q}$ pathway was assayed measuring the intracellular Ca^{2+} response after SP addition. 293T cells stably expressing ACP-NK1R were seeded into a 96-well plate (Perkin-Elmer, Waltham, MA) and grown in DMEM/F12 10% NBCS for 24h. Cells were loaded with Fluo4-NW (Life Technologies) in Hanks' balanced salt solution-HEPES according to manufacturer instructions. After 30 min at 37°C, cells were placed in a FLEX Station (Molecular Devices, Sunnyvale, CA). A first operation cycle was used to add buffer, nocodazole, cytochalasin B, Dyngo-4a, PitStop 2, or m β CD at appropriate concentrations. In a second operation cycle, SP was added at concentrations ranging from 10^{-12} to 10^{-7} M to obtain a dose-dependent response curve, from which maximum responses were extracted.

2.3.5 Receptor labeling

293T cells stably expressing ACP-NK1R were washed once with DMEM/F-12 medium 10% NBCS supplemented with 1% w/v bovine serum albumin (BSA). Labeling was performed by incubating the cells for 15 min at 37°C in DMEM/F-12 10% NBCS containing 1% BSA, 10 mM $MgCl_2$, 1 μ M PPTase (4'-phosphopantetheinyl transferase), and 5 μ M CoA-biotin. After incubation and prior to the second step of labeling, cells were washed three times with DMEM/F-12 10% NBCS supplemented with 1% BSA. Cells were then incubated for 5 min at room temperature with 10 pM streptavidin-coated CdSe-ZnS core-shell QDots 655 (Invitrogen, Life Technologies) in Dubelcco's PBS containing Ca^{2+} and Mg^{2+} and supplemented with 1% BSA. Prior to SPT measurements, cells were rinsed three times in colorless DMEM complemented with 1% BSA to remove unbound QDots. To account for cell variability and avoid NK1R unrelated effects, experiments on inactive NK1R state without addition of chemicals have been performed systematically before each new experiment.

2.3.6 Microscopy

For single-molecule microscopy, cells were mounted on a modified epi-fluorescence wide-field microscope (Axiovert 200, Zeiss, Feldbach, Switzerland). To observe QDots 655, light of a 488 nm Obis diode laser (Coherent Inc., Santa Clara, CA) was directed by a dichroic mirror (Q645LP, Chroma Corp, McHenry, IL) into the microscope objective (C-Apochromat 63X/1.2 numerical aperture water corrected, Zeiss) to illuminate a 15- μ m diameter region of the sample. Fluorescence was collected by the same objective, passed through a filter (HQ710/100, Chroma) and a 1.6x Zeiss Optovar, and imaged on an electron-multiplying charge-coupled device camera (Ixon 887BV, Andor Technology, Belfast, UK). Single-molecule trajectories were recorded at a frequency of 30 Hz with excitation intensities around 0.1 kilowatt/cm² for 33 s. For confocal scanning microscopy, cells were mounted on Zeiss LSM 510 microscope (Zeiss). QDots were excited with the 488 nm line of an Argon ion laser. Fluorescence signal was acquired with a 63X, 1.2 numerical aperture water immersion objective (Zeiss), filtered through an HFT 488/561 dichroic mirror and a 650 nm long pass filter (both Zeiss), and detected with

an avalanche photodiode (Perkin-Elmer).

2.3.7 Single-molecule tracking

Image sequences were treated using a home-written software in Igor Pro (Wavemetrics, Lake Oswego, OR). Each image of a single-molecule time series was restored using a noise filter to remove: (i) Long-range structures from inhomogeneous laser profile, detector fluctuation and autofluorescence regions. (ii) Short-range discretization noise and charge-coupled device spikes [189]. Local maxima were determined on the filtered image. Each local maximum was then fitted using a 2-dimensional Gaussian fit. Size, shape and fluorescence intensity time profile of a fitted fluorescent peak was verified to match single-molecule features. Selected fluorescence peaks were then linked over an image series to obtain trajectories. To avoid bias in subsequent steps of analysis only cells with more than 90% of approved visible labels were considered.

2.3.8 Analysis of individual trajectories

Diffusion coefficient, length of confinement region, moment scaling spectrum and velocity were calculated from individual trajectories as described elsewhere [190]. To extract a maximal amount of information, long trajectories were segmented using a sliding window of 100 frames. Each of the segmented trajectories was treated as an individual and analyzed to obtain five mobility related features:

1. Initial diffusion coefficient D_{1-10} [187, 121]. This initial diffusion is computed by fitting the first 10 time intervals of a standard mean square displacement (MSD) versus time lag (t_{lag}) curve. It corresponds to a maximal time interval of 200 ms, during which the diffusion is less affected by long-range features.
2. Hurst parameter, S_{MSS} [157].
3. Length, L , which is the diagonal of the smallest rectangle containing 95% of the point position.
4. Asymmetry [191].
5. Efficiency [192].

These features were then used to construct a vector, which described with high specificity the mobility state of the particular trajectory segment.

2.3.9 Population analysis

D_{1-10} and S_{MSS} values characterize the mobility properties of individual receptors and, by extension, those of a receptor population. These two values were obtained with two independent

calculations from the same dataset. Median values of D_{1-10} and S_{MSS} were calculated for each experimental condition. Boxplots were then computed to obtain population extent and 95% confidence interval (notches) using R (R Foundation for Statistical Computing). D_{1-10} and S_{MSS} values were used to compare different experiments. Two-dimensional probability functions of D_{1-10} and S_{MSS} were determined using the values obtained with the segment feature analysis. 2D mobility patterns were obtained using the *kde2d* function of R on D_{1-10} and S_{MSS} . This two-dimensional kernel density estimator was then used to establish a mobility pattern for each condition. Bandwidths of 0.11 on the x-axis, corresponding to $\log_{10}(D_{1-10})$ and 0.03 on the y-axis, corresponding to S_{MSS} were used, unless otherwise stated.

2.3.10 Classification of individual trajectories

Trajectories were classified according to two methodologies: (i) Ensemble analysis, calculating the proportion of trajectories exhibiting defined characteristics from the complete two-dimensional probability function described above. (ii) A priori, or single-trace, classification assigning a single trace to a category depending on the values of the mobility parameters described above. For a priori classification, a linear support vector machine (SVM) has been used. Three homogenous sets of real trajectories (shown on Figures 2.2C, 2.2E, and 2.2G) served as training set. The SVM was based on a 4-dimensional vector comprising D_{1-10} , S_{MSS} , asymmetry and efficiency. The training set was composed of 6969 type I, 5500 type II, and 7524 type III segments of trajectories. The same classification machine was used to construct a time dependent distribution. A sliding time window of 160 s was used to extract the evolution of the mobility parameters in time. The classification was performed for each time frame using the same support-vector machine as above.

2.3.11 Dimension of confined regions

The dimension of a confined region (L) in the case of restricted receptor diffusion is not a straightforward value to obtain. It is generally estimated by fitting a MSD vs t_{lag} curve of either a single trajectory or an ensemble of trajectories using a complete [29] or a simplified [7] function of t_{lag} . Here we chose a simplified definition of the confinement length, as the diagonal of the smallest rectangle enclosing 95% of the trajectory. This definition has been retained to avoid artifacts due to noise and interdependence of L and D .

2.4 Results

2.4.1 Heterogeneous mobility of the NK1R in the plasma membrane of 293T cells

To track a particular receptor equipped with one QDot, we used a 293T cell line stably expressing ACP-NK1R [187, 162]. The ACP-NK1R was labeled by the following sandwich method. We first covalently linked CoA-biotin to the ACP tag of the receptor and then bound to the biotin a

Chapter 2. Mobility of individual NK1 receptors

streptavidin-coated QDot [159]. Labeling with QDots did not prevent receptor endocytosis. The highly specific labeling of a few NK1Rs at the plasma membrane of a living cell, allowed us to follow trajectories of individual NK1Rs over time periods between 30 seconds and 2 minutes at 33 ms temporal resolution (see [supplemental Movie S1](#))¹.

Trajectories of single receptors diffusing on the dorsal cell membrane were obtained from time-lapse series of 1000 fluorescence images recorded at 30 frames per second using a wide-field epi-fluorescence microscope. NK1R showed five distinguishable mobility regimes in the plasma membrane; (i) free Brownian diffusion, (ii) slow diffusion in confined regions, (iii) fast diffusion in confined domains, (iv) directed motion, and (v) immobile receptors (Figure 2.2A).

Here, we determined the short-term diffusion coefficient, D_{1-10} , and the Hurst parameter, S_{MSS} [157]. D_{1-10} is related to the physical properties of the surrounding membrane and the interaction of the receptor with its close environment [188, 162, 29]. S_{MSS} describes the overall mode of motion; values below 0.5 are typical for confined diffusion, values equal or close to zero represent immobile molecules, Brownian movements are characterized by S_{MSS} values around 0.5, whereas directed movements show S_{MSS} values above 0.5 [157].

In order to augment the information content extracted from each single-molecule trace, a window of 100 frames was moved along the trajectory, and each resulting segment was analyzed as an independent trajectory. The two central parameters D_{1-10} and S_{MSS} were calculated from each segment and displayed as a two-dimensional probability density function, named “mobility pattern”. This novel representation method allowed for resolving highly heterogeneous receptor populations as well as for following their evolution over time.

Receptors in the basal state (Figures 2.2A-B) displayed distinct diffusion modes. Freely diffusing receptors had characteristic diffusion coefficients D_{1-10} between 0.016 and 0.05 $\mu\text{m}^2/\text{s}$ and S_{MSS} values > 0.3 . Importantly, receptors with S_{MSS} values between 0.3 and 0.5 diffuse in the plasma membrane without boundaries even if they display anomalous behavior. Receptors with confined diffusion showed diffusion coefficients D_{1-10} ranging from 0.002 to 0.02 $\mu\text{m}^2/\text{s}$ and S_{MSS} values spread between 0.1 and 0.3. Typically confined diffusion was restricted to domains of 120–550 nm size and in a few cases to 70–800 nm domains. Receptors were assigned as immobile when their D_{1-10} values were lower than 0.002 $\mu\text{m}^2/\text{s}$ and their S_{MSS} values lower than 0.1. Fast-confined receptors had diffusion coefficients larger than 0.02 $\mu\text{m}^2/\text{s}$ and $S_{MSS} < 0.15$. Less than 2% of NK1Rs exhibited directed motion, and these comprised two distinct cases: receptors transported in the membrane plane outside of domains or receptors diffusing freely in moving nanodomains.

To simplify the analysis, receptors were classified into three categories: type I comprised the freely diffusing and directed receptors, type II the confined and immobile receptors, and type III the fast-confined receptors as described above. Representative traces of each type and their corresponding mobility pattern are shown on Figures 2.2C-H. The interchange rate between

¹<http://www.jbc.org/content/290/46/27723/suppl/DC1>

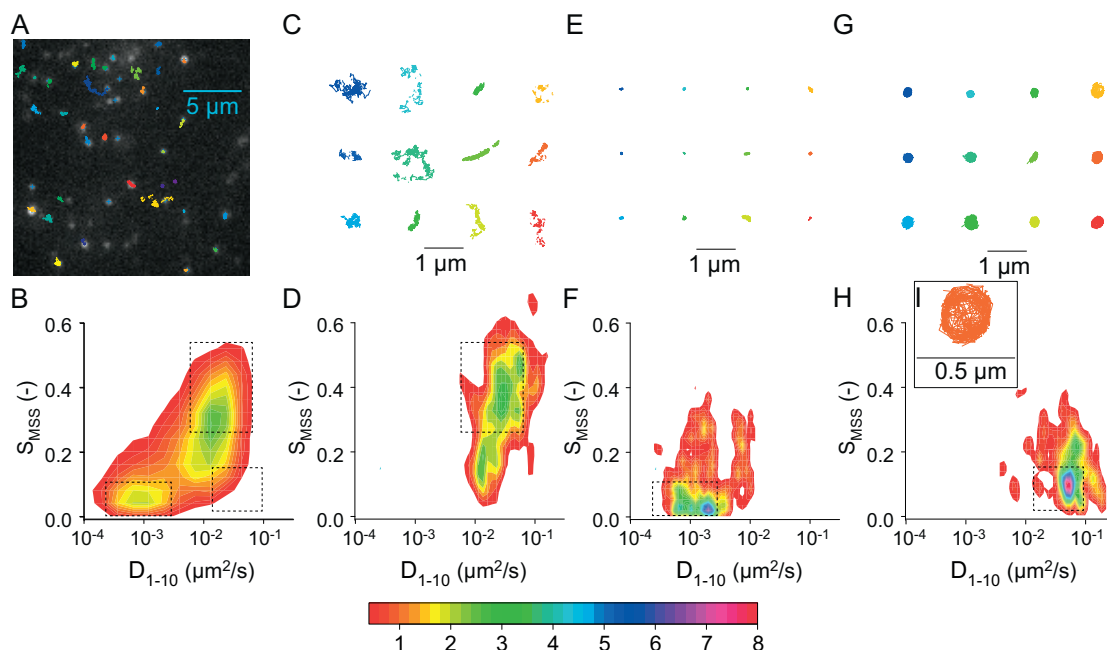


Figure 2.2: **Heterogeneous diffusion of NK1R in the plasma membrane of 293T cells.** Diffusion trajectories of individual NK1Rs labeled with QDots 655 are measured by SPT in the plasma membranes of the cells. The mobility patterns of the receptor are presented as two-dimensional probability density functions calculated from measured trajectories, a selection of which are shown in C, E, and G. S_{MSS} of the trajectory segments are plotted versus D_{1-10} . D_{1-10} and S_{MSS} describe the diffusion coefficient and the type of motion of the receptor, respectively. (A) Single-receptor trajectories from a single cell obtained at 30 Hz with an acquisition time of 29 ms. (B) Mobility pattern of 1342 individual receptors measured in the basal state. Boxes indicate the regions of the different mobility types, depicted in D, F and H. (C) Typical traces of type I diffusion with average $D_{1-10} > 0.008 \mu\text{m}^2/\text{s}$ and $S_{MSS} > 0.25$. The 12 trajectories depicted were selected from a collection of 633 individual receptors satisfying these conditions. (D) Mobility pattern of type I receptors of which selected trajectories are shown in C. (E) Typical traces of type II diffusion with average $D_{1-10} < 0.002 \mu\text{m}^2/\text{s}$ and $S_{MSS} < 0.1$. The 12 trajectories depicted were selected from a collection of 483 individual receptors satisfying these conditions. (F) Mobility pattern of type II receptors of which selected trajectories are shown in E. (G) Typical traces of type III diffusion with average $D_{1-10} > 0.02 \mu\text{m}^2/\text{s}$ and $S_{MSS} < 0.15$. The 12 trajectories depicted were selected from a collection of 131 individual receptors satisfying these conditions. (H) Mobility pattern of type III receptors of which selected trajectories are shown in G. (I) Closer view of a typical type III receptor trajectory. The color code scales with the indicated frequency (a.u.) of states.

Chapter 2. Mobility of individual NK1 receptors

these three different receptors was very low, less than 3%, during 30 s measurement windows corresponding to an interchange rate of 10^{-3} s^{-1} .

The mobility pattern of NK1Rs in the basal state exhibited two clear distinct peaks (Figure 2.2B) corresponding to freely diffusing (type I) and to restricted (type II) receptors, respectively. For each populations, both diffusion coefficients and Hurst parameters did not show a normal distribution; instead, the logarithm of D had a bimodal and S had multimodal distribution (Figure 2.3A). The median and the range of these distributions served as a basis for comparing receptor mobility between different experiments. Although diffusion trajectories of individual NK1Rs were highly heterogeneous in 293T cells (Figure 2.2A), the mobility pattern of the ensemble population (Figure 2.2B) was totally reproducible over days of measurement under identical experimental conditions.

In the following, the NK1R mobility was characterized either globally or as type I, II or III. The overall parameters were obtained by including all the trajectories measured during an experiment, whereas the values for the particular mobility types were obtained considering only the trajectories of the corresponding type.

2.4.2 Receptor immobilization after activation

To probe the effect of an activating ligand on NK1R mobility, the cells were stimulated with various amounts of the natural agonist SP. After addition of SP, the portion of receptors confined in nanometer-sized domains significantly increased. This immobilization effect is clearly visible by comparing [supplemental Movie S2](#) and [supplemental Movie S3](#)², which were recorded in absence or presence of SP, respectively. Figures 2.3A and 2.3B show the two-dimensional distribution of D_{1-10} and S_{MSS} values for single receptor trajectories before and after receptor activation, respectively. Figures 2.3C and 2.3D show the corresponding mobility patterns evaluated as described before. The mobile receptor population (type I, high values of D_{1-10} and S_{MSS}) decreased in favor of the confined receptor population (type II, low values of D_{1-10} and S_{MSS}), in which the immobile receptor subpopulation ($D_{1-10} < 2 \cdot 10^{-3} \mu\text{m}^2/\text{s}$, $S_{MSS} < 0.1$) increased substantially. This transition occurred in the first minutes after addition of SP. Interestingly, this immobilization depended on the concentration of added SP with an EC_{50} of about 100 pM for the average S_{MSS} (Figure 2.3E).

2.4.3 Temporal classification of trajectory segments

To reach an accurate and reliable classification of trajectories, we applied a machine learning evaluation procedure. The support-vector machine (SVM) was based on the four mobility parameters D_{1-10} , S_{MSS} , efficiency and asymmetry (for definition see “Experimental procedures”), which were calculated from segments of archetypal trajectories. SVM was run for both basal and activated states of the receptors. The dataset of receptors in the activated state was

²<http://www.jbc.org/content/290/46/27723/suppl/DC1>

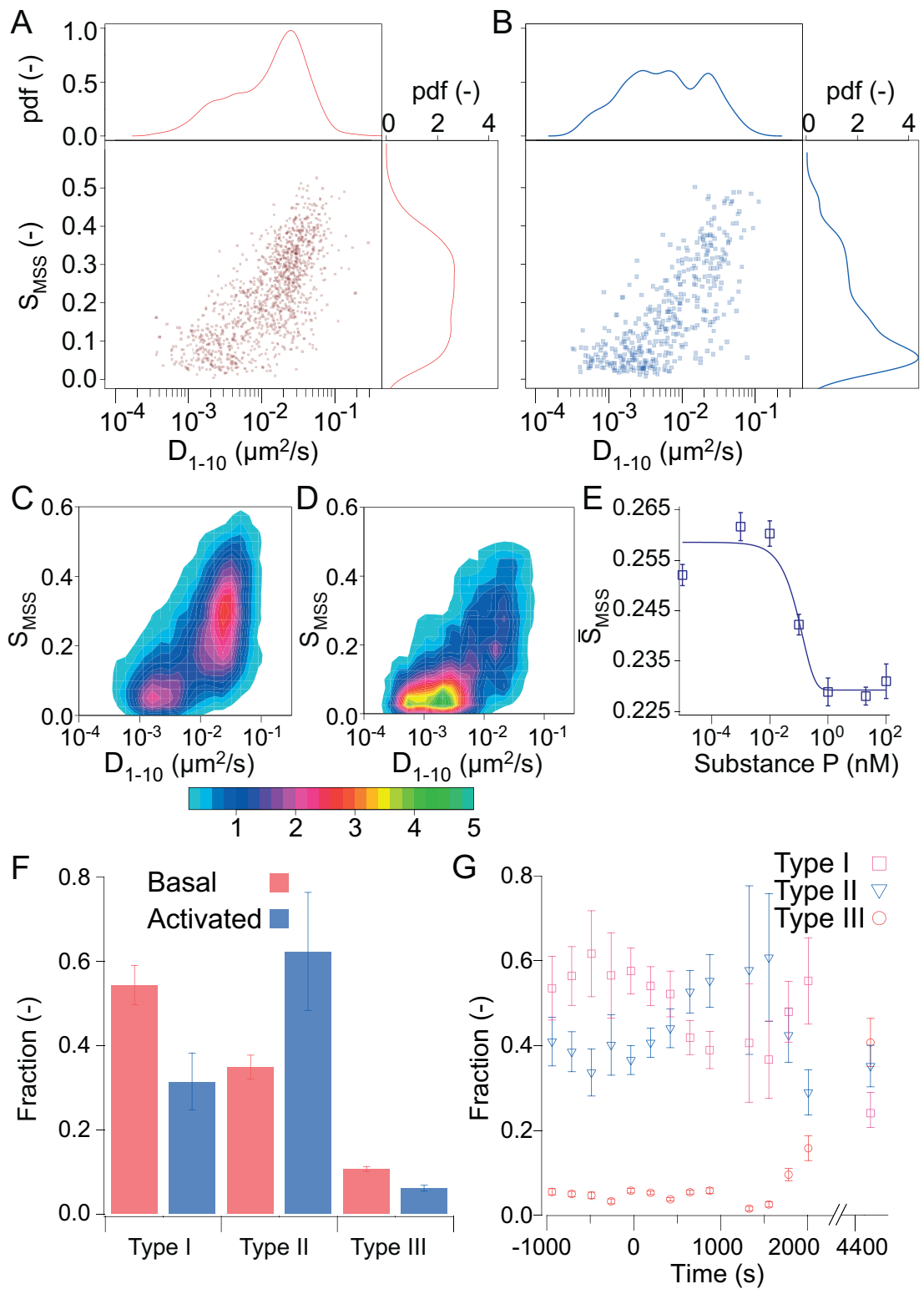


Figure 2.3: (legend on next page).

Chapter 2. Mobility of individual NK1 receptors

Figure 2.3: (*figure on previous page*). **Effect of SP binding on NK1R diffusion in 293T cells.** S_{MSS} vs D_{1-10} plot of 1207 individual receptors in absence of agonist. Probability density function (pdf) of D_{1-10} (bandwidth = 0.11 in the logarithmic scale) (top) and of S_{MSS} (bandwidth = 0.03) (right). (B) Same representation as in A of 433 NK1R in presence of 83 nM SP. (C) Mobility pattern of NK1R in the basal state. (D) Mobility pattern of NK1R in the first 30 minutes after addition of 83 nM SP. Color code at the bottom of C and D scales with the indicated frequency (a.u.) of states. (E) Dependence of NK1R immobilization on SP concentration. The average value of the Hurst parameters \bar{S}_{MSS} corresponds to the average receptor mobility for each concentration. An $EC_{50} \approx 100$ nM SP was calculated for the mobility change by fitting the \bar{S}_{MSS} vs SP concentration data with a standard Hill function. (F) Support-vector machine classification of trajectory segments according to the three defined types, before and after addition of 83 nM SP. (G) Time-evolution of the three classes of trajectory segments. A sliding time window of 160 seconds has been used to obtain the support-vector machine results in F and G. SP was added at $t = 0$. The evaluated time frames comprised between 21'747 and 68'834 trajectory segments. Error bars represent S.D.

limited to trajectories acquired during the first 1000 s after addition of SP. An increase of 27% of type II receptor population correlated with a decrease of 23% of type I receptor population, rapidly followed receptor activation, whereas the fraction of type III receptors remained stable (Figure 2.3F). To follow the intrinsic changes of receptor mobility over time, we measured the respective fractions of the mobility types during 1000 s at basal state (Figure 2.3G). No significant changes were detected during this time interval. After addition of SP, the type II receptor population increased rapidly with a correlated decrease of type I receptor population. 30 minutes after activation, type I receptors recovered to its initial level, while the type III receptor population started to increase significantly (Figure 2.3G). This distinct fraction showed a high mobility ($D > 0.02 \mu\text{m}^2/\text{s}$) and a strong confinement ($S_{MSS} < 0.2$) (Figure 2.2H) in circular 200 - 600 nm sized domains (Figures 2.2G and 2.2I). After long-term exposition to the agonist, the relative majority of receptors showed typical type III trajectories (Figures 2.2G and 2.3G).

2.4.4 Contribution of the Rho/ROCK pathway

This intriguing behavior of type III receptors may correspond to receptors diffusing in membrane blebs or microvesicles. Actually, in 293T cells, activation of NK1R with SP stimulates formation of membrane blebs and microvesicles derived from the cell membrane through the Rho/ROCK pathway [83]. To investigate the effect of this secondary pathway on receptor mobility and localization, Y-27632, a Rho-associated coiled-coil kinase inhibitor was added to the cells prior to SP addition. After stimulation with SP in the presence of Y-27632, receptors were immobilized in the plasma membrane as in the absence of the inhibitor, with a similar shift from mobile (type I) to immobile and confined (type II) receptor populations (Figures 2.4A and 2.4C). After 60 minutes of combined SP and Y-27632 exposition (Figure 2.4D), the NK1R mobility was comparable with that of the basal state (Figure 2.4A). Importantly, the fast-confined receptor population (type III) did not increase, unlike in the absence of the

Rho/ROCK pathway inhibitor (Figure 2.4B). This shows that the type III receptor population is directly linked to the Rho/ROCK signaling pathway.

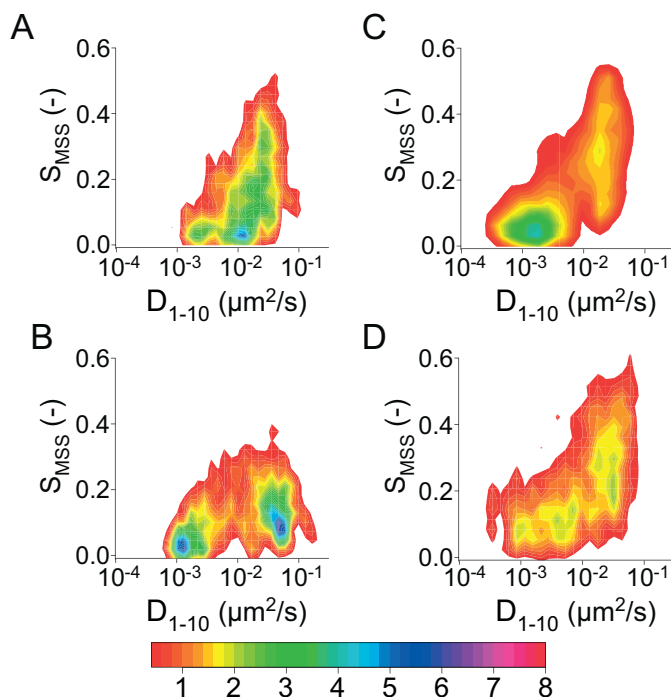


Figure 2.4: **Long-term evolution of NK1R mobility after SP exposition and Rho-ROCK pathway inhibition.** (A) Mobility pattern of the NK1R in the basal state, measurements started 1.5h after receptor labeling. (B) Measurements started 1.5 after addition of 83 nM SP and 1.5h after receptor labeling. (C) Measurements started just after SP addition and 30 min after labeling in presence of Y-26732, a Rho/ROCK pathway inhibitor. (D) Measurements started 1h after SP addition and 1.5h after receptor labeling in presence of Y-26732, a ROCK inhibitor. The color code scales with the indicated frequency (a.u.) of states.

2.4.5 Role of the cytoskeleton on NK1R confinement

To determine the origin of the important fraction of confined receptors (type II) at the basal state, we first investigated the role of the cytoskeleton and cholesterol, two key players often associated with protein compartmentalization in the plasma membrane.

GPCRs can interact directly or indirectly with the cell's cytoskeleton [176, 193, 194]. Here we probed the influence of the cytoskeleton on NK1R diffusion using cytoskeleton-depolymerizing toxins. To investigate the interactions of the NK1R with microtubules, the cells were incubated with nocodazole, an anti-neoplastic agent interfering with microtubule polymerization. This resulted in a significant decrease of the overall mobility of the NK1R, as seen by the median short-term diffusion coefficient (Figure 2.5E). This effect correlated with a significant increase of type II fraction, while the diffusion coefficient of the type I receptors remained unaffected (Figures 2.5A-B).

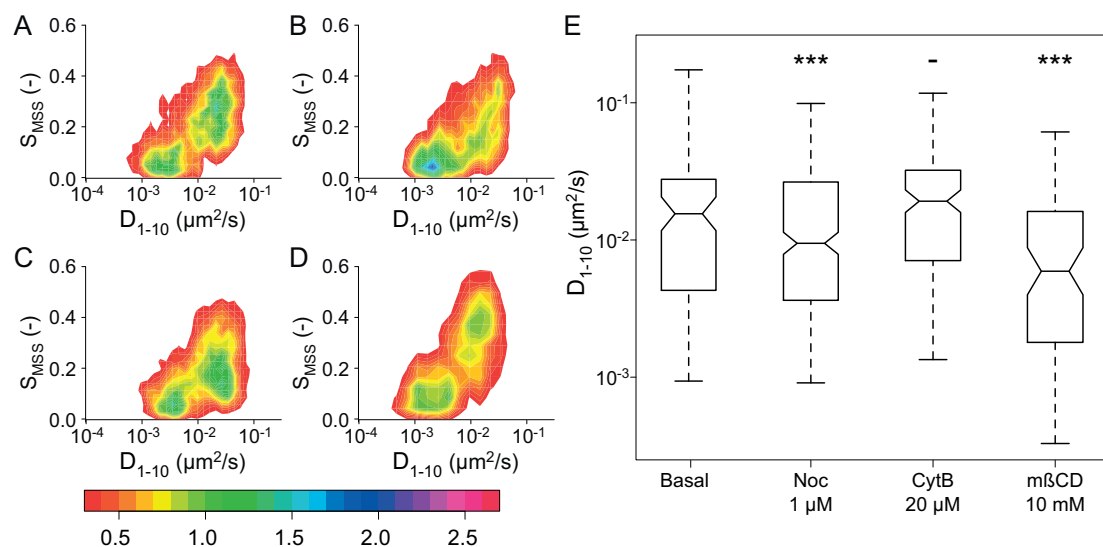


Figure 2.5: Modulation of NK1R mobility in 293T cells by cytoskeleton disruption and cholesterol depletion. (A) Mobility pattern of the NK1R in the basal state. This control pattern has been established using all basal state measurements performed before addition of chemicals. (B) Mobility pattern after addition of 1 μM nocodazole. (C) Mobility pattern after addition of 20 μM cytochalasin B. (D) Mobility pattern after addition of 10 mM m β CD. The color code scales with the indicated frequency (a.u.) of states. (E) Boxplot of D_{1-10} in presence of chemicals modifying cell cytoskeleton and membrane cholesterol content: basal state receptors ($n=314$), in presence of nocodazole ($n=294$), cytochalasin B ($n=146$) and m β CD ($n=60$). The median is drawn as a horizontal line. Notches indicate the 95% confidence interval of the median. Boxes represent the interquartile ranges of the distribution. Significance has been determined by a Wilcoxon ranking test on the distribution where each condition is compared with the related basal state, with – indicating no difference, and *** $p < 0.001$ with the null hypothesis (H_0) that population A is not different from population B. Trajectories of the receptors in the basal state were measured on the same cells before addition of chemicals.

The hindered and heterogeneous mobility observed in SPT experiments can stem from contacts of the receptors with the actin based membrane skeleton [195, 10]. To probe the existence of such interactions, cells were treated with cytochalasin B, an inhibitor of actin filament polymerization. Cytochalasin treatment did not significantly change the overall median diffusion coefficient (Figure 2.5E). More specifically, D_{1-10} of the type I receptor population remained unaffected. However, the population of confined receptors increased substantially, resulting in significantly lower S_{MSS} values as revealed by the associated mobility pattern (Figure 2.5C), in which the type III receptor population increased and the type I decreased. Importantly, neither the population nor the mobility features of type II receptors were affected by actin depolymerization. These results indicate that the restricted mobility of the NK1R is not due to direct interactions with the cell's cytoskeleton.

2.4.6 Decrease of receptor mobility after cholesterol depletion

Cholesterol has been shown to play a role in the localization of NK1R in plasma membrane domains [196]. To investigate the effect of cholesterol content in the plasma membrane on NK1R diffusion, the cells were treated with methyl- β -cyclodextrin (m β CD). We found that membrane cholesterol depletion by m β CD decreased the overall mobility of the receptor (Figure 2.5E). In particular, we observed two independent effects: (i) a shift of the mobility pattern toward confined diffusion of type II (Figure 2.5D), and (ii) a decrease of the median diffusion coefficient of the type I receptor population to $0.011 \mu\text{m}^2/\text{s}$, which differs significantly from the values observed for receptors in the basal state (0.016 to $0.025 \mu\text{m}^2/\text{s}$).

2.4.7 NK1R interaction with clathrin

The NK1R is recycled through the CME pathway [184]. Since the role of cytoskeleton and cholesterol appeared to be of minor importance in receptor confinement, we investigated the influence of clathrin on NK1R mobility. Three different CME inhibitors have been used to block formation and internalization of CCPs at different steps: (i) PitStop 2, which impairs association of amphiphysins with the clathrin terminal domain [197], (ii) Dynasore, which inhibits dynamin 1 and 2 GTPase activity [198], and (iii) Dyngo-4a, a potent Dynasore analogue [199]. Addition of each inhibitor significantly shifted receptor mobility towards restricted motion (Figures 2.6A-D). The type II receptor population increased without modification of the overall shape of the distribution, namely without a shift towards the subpopulation of immobile receptors. No significant differences were observed between the three different inhibitors. The mobility patterns were stable for more than one hour. During this timeframe, no noteworthy changes in cell morphology were observed.

In presence of the CME inhibitors, stimulation of the cells with SP (83 nM) further reduced NK1R mobility. Indeed the short-term diffusion coefficients (D_{1-10}) of single trajectories significantly decreased (Figure 2.6E), while the confinement was not affected, as illustrated by the stable values of S_{MSS} (Figure 2.6F). With Dyngo-4a (Figure 2.6B) and Dynasore (Figure 2.6D)

Chapter 2. Mobility of individual NK1 receptors

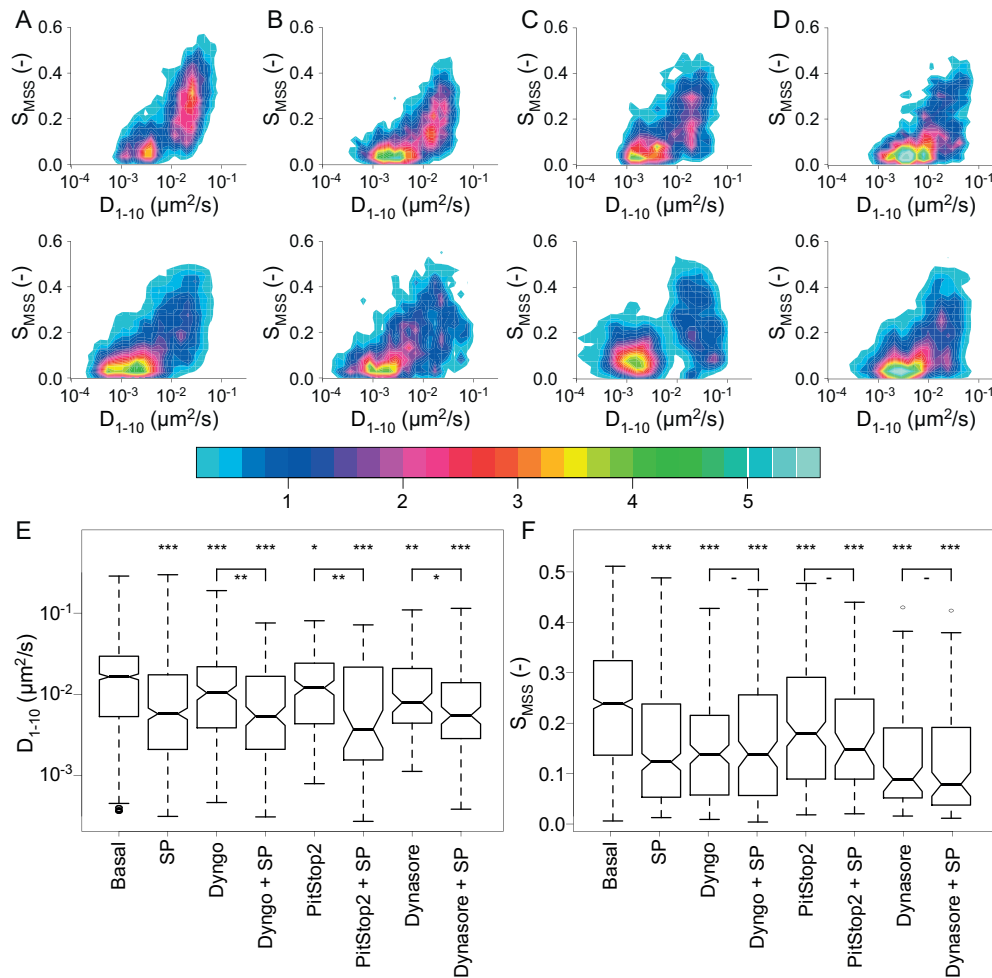


Figure 2.6: Modulation of NK1R mobility in 293T cells by CME impairment. (A) Mobility pattern of NK1R in the absence of CME inhibitors before (top) and after (bottom) addition of 83 nM SP. (B) Mobility pattern of NK1R in presence of 30 μM Dyngo-4a before (top) and after (bottom) addition of SP. (C) Mobility pattern of NK1R in presence of 30 μM PitStop2 before (top) and after (bottom) addition of SP. (D) Mobility pattern of NK1R in presence of 80 μM Dynasore before (top) or after (bottom) addition of SP. The color code scales with the indicated frequency (a.u.) of states. (E), (F) Boxplots of the NK1R mobility parameters from full-length receptors trajectories after addition of CME inhibitors before and after activation with SP. The median is drawn as a horizontal line. Notches indicate the 95% confidence interval of the median. Boxes represent the interquartile ranges of the distribution. Significance has been determined by a Wilcoxon ranking test on the distribution where each condition is compared with the related basal state, with – indicating no difference, * $p < 0.05$, ** $p < 0.01$, and *** $p < 0.001$ with the null hypothesis (H_0) that population A is not different from population B. (E) Boxplot of the diffusion coefficient D_{1-10} in absence of CME inhibitors ($n=217$, with SP $n=104$), after addition of 30 μM Dyngo-4a ($n=163$, with SP $n=155$), after addition of 30 μM PitStop 2 ($n=127$, with SP $n=60$), and after addition of 80 μM Dynasore ($n=91$, with SP $n=110$). (F) Boxplot of the Hurst parameter S_{MSS} for the same trajectories as in E.

the type I receptor population significantly decreased after activation. The type II receptor population increased and displayed a broader distribution of D_{1-10} . In both experiments a significant amount of receptors diffused in domains. Cells treated with PitStop 2 (Figure 2.6C) also displayed a strong reduction of type I receptor population, whereas the distribution of type II receptor population showed a narrower distribution around immobile receptors ($D_{1-10} < 0.002 \mu\text{m}^2/\text{s}$, $S_{MSS} < 0.1$) compared to the two dynamin inhibitors.

To investigate the influence of clathrin on the receptor further, we specifically depleted the cellular content of clathrin using siRNA. We found an increase of the overall mobility of NK1R in the plasma membrane; the mobility pattern showed a significant increase of the type I receptor population (Figures 2.7A-B). Furthermore, receptor confinement decreased markedly with a 37% higher value for S_{MSS} (Figure 2.7D), while D_{1-10} increased only slightly (Figure 2.7C).

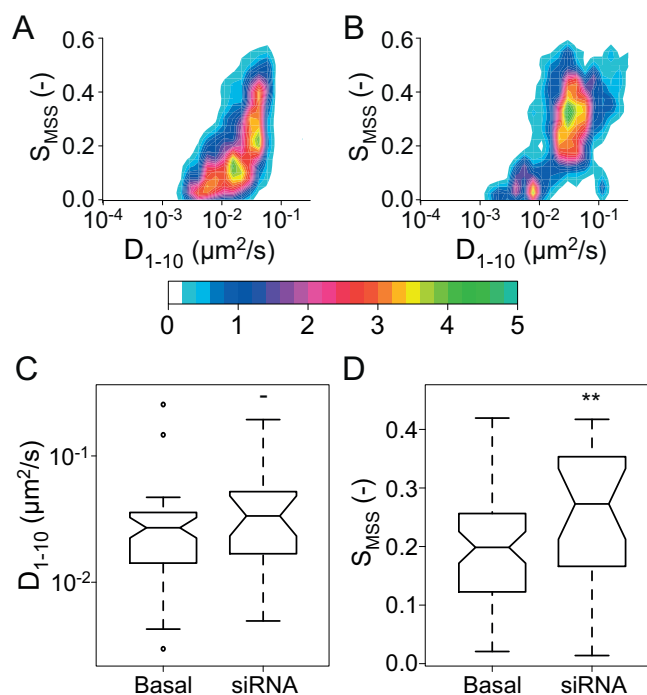


Figure 2.7: Mobility of NK1R in the plasma membrane of 293T cells after siRNA-mediated clathrin depletion. (A) Mobility pattern of NK1R in non-transfected control cells. (B) Mobility pattern of NK1R after siRNA knockdown of the clathrin heavy chain. For both A and B, bandwidths are $D_{1-10} = 0.21$ in the logarithmic scale and $S_{MSS} = 0.09$. The color code scales with the indicated frequency of states (a.u.). (C) Boxplot of the NK1R diffusion coefficient D_{1-10} and (D) of the Hurst parameter S_{MSS} in absence ($n=61$) and in presence ($n=23$) of siRNA against clathrin. The median is drawn as a horizontal line. Notches indicate the 95% confidence interval of the median. Boxes represent the interquartile ranges of the distribution. Significance has been determined by a Wilcoxon ranking test on the distribution where each condition is compared with the related basal state, with – indicating no difference, and ** $p < 0.01$ with the null hypothesis (H_0) that population A is not different from population B.

2.4.8 Impairment of NK1R-mediated Ca^{2+} signaling

The impact of the different chemical modulators used in the present study on NK1R activity was probed using a standard Ca^{2+} assay based on the fluorescent indicator *Fluo-4 NW*. Microtubule or actin filament disruption with nocodazole or cytochalasin B, did not affect the cellular Ca^{2+} response induced by SP, whereas removal of cholesterol with $m\beta\text{CD}$ almost abolished Ca^{2+} signaling (Figure 2.8A). Addition of Dyngo-4a and PitStop 2, which down-regulates CME, also led to a significant decrease of the Ca^{2+} response (Figure 2.8B). These results point out the importance of cholesterol but also clathrin in the regulation of NK1R activity.

To evaluate the ability of NK1R to bind SP in presence of the CME inhibitors, a fluorescent derivative of SP (SP-Cy5) was added to the cells, and binding of the fluorescent agonist was monitored using confocal microscopy. Dyngo-4a, PitStop 2 and Dynasore did not prevent SP-Cy5 binding (Figures 2.8C-E).

2.5 Discussion

Here, we have investigated the mobility features of the NK1 receptor with an unprecedented level of mechanistic understanding. We used mobility patterns as a new, high-content graphical representation of single-molecule mobility. This representation is based on a two-dimensional density function of the short-range diffusion coefficient D_{1-10} , versus the mobility parameter S_{MSS} , which is directly associated with the mode of motion of the receptor. This enabled us to visualize and analyze the complex information contained in a particular experiment within a single graph, facilitating substantially comparison of results obtained under different experimental conditions. Moreover, this method of analysis allowed us to easily define and classify the diffusing particles into different types according to their mobility regime.

Our study revealed that in spite of the very broad distribution of the mobility and sizes of membrane confinement, the overall NK1R mobility pattern remains highly reproducible between different days of experiment. This suggests the presence of a very distinct and stable network of functional interactions between the receptor and other cellular components. As presented in the results section, NK1R can be classified into three major classes. Receptors assigned to type I are free to diffuse in the cellular membrane. Their general diffusion properties are accessible by other measurement techniques such as fluorescence recovery after photobleaching (FRAP) or fluorescence correlation spectroscopy (FCS). The overall features of type I receptors are comparable to those observed by single-molecule tracking of other GPCRs [188, 200, 201, 202]. The low S_{MSS} values measured here correlate with a restricted diffusion of the NK1R. A similar behavior was observed for other receptors in living cells and is often explained by multiple effects such as the rough, irregular shape of the plasma membrane, transient interactions with other membrane proteins, the heterogeneous composition of the plasma membrane, or the recruitment in caveolae [187, 26, 203, 204, 205]. The diffusion coefficients of GPCRs we and others have observed in the membranes of living cells are considerably lower than those

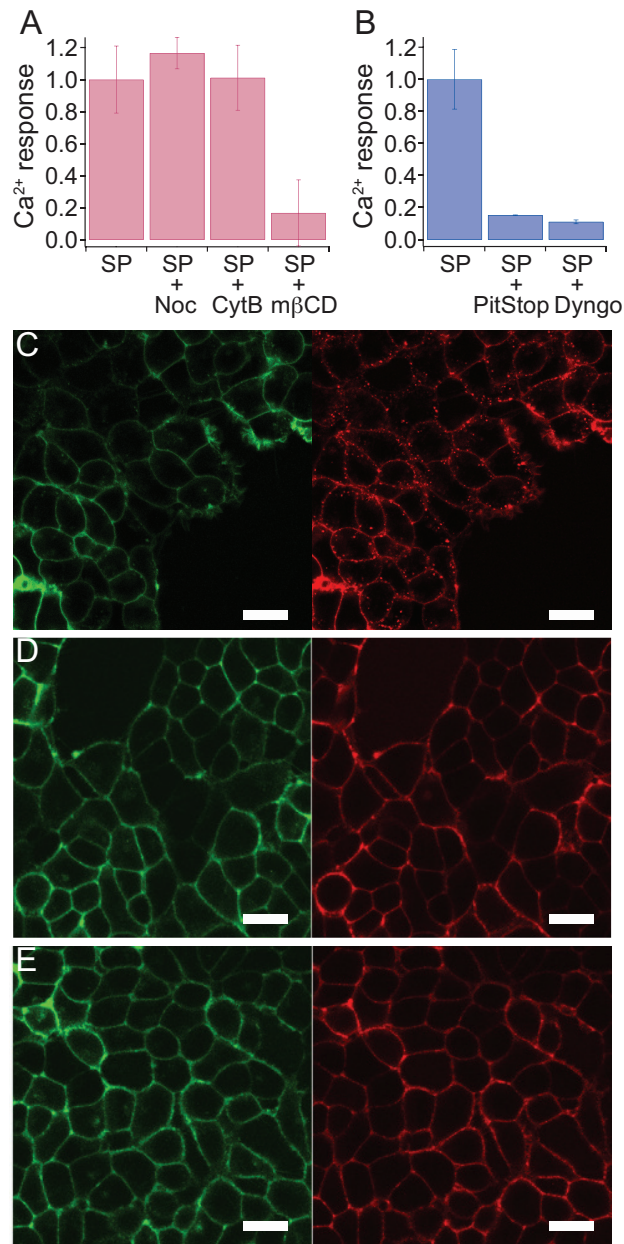


Figure 2.8: **Efficiency of the $G_{\alpha q}$ activation pathway in 293T cells after cytoskeleton disruption, cholesterol depletion and CME inhibition (A and B) and capacity of the NK1R to bind SP in presence of the CME inhibitors (C-E).** (A) Intracellular Ca^{2+} responses measured with Fluo-4 in the presence of 83 nM of agonist SP before and after addition of (i) nocodazole which disrupts microtubules, (ii) cytochalasin B which prevents F-actin fiber formation, and (iii) mβCD which depletes cholesterol from the plasma membrane. (B) Intracellular Ca^{2+} responses before and after CME impairment by PitStop 2 and Dyngo-4a. (C-E) Fluorescence confocal micrographs showing 293T cells stably expressing ACP-NK1R labeled with CoAlexa488 before (left), and after adding 50 nM of the agonist SP-Cy5 (right), in absence of CME inhibitor (C), in presence of Pitstop 2 (D), or Dyngo-4a (E). Scale bars: 20 μm.

Chapter 2. Mobility of individual NK1 receptors

of other membrane proteins of similar size or that of rhodopsin as an example of a class A GPCR in pure lipid bilayers [206, 27]. The use of QDots as fluorescent label to track individual receptors allowed us to validate in an accurate and reliable manner previous single-molecule diffusion measurements using organic dyes by Prummer *et al.* [187]. Consequently, the use of QDots does not interfere with the receptor's diffusion properties.

Low diffusion coefficients are often explained by direct interactions of the membrane protein of interest with components of the cytoskeleton [207, 208, 209]. According to the picket-fence model [10], drug treatment causing actin depolymerisation should result in an increased receptor diffusion due to the reduction of actin filament barriers. The NK1R does not follow this behavior. In the present case, the type I mobility receptor population did not increase after actin-fiber or microtubule depolymerization, strongly suggesting a lack of direct interaction of type I NK1Rs with the cytoskeleton. The relative low mobility of type I receptors could be explained by the high propensity of NK1R to form diffusing membrane domains a few tens of nanometers in size with high receptor density [196].

A high fraction of the NK1Rs exhibited a strictly restrained mobility and was therefore classified as type II. Indeed more than one third of the receptors in the basal state were found to be confined in submicrometer-sized domains. The low interchange rate between receptors of type II and other mobility regimes indicated that this restricted diffusion is not a consequence of the fast transient recruitment described in the picket-fence model of the plasma membrane [27], but is more likely due to the existence of very stable membrane structures in which the NK1R is integrated. The low diffusion coefficients measured for type II receptors did not depend on intact actin filaments or microtubule structures, as no differences have been observed in type II diffusion features upon treatment of cells with cytochalasin B or nocodazole. The low D_{1-10} values observed are very likely due to molecular crowding related to membrane regions of high protein-content. The high frequency of our measurements (30 Hz), combined with the very high accuracy generated by the use of QDots to localize individual receptors permitted us to exclude effects of domain size on the apparent diffusion coefficients observed elsewhere for other GPCRs with less photostable fluorophores [205, 210]. A small part of the receptors in the basal state remained immobile; this population probably stems from constitutively internalized receptors. Although our results do not yield any indication of direct or mediated interactions by a simple protein assembly of the NK1R with the cell's cytoskeleton, the NK1R is nevertheless tightly related to its surrounding. Indeed disruption of the cytoskeleton had an indirect influence on the mobility pattern of the receptor through structural modifications of the membrane.

Depolymerization of actin filaments is known to stimulate cell blebbing [211, 212]. Under certain conditions, these blebs can be released as native microvesicles containing functional NK1R [213]. The high fraction of type III receptors after cytochalasin B treatment is related to membrane blebbing. The protein content of native vesicles is different from that of the cell's plasma membrane; in particular they lack cytoskeletal structure [214]. This explains the high D_{1-10} observed for this population. Furthermore, the sub-micrometer size of the confinement

region is in total agreement with the results obtained elsewhere [212, 213].

SP is a potent natural agonist of the NK1R. It triggers multiple signaling pathways and receptor recycling. After activation, the NK1R is recycled via two distinct pathways: In a fast process, receptors are recruited in plasma membrane domains or in early endosomes in close proximity to the plasma membrane [61, 186]; in a slow process, the receptors are transported to low pH perinuclear late endosomes [215, 216]. Both pathways are initiated by receptor phosphorylation and subsequent arrestin binding. Our SPT results in presence of SP, show a substantial decrease of NK1R mobility, consistent with an increased recruitment of the receptors in structures related to the recycling pathways. This effect correlates with a decrease of the overall diffusion coefficient, mainly due to an increase of confinement as seen by an important shift from type I to type II receptors on the mobility patterns. Interestingly, only 30% of the receptors undergo a change of mobility after activation. It has been shown elsewhere that other cargo proteins associate transiently with CCPs during their formation and can dissociate before pit termination or internalization; the dwell times of this process display a very broad distribution from the second to hundred-second regime [217]. Taking this mechanism into consideration, our results can be explained by an increase of the receptor affinity for CCPs after agonist binding, thus increasing the dwell time and favoring the internalization against release of the receptor in the plasma membrane.

It is remarkable that this immobilization effect associated with receptor recruitment in CME pathway depends on agonist concentration. The dose response curve resulting of the measurement of the average Hurst parameter with increasing SP concentrations shows an EC_{50} value of about 100 pM, which is comparable to the EC_{50} of the intracellular Ca^{2+} response indicating that the ligand coordinated receptor immobilization might regulate the intracellular response. The NK1R mobility change induced by the presence of low concentrations of agonist in the environment would quickly regulate the cell response and therefore limit the intracellular Ca^{2+} release in case of long-term agonist exposition.

An unexpected important result is that the decrease of CME functionality induced by the clathrin-/dynamine-inhibitors Pitstop 2, Dyngo-4a, or Dynasore leads to a substantial increase of type II receptors confined in submicrometer membrane domains. Besides inhibition of endocytosis, these molecules induce an accumulation of clathrin at the plasma membrane, forming long-lived clathrin structures [218], including membrane-attached vesicles [219]. Clathrin can also exist in large patches on the plasma membrane without forming functional pits or invagination [220, 221, 222]. The correlated decrease of both the diffusion coefficient and the Hurst parameter after inhibition of clathrin or dynamine indicates a stable interaction of NK1R with these clathrin-related structures. Importantly, this is observed with all three CME inhibitors indicating a specific clathrin effect. It is thus possible to exclude domain recruitment due to clathrin-independent membrane processes, which could be affected by dynamine inhibitors [223]. Receptors are accumulating in a pre-internalized state, that is either in clathrin lattices, pre-pits [224], coated pits [225, 226], or in superficial early endosomes [185]. The fast accumulation of NK1R after CME inhibition strongly suggests a high association

Chapter 2. Mobility of individual NK1 receptors

rate with these structures. Further support for the specific interaction of clathrin with the NK1R comes from the observation that the distinct membrane organization of the receptor is strongly affected after clathrin depletion.

Interaction of NK1R with clathrin-dependent structures and immobilization of activated receptors are sequential events. In the absence of CME inhibitors, a large fraction of the receptors are localized in relatively stable domains in an intermediary mobility state between freely diffusing and internalized receptors. CME-inhibitors promote this state by increasing the clathrin content at the membrane. In this state, receptors are diffusing in domains with lower diffusion coefficients and lower Hurst parameters. After activation with SP, the Hurst parameters remained unchanged, while the diffusion coefficients further decreased. The interactions involved in domain recruitment and in immobilization after activation are distinct. Non-activated receptors interact with clathrin-dependent structures, forming transient membrane domains, whereas activated receptors bind specifically to CCP through β -arrestin and AP2.

CME inhibitors also strongly impaired receptor-mediated intracellular calcium signaling. This decrease of the NK1R canonical activity can arise from several, non-exclusive reasons: (i) The agonist binding site is not accessible due to the shape of the invagination as depicted on Figure 1, (ii) G-proteins cannot bind the intracellular region of the receptor due to the densely packed clathrin structures [227], (iii) receptor signaling is impaired by molecular crowding [228]. Interestingly, disruption of microtubules, known to inhibit CME [229], does not alter NK1R activity in our case.

The correlation between the clathrin-dependent change of receptor mobility and the decrease of its activity, combined with the presence of a high fraction of type II receptors before activation, implies a clathrin-based mechanism for regulation of NK1R activity. Thereby, type II receptors could act as a non-activated receptor reservoir directly and quickly available at the cell membrane. This reservoir would have major implications in cell response to an agonist. In particular, it would allow responding to successive or long-term agonist exposures. Indeed, for a short exposition time to an agonist, only a fraction of the receptors must respond. A gradual release of receptors from an inactive membrane reservoir could increase the response in case of prolonged agonist exposition. Furthermore, such a mechanism would allow multiple intracellular Ca^{2+} responses to sequential agonist waves, without the need of newly membrane-inserted receptors. This model is also compatible with the fast resensitization observed elsewhere [186], albeit without the need of preliminary activation of NK1R.

Cholesterol removal with $m\beta\text{CD}$ affects NK1R mobility and activity in a similar manner as CME inhibition. Indeed, cholesterol depletion provokes a substantial decrease of the overall diffusion of the receptor and practically abolished the intracellular Ca^{2+} response. Thus, cholesterol, like clathrin, plays a major role on receptor mobility and is of critical importance for its activity, corroborating the close link between mobility and activity.

The fast diffusing type III receptor population confined in circular domains, which appears 30

minutes after NK1R activation with SP, results from the presence of receptors in membrane blebs or microvesicles. Membrane blebs are balloon-like structures of the plasma membrane in which the cytoskeleton elements are generally absent, leading to enhanced molecular diffusion. Tank *et al.* found a considerable increase of the diffusion coefficients for both membrane proteins and lipids [230], comparable to those found in liposomes [10]. Besides the canonical signaling pathway leading to Ca^{2+} release from the endoplasmic reticulum, SP induces cell membrane blebbing through the Rho/ROCK pathway by contraction of the actomyosin cell cortex [83].

Y-27632 is a highly specific and efficient cell-permeable Rho-associated coiled-coil kinase (ROCK) inhibitor, which prevents NK1R-induced blebbing without affecting the apoptotic state of the cells [83]. The mobility pattern resulting from NK1R trajectories measured in cells treated with this inhibitor and stimulated with SP is characterized by the absence of type III receptors. It demonstrates that the type III receptor population is directly dependent on the activation of the Rho/ROCK pathway and thus on the presence of membrane blebs. Membrane blebbing and excretion of microparticles are often associated with apoptosis. However, in our case it has been shown that membrane blebbing is induced by activation of the NK1R by SP and is hence an apoptosis-independent phenomenon. This particular cellular mechanism may be of great importance for intercellular communication [84].

2.6 Conclusion

In summary, single-particle tracking and multi-parameter analysis allowed us to describe in detail the diffusional behavior of the NK1 receptor in the plasma membrane of living cells. The bimodal distribution of freely diffusing and confined receptors observed in the basal state is strongly shifted towards restricted mobility by receptor activation, whereas a new population of fast diffusing receptors in circular domains, corresponding to receptors in membrane blebs, resulted 30 minutes after activation of the Rho/ROCK pathway. Blocking of the CME pathway using different inhibitors leads to receptor confinement, which is correlated to a significant decrease of the receptor canonical pathway activity. Our results point to the central importance of clathrin, not only in receptor endocytosis and turnover but also in NK1R membrane homeostasis and fine regulation of its activity.

3 A monovalent StrepTactin for cross-linking-free labeling of membrane receptors

3.1 Abstract

Specific, stoichiometric and long-lasting tagging of biologically relevant molecules with fluorescent labels is of critical importance for single-molecule microscopy. The biotin-streptavidin couple is often used to label proteins in living cells. In some cases, however, it may be prone to cross-linking artifacts interfering with biological functions. Here, we present a novel method to label directly Strep-tagged or biotinylated membrane receptors with high affinity and virtually no risk of cross-linking. Monovalent StrepTactin (mST) is a combination of one StrepTactin subunit with three inactive streptavidin subunits. Under strict stoichiometric control of the two subunits prior to refolding, we obtained a good yield of pure mST. Fluorescent derivatives of mST were used for live-cell imaging of plasma membrane receptors. Semiconductor quantum dot-mST conjugates were particularly well suited for long-term tracking of biotinylated receptors at the single-molecule level.

3.2 Introduction

Streptavidin (SA) is a ~53 kDa homotetrameric protein isolated from the bacterium *Streptomyces avidinii* [231]. Due to its extraordinarily high affinity for biotin, it is extensively used in biotechnology and molecular research for detection, purification, cross-linking and labeling of biomolecules [232, 233, 234]. The dissociation constant (K_d) of the biotin-SA system is on the order of 10^{-15} M [165], making it the strongest noncovalent biological interaction known.

SA-based applications often require the biotinylation of the target molecules. Biotinylation can be performed through chemical means or using enzymatic methods [235]. Although chemical biotinylation methods are technically straightforward and offer a greater flexibility, their lack of target selectivity prevents in particular their use for live cell imaging of membrane proteins. In this case, enzymatic biotinylation, which allows to link biotin at a unique specific site in the

K_d (mol/L)	SA	ST
Biotin	10^{-14} [165]	$< 10^{-13}$ [242]
StrepTag II	10^{-4} [243]	10^{-6} [244]

Table 3.1: **Dissociation constants (K_d).**

protein of interest, is more appropriate. The most commonly used method links by genetic engineering a small peptide tag (termed acceptor peptide) to the N- or C-terminus of the protein of interest and to use a biotin ligase (BirA) that will catalyze the covalent attachment of biotin to a specific lysine residue of the tag [236].

The fact that the tetrameric SA can bind up to four biotinylated ligands imposes, in some cases, a severe limitation of the method. The multivalency can cause target aggregation, which may influence the biomolecule function or dynamics. Many efforts have been undertaken to engineer a monomeric streptavidin. Unfortunately the biotin-binding affinity of such proteins remained many orders of magnitude lower than that of wild-type streptavidin [237] [238].

Howarth *et al.* have developed a monovalent tetrameric streptavidin (mSA) in which only one of the four binding sites is functional [239]. This engineered recombinant form of streptavidin is not subject for cross-linking and its single biotin binding site has an affinity and off rate similar to the tetravalent version [239, 240].

Here we adapt the approach of Howarth *et al.* to StrepTactin (ST), a triple mutant of SA (Figure 3.1A-B). ST also binds biotin with femtomolar affinity, but the main feature of this engineered SA is its optimized binding site for the *Strep-Tag II*, a short peptide tag of only eight amino acid residues (Figure 3.1C) which can be fused to any protein of interest [241]. The affinity of ST for the Strep-Tag II is almost 100 times stronger than that of SA (Table 3.1). Monovalent StrepTactin (mST) may therefore be of particular interest for direct, cross-linking-free labeling of membrane proteins. In the following we evaluate the ability of fluorescent mST conjugates for live-cell imaging and single-molecule tracking of membrane receptors.

3.3 Experimental procedures

3.3.1 mST expression and purification

pET21a-streptavidin-dead and *pET21a-streptavidin-alive* plasmids were a gift from Alice Ting (Addgene plasmids # 20859 and # 20860, respectively). *pET21a-StrepTactin-alive* was generated by Menno Tol from *pET21a-streptavidin-alive* using site-directed mutagenesis. *E. Coli BL21(DE3) pLysS* cells (Invitrogen) transformed with *pET21a* expression plasmid encoding StrepTactin-*alive* subunit or streptavidin-*dead* subunit were induced at an OD_{600} of 0.6 with 0.5 mM isopropyl β -D-1-triogalactopyranoside (IPTG). After 16h incubation at 37°C, cells were harvested by centrifugation (4,200g, 20 min, 4°C), resuspended in ice-cold wash buffer (50 mM Tris-HCl, pH 8.0, 500 mM sucrose), centrifuged again (20,000g, 30 min, 4°C) and



Figure 3.1: **StrepTactin and Strep-Tag II.** (A) Protein sequence alignment of ST, SA and SD. Mutations between ST / SD and SA are highlighted in purple and yellow, respectively. 6xHis purification tag at the N-terminus of ST and SA is in light blue. (B) X-ray structure of ST. The four monomers are represented in different colors. Taken from [245]. (C) Chemical structure of Strep-Tag II (WSHPQFEK).

resuspended in ice-cold lysis buffer 50 mM Tris-HCl pH 8.0, 1 mM EDTA). Cells were broken by sonication and the crude cell extract was centrifuged (20,000g, 30 min, 4°C). The supernatant was discarded whereas the inclusion body-rich pellet was washed three times in ice-cold lysis buffer. Following the last centrifugation (200,000g, 30 min, 4°C) step, inclusion bodies were solubilized in guanidinium hydrochloride (GuHCl) (6 M, pH 1.5). Solubilized samples were homogenized and incubated at 50°C for 10 min. Insoluble material was removed by centrifugation (20,000g, 10 min, 4°C) whereas the supernatant was dialyzed twice against GuHCl in order to remove trace of biotin. The unfolded *alive* and *dead* subunits were mixed in a 1:9 ratio, after having previously determined their relative concentration from OD₂₈₀ values. mST was generated by dilution of the mixture into Dulbecco's phosphate-buffered saline (DPBS) (Invitrogen) under vigorous agitation. After ultracentrifugation (20,000g, 30 min, 4°C) and filtration at 0.22 μm to remove aggregates, the protein was loaded onto a Ni-NTA affinity column (GE Healthcare) in presence of 30 mM imidazole to prevent non-specific binding. His-tagged proteins were allowed to bind to the column using a continuous flow of 2 ml/min and with at least two successive passages. Elution was performed using a linear imidazole gradient to a final value of 500 mM. Purified proteins were concentrated using 30 kDa molecular mass cut-off (MWCO) concentrators (Millipore) to a final volume of ~1ml. The purified proteins were analyzed by sodium dodecyl sulphate-polyacrylamide gel electrophoresis (SDS-PAGE). In order to remove imidazole, the protein solution was passed

Chapter 3. Monovalent StrepTactin

through a NAP-10 column (GE Healthcare), which has been equilibrated with DPBS previously, and elution was performed using with the same buffer. The concentration of proteins was determined by measuring A_{280} with a Nanodrop 2000 (Thermo Scientific) assuming 1 Abs = 1 mg/ml. Finally the concentrated sample was supplemented with 1 mM EDTA and 30% glycerol (for cryopreservation), aliquoted, flash frozen in liquid nitrogen, and stored at -80°C .

Tetravalent StrepTactin was purified similarly, except that only *alive* submits were used for the refolding step.

3.3.2 Conjugation of Atto635 to mST

mST was conjugated to Atto635 N-hydroxysuccinimide (NHS) ester fluorochrome (Atto-Tec) following manufacturer's instructions. First, mST solution was passed through a NAP-5 column (GE Healthcare) pre-equilibrated with DPBS (pH 7.4) to remove EDTA (that would react with NHS-ester). Eluted mST was then concentrated to 0.5 mg/ml with a 10 kDa MWCO concentrator (Millipore). Conjugation reaction was initiated by mixing 20 μg of the protein with a 10-fold molar excess of Atto635-NHS ester. The reaction was allowed to proceed for 40 min at room temperature on a rotating wheel. Purification was performed by size-exclusion chromatography using a NAP-5 column equilibrated with DPBS. After concentration to 0.2 mg/ml, 0.1% of BSA (Sigma-Aldrich) was added and mST-Atto635 was aliquoted and stored frozen at -20°C protected from light.

3.3.3 Functionalization of QDots with mST

Amine-functionalized PEG-coated quantum dots (QDot 655 ITK amino (PEG), Invitrogen) were used for the preparation of mST-QDots. QDots were activated with bifunctional crosslinker BS³ (bis(sulfosuccinimidyl)suberate), followed by covalent conjugation with mST. QDots (200 μl , 0.2 nmol) were mixed with a 100-fold molar excess of BS³. The mixture was incubated for 30 minutes at room temperature on a rotating wheel and then passed through a NAP-5 column pre-equilibrated with DPBS to remove excess of crosslinker. Eluted QDots were added to a 10-fold molar excess of mST (mST:QD ratio of 10:1). After 4 hours incubation at room temperature, the reaction was quenched by adding glycine to a final concentration of 50 mM. mST-QDots were purified using a 100 kDa MWCO ultrafiltration device for at least six times with borate buffer (50 mM, pH 8.3). mST-QDots were stored in borate buffer at 4°C .

3.3.4 Fluorescence Correlation Spectroscopy (FCS)

Biotin-Atto633 (M 962) conjugate and streptavidin (M 52,800) were obtained from Atto-Tec and Sigma-Aldrich, respectively. All dilutions were made in DPBS buffer, pH 7.4. A fixed concentration of biotin-Atto633 (20 nM) was titrated with increasing concentrations of streptavidin, StrepTactin or mST (0-50 nM). All samples were incubated 20 min at room temperature in the dark before measurement.

3.3. Experimental procedures

FCS measurements were performed using a LSM 510 Meta laser scanning microscope based on an Axiovert 200M microscope stand equipped with a ConfoCor 3 FCS unit (Zeiss). This allowed acquisition of photon-time traces and online correlation of the data. Biotin-Atto633 was excited at 633 nm by the built-in He-Ne laser (Lasos Lasertechnik). An acousto-optical filter (AOTF) was used to adjust the exciting beam from the microscope objective (40x C-Apochromat, NA 1.2, water immersion, Zeiss) in order to minimize photobleaching and photophysical effects. The fluorescence signal was collected through a LP650 emission filter.

Determination of the lateral beam waist radius ω_{xy} of the laser was performed by measuring the translational diffusion time constant τ_d of Alexa Fluor 647 (Invitrogen) with known diffusion coefficient ($D = 3.3 \cdot 10^{-6} \text{ cm}^2 \text{ s}^{-1}$) [246] according to equation 3.1.

$$\omega_{xy} = (4D\tau_d)^{1/2} \quad (3.1)$$

A droplet (30-50 μl) of the sample solution was put on a coverslip mounted on the top of the objective just before the start of the measurement which occurred 200 μm above the glass surface. Fluorescence intensity time traces and correlation curves were recorded for ten times 10 s.

The correlation curves obtained from the FCS measurements were fitted with a three-dimensional diffusion model of multiple species using a Marquardt algorithm with IGOR Pro (WaveMetrics), according to equation 3.2:

$$G(\tau) = 1 + \frac{1}{N} \cdot \sum_{i=1}^m f_i \cdot \left(1 + \frac{\tau}{\tau_{d_i}}\right)^{-1} \cdot \left(1 + \frac{1}{S^2 \tau_{d_i}}\right)^{-1/2} \quad (3.2)$$

where N is the total number of fluorescent molecules in the observation volume, f_i is the fraction of species i from a total number of species m with diffusion time τ_{d_i} , and S is the structure parameter defined by the ratio of the longitudinal to the radial dimension of the laser focal spot.

To taken into account triple state, the second term may be multiplied by:

$$\left(1 + \frac{Tr}{1 - Tr} \cdot e^{-\frac{\tau}{\tau_{Tr}}}\right) \quad (3.3)$$

where Tr is the triplet amplitude and τ_{Tr} the triplet lifetime.

Finally the molecular mass M of the diffusing species can be estimated with equation 3.4:

$$\tau_d = \frac{3\pi\omega_{xy}^2\eta}{2kT}(M)^{1/3} \quad (3.4)$$

where η the viscosity of the sample, k the Boltzmann's constant and T the temperature.

3.3.5 Surface Plasmon Resonance (SPR)

SPR measurements were carried out using a Biacore 3000 instrument (GE Healthcare). Protein immobilization was performed in DPBS buffer at a flow rate of $5 \mu\text{l}\cdot\text{min}^{-1}$. Binding experiments were performed in buffer containing 10 mM HEPES, pH 7.4, 150 mM NaCl, 0.02% C_{12}E_9 at a flow rate of $10 \mu\text{l}\cdot\text{min}^{-1}$. mST was covalently coupled to the surface of a sensor chip CM5 (GE Healthcare) using standard amine coupling procedure (EDC/NHS coupling). Strep-tagged 5-HT₃R (100 nM) [247] was injected on the mST-functionalized surface of the sensor chip. BiaEvaluation 4.1 (GE Healthcare) and IGOR Pro softwares were used for data processing.

3.3.6 Cell culture

HEK293 cells stable cell lines were maintained at 37°C under a humidified 5% CO₂ atmosphere in tissue culture-treated flasks (TPP) containing DMEM:F12 medium with GlutaMAX (Invitrogen) and 10% NBCS (Invitrogen). ACP-NK1R stable cell line [196] were grown in presence of 200 $\mu\text{g}/\text{ml}$ of hygromycin B (Roche). Strep₄-5-HT₃R tetracycline-inducible cell line [247] was grown in presence of 200 $\mu\text{g}/\text{ml}$ hygromycin B and 10 $\mu\text{g}/\text{ml}$ blasticidin (Invitrogen). When cells reached 80-100% confluency they were trypsinized, and re-seeded by 50-fold dilution into fresh medium. For confocal microscopy and single-particle tracking experiments cells were grown in DMEM:F12 medium with 10% NBCS but without antibiotics on 8-well chambered glass slides (Nunc) for 24-48h.

3.3.7 Labeling of Strep-tagged receptors

Strep-tagged 5-HT₃R was expressed either transiently or stably in HEK293 cells. Transient transfection with *pcDNA5/TO*-Strep₄-5-HT₃R vector [247] was performed using Lipofectamine 2000 (Invitrogen) following the manufacturer's instructions. Expression of Strep-tagged 5-HT₃R from the stable cell line [247] was induced with tetracycline (2 mg/ml) for 48h. Prior to labeling, cells were washed once with DPBS containing 1% BSA. Cells were then incubated with either 100 nM mST-Atto635 (confocal imaging), 10 nM mST-QDots (confocal imaging) or 100 pM mST-QDots (SPT) for 10 minutes at room temperature. Cells were washed three times with colorless DMEM (Invitrogen) containing 1% BSA prior to measurements.

3.3.8 Labeling of biotinylated receptors

HEK293 cells stably expressing ACP-NK1R [196] were labeled with CoA-biotin as described previously (chapter 2, p. 43). Cells were then washed three times with DPBS 1% BSA prior to incubation with 100 pM of mST-QDots for 10 minutes at room temperature. Cells were washed three times with colorless DMEM 1% BSA prior to measurements.

3.3.9 Microscopy

Confocal microscopy Laser-scanning confocal micrographs were recorded by using a LSM510 confocal microscope (Zeiss). Atto635 was excited at 633 nm by the built-in HE-Ne laser focused by a NA 1.2 63x water-immersion objective (Zeiss). QDots 655 were excited at 488 nm by the built-in Ar-ion laser. Fluorescence was detected using photomultiplier tubes (PMT). The imaging parameters were kept constant whenever intensity of fluorescence was compared.

Single-Particle Tracking (SPT) 8-well plates were mounted on a modified epi-fluorescence wide-field microscope (Axiovert 200, Zeiss). mST-QDots were excited at 488 nm (Obis diode laser, Coherent Inc.). A circularly polarized laser beam was directed by a Q645LP dichroic mirror (Chroma Corp.) into the microscope objective (C-Apochromat 63x W Corr, 1.2 NA, Zeiss) to illuminate a 15- μm diameter region of the sample. Fluorescence emission was collected by the same objective, passed through a HQ710/100 filter (Chroma Corp.), a 1.5x Optovar (Zeiss), and imaged on a intensified charge-coupled device (CCD) camera (Ixon 887BV, Andor Technology). Single-molecule images were recorded at a frequency of 30 Hz with excitation intensities of 0.1 kW/cm² during 33 s (i.e. 1000 frames). Measurements were taken at the apical membrane of the cells.

SPT data evaluation Single-molecule trajectories were reconstructed from the positions of the fluorescent spots over time using a home-written software in IGOR Pro as described previously (chapter 2, p. 44). Trajectories were segmented using a sliding window of 100 frames. Initial diffusion coefficient (D_{1-10}) and Hurst parameter (S_{MSS}) were calculated for each individual trajectory from the segments constituting the trajectory (average). Boxplots were computed using R (R Foundation for Statistical Computing).

3.4 Results and discussion

3.4.1 Production of monovalent StrepTactin

Our goal was to produce a StrepTactin tetramer with only one functional binding site. To achieve this we were inspired by the work of Mark Howarth and Alice Ting who developed an elegant strategy to generate a monovalent streptavidin composed of three “*dead*” subunits which have negligible biotin binding, and one “*alive*” subunit which is fully functional [239].

Chapter 3. Monovalent StrepTactin

The *dead* subunits were from a triple mutant (N11A, S15D, S33A) of streptavidin, whereas the *alive* subunit was a wild-type streptavidin subunit fused with a 6xHis-tag at the C-terminus [239]. In our case the *alive* subunit was replaced by a StrepTactin subunit (E32V, S33T, V35R). The procedure used for generating monovalent StrepTactin is illustrated in Figure 3.2. The two subunits, which were expressed separately in *E. Coli*, resulted in the formation of inclusion bodies. After extraction and dissolution of the inclusion bodies in guanidinium hydrochloride, the two unfolded subunits were mixed with an *alive:dead* ratio of 1:9 and then refolded by dilution into DPBS buffer. By using a large excess of *dead* subunits compared to *alive* subunits, we maximized the formation of mST while minimizing the formation of higher oligomeric forms of ST. It is important to notice that because the *dead* subunit does not have a 6xHis-tag, the homotetramer composed of *dead* subunits, which is the other majority species formed during the refolding step is not purified.

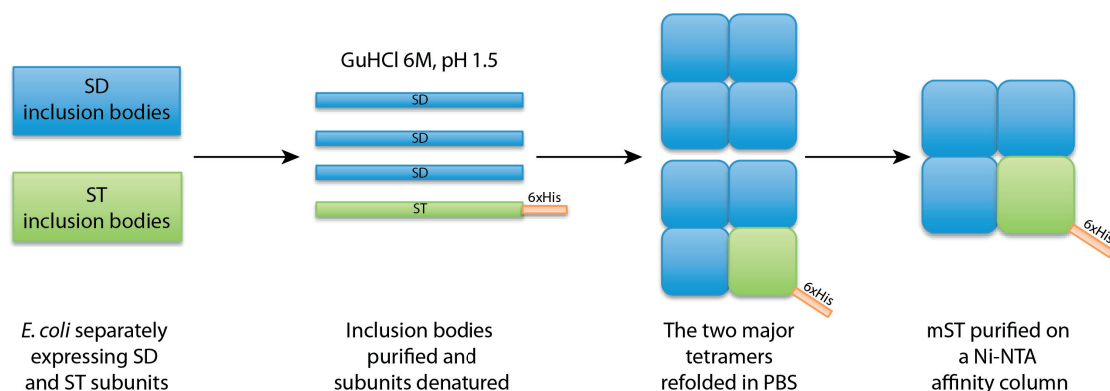


Figure 3.2: **Generation of mST.** Streptavidin-*dead* (SD) and StrepTactin-*alive* (ST) were expressed separately in *E. coli*. Inclusion bodies were extracted and solubilized in 6 M GuHCl (pH 1.5). To generate mST, SD and ST subunits were combined in a 9:1 ratio and refolded by rapid dilution in DPBS. This refolding generated a mixture of mST and SD tetramers. mST, which has a His-tagged subunit, was purified by Ni-NTA affinity chromatography.

3.4.2 Verification of tetramer subunit composition

In order to check the tetramer composition, we broke it into monomers by boiling the sample before loading on SDS-PAGE (Figure 3.3). The two distinct bands just below 15 kDa correspond to the *dead* and *alive* subunits (Figure 3.3A, 2nd lane). The *alive* subunit (upper band) has a higher mass due to the presence of the 6xHis-tag. Under similar conditions, homotetrameric StrepTactin resulted in a single band (Figure 3.3B, 2nd lane). These results are in agreement with the subunit composition of mST.

3.4.3 Binding to biotin

To assess the binding of biotin to mST, fluorescence correlation spectroscopy (FCS) was used. FCS is a powerful single-molecule detection technique that exploits temporal fluorescence

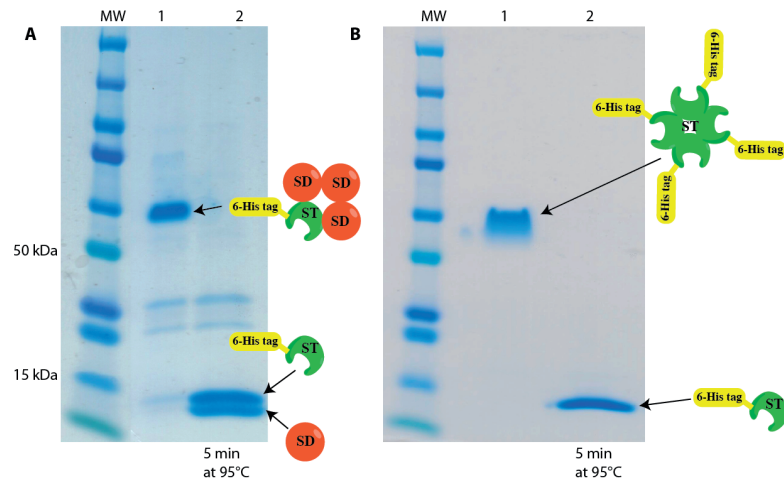


Figure 3.3: Coomassie blue stained SDS-PAGE of StrepTactin tetramers under nondenaturing conditions (lane 1) or denaturing conditions (95°C, 5 min) to break the tetramers into monomers (lane 2). A. Monovalent StrepTactin (mST). B. Tetraivalent StrepTactin.

intensity fluctuations produced by a small number of fluorescently labeled molecules diffusing into and out of the confocal detection volume of about 10^{-15} L (Figure 3.4A-B) to characterize diffusional mobility, concentration, and brightness of the labeled molecules [248].

The time a molecule spends in the detection volume (diffusion time, τ_d) is directly related to its molecular mass M according to equation 3.4. An increase in diffusion time shifts the autocorrelation curve also to longer correlation times. Thus freely diffusing biotin can be easily discriminated from bound biotin by measuring the respective diffusion time. The autocorrelation data and fitting curves for biotin-Atto633 in absence or in presence of an excess of mST are shown in Figure 3.4C. Using a three-dimensional one-component fit we obtained diffusion times of $\tau_d=58$ and $\tau_d=227 \mu\text{s}$ for free biotin and bound biotin, respectively. These values correspond to species having a molecular mass of about 1 and 60 kDa, which is in good agreement with the theoretical values of M of biotin-atto633 and mST. This result indicates that our mST construct is functional with respect to biotin binding.

We attempted to evaluate the valency of our mST construct by a FCS titration approach in which a fixed concentration of biotin-Atto633 (20 nM) was titrated with increasing concentrations of SA, ST or mST (0-50 nM). The resulting autocorrelation curves are displayed in Figure 3.4D-F. Due to the numerous parameters that can influence the FCS measurements of the present experiment, such as the brightness of the diffusing species (multiple species of different brightness for SA and ST, quenching phenomenon), the accuracy of the concentration of the different samples, and the potential presence of non-labeled biotins or free dyes, a quantitative analysis turned out to be difficult. From a qualitative perspective however, the differences between the three tetramers are obvious. Titrations with SA (Figure 3.4D) and ST (Figure 3.4E), which have both four biotin binding sites, display almost identical behavior with a sudden shift of the correlation curves to longer times at a given concentration. In the case

Chapter 3. Monovalent StrepTactin

of mST (Figure 3.4F), this shift is more gradual. This finding supports the fact that our mST construct has a unique biotin binding site.

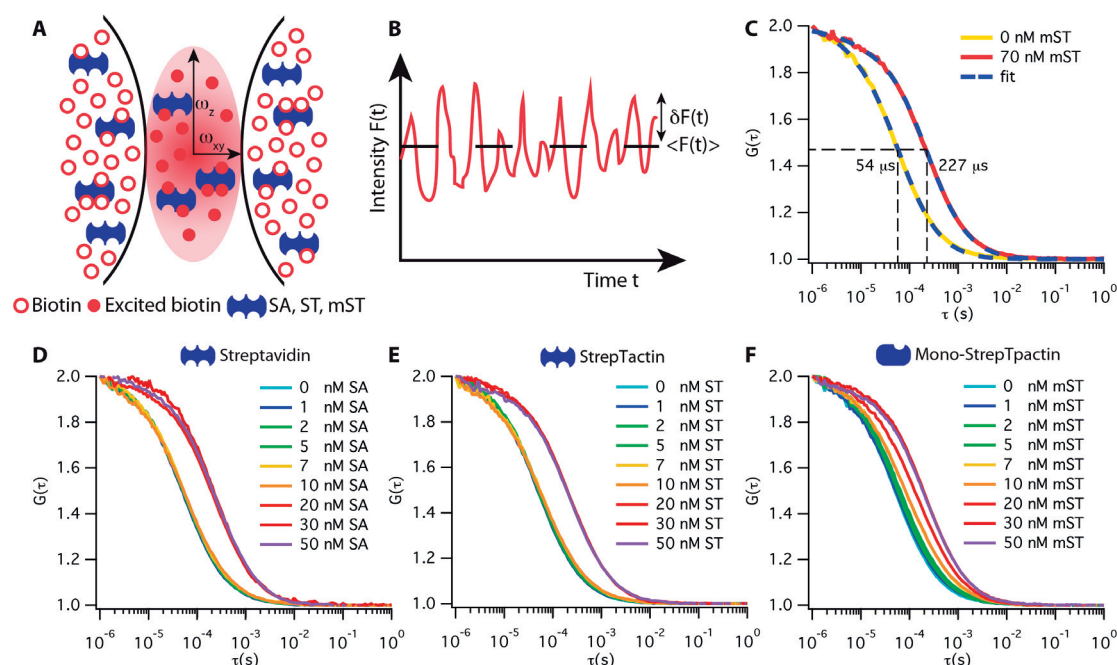


Figure 3.4: FCS to probe interaction of streptavidin (SA), StrepTactin (ST) and monovalent StrepTactin (mST) with biotin. (A) Scheme of FCS. A tightly focused laser beam (red ellipse) excites fluorophores linked to biotin (red filled circles). (B) Excited biotin leads to fluctuations in the fluorescence time trace. (C) Autocorrelation functions (ACFs) for 20 nM of biotin-Atto633 in absence or presence of 70 nM of mST. The ACFs were fitted with a 3D 1-component diffusion model (blue dashed lines). (D) ACFs for 20 nM biotin-Atto633 titrated with SA from 0 to 50 nM. (E)-(F) Same as (D), but with ST and mST, respectively.

3.4.4 Binding to Strep-Tag II

mST binding to Strep-tagged proteins was investigated by surface plasmon resonance (SPR) spectroscopy [249]. This label-free technique exploits the phenomenon of SPR to monitor bimolecular interactions in real-time. Its principle is schematically represented in Figure 3.5. Monochromatic p-polarized light is applied to the surface of a gold-coated sensor chip. The intensity of the reflected light drops at certain incident angle (SPR angle) due to plasmon resonance. The SPR angle is very sensitive to the refractive index of the solution near the surface of the sensor. Interaction of any molecules with the surface induces an increase of the refractive index, which causes a shift of the SPR angle. Injection of solubilized, purified Strep-tagged 5-HT₃R_s (kindly provided by Cédric Deluz [247]) on a mST-functionalized sensor chip led to a strong increase of the SPR signal (Figure 3.5 - right), demonstrating the binding functionality of mST toward Strep-Tag II.

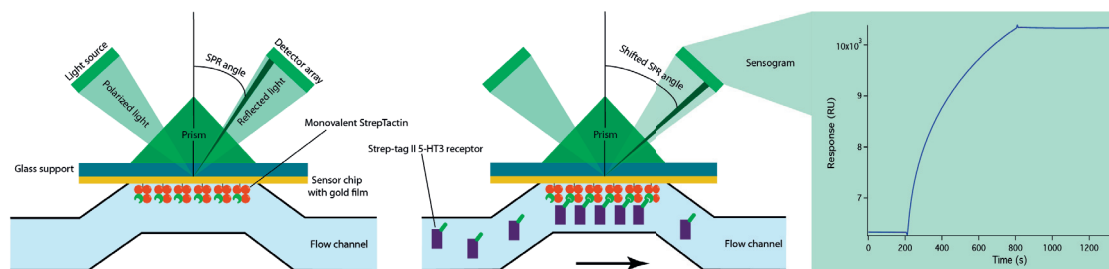


Figure 3.5: **Biacore's SPR biosensor to measure binding of mST to StrepTagII-5-HT₃R.** Gold surface covered with a layer of carboxymethylated dextran (not shown) was functionalized with mST via EDC/NHS mediated amino coupling procedure. Then solubilized Strep-tagged 5-HT₃R was injected on the surface. The binding of the latter to mST resulted to an increase of the SPR signal measured in resonance units (RU). The recorded sensogram is shown on the right.

3.4.5 Organic dye-mST conjugate for labeling membrane receptors in living cells

In order to test the binding functionality of our mST construct on living cells, mST was conjugated to the organic dye Atto635 via NHS ester reaction to primary amines (Figure 3.6A). mST-Atto635 was characterized using FCS. The molecular brightness (i.e. the mean fluorescence count rate per molecule or CPM) of mST-Atto635 was about 1.5 times that of the free dye, indicating that we are close to a 1:1 ratio (Figure 3.6B). Fluorescence confocal microscopy showed that mST-Atto635 is able to specifically bind Strep-tagged receptors in the plasma membrane of living cells (Figure 3.6C).

3.4.6 mST-QDot conjugate for tracking individual receptors in living cells

Fluorescent semiconductor QDots have recently emerged as a powerful tool to probe biological processes at the single-molecule level [129]. The major advantage of QDots over fluorescent dyes and proteins is their extremely high brightness and photo-stability, thus allowing high resolution and long term tracking of individual molecules [250]. Here we functionalized CdSe:ZnS QDots with mST and evaluated their potential for labeling and tracking cell membrane receptors.

QDots were coupled to mST via an amine-to-amine crosslinker (Figure 3.7A). Fluorescence confocal microscopy (Figure 3.7B) showed that 10 nM of mST-QDots stained the membranes of cells expressing Strep-tagged 5-HT₃R but not those not expressing the receptor. mST-QDots are therefore suitable for ensemble measurements.

Lowering the concentration of mST-QDots in order to label only a few receptors per cells was not successful. Despite testing numerous labeling conditions by varying concentration and incubation time, the difference between cells expressing and not expressing Strep-tagged 5-HT₃R was insignificant (data not shown). This suggests that affinity of mST towards the StrepTag is not strong enough to reliably track single molecules in living cells.

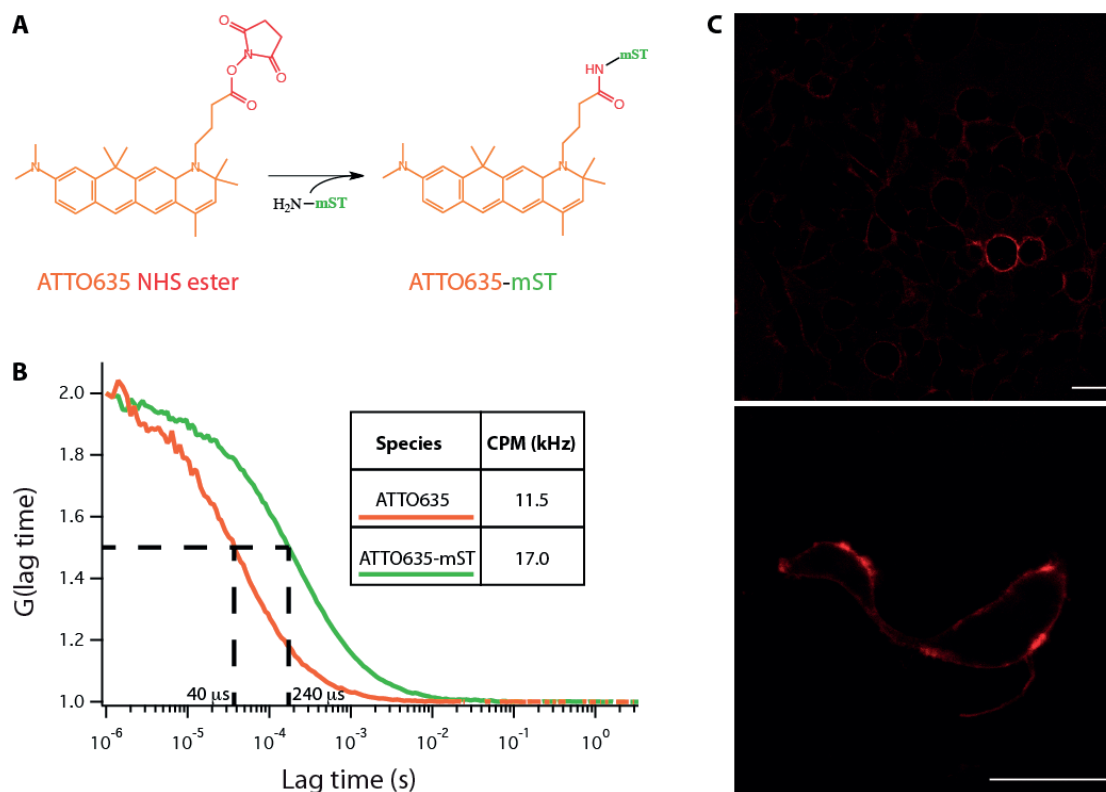


Figure 3.6: mST-organic dye conjugation and characterization. (A) Conjugation reaction between an organic dye, Atto635-NHS ester, and an amino group of mST yielding a stable carboxamide-linked conjugate. (B) ACFs and molecular brightness (CPM) for mST-Atto635 conjugate and free dye. (C) Confocal fluorescence images showing living HEK293 cells stably (top) or transiently (bottom) expressing Strep-tagged 5-HT₃R labeled with 100 nM mST-Atto635.

To track individual membrane receptors through mST, a biotin molecule had to be attached to the receptors. Cells stably expressing ACP-NK1R, labeled with CoA-biotin, and incubated with 100 pM of mST-QDots, resulted in the presence of a few tens of diffusing QDots (Figure 3.7 C, left), whereas QDots were absent from the plasma membrane of cells not expressing ACP-NK1R, but still labeled with CoA-biotin (Figure 3.7 C, right). Individual receptor trajectories from a single cell and their corresponding MSD vs t_{lag} plots are shown in Figure 3.7D. Diffusion of the NK1R is very heterogeneous and transitions between modes of motion during the course of some trajectories were observed (Figure 3.8).

3.4.7 SA-QDots vs. mST-QDots to track membrane receptor dynamics

A major drawback of the widely used streptavidin-biotin couple is the potential risk of cross-linking (i.e. one Qdot binds to several receptors). Receptor cross-linking may strongly affect the diffusion and internalization of membrane receptors or even influence their signaling function [121]. In this respect, we were concerned that the commercial SA-QDots previously

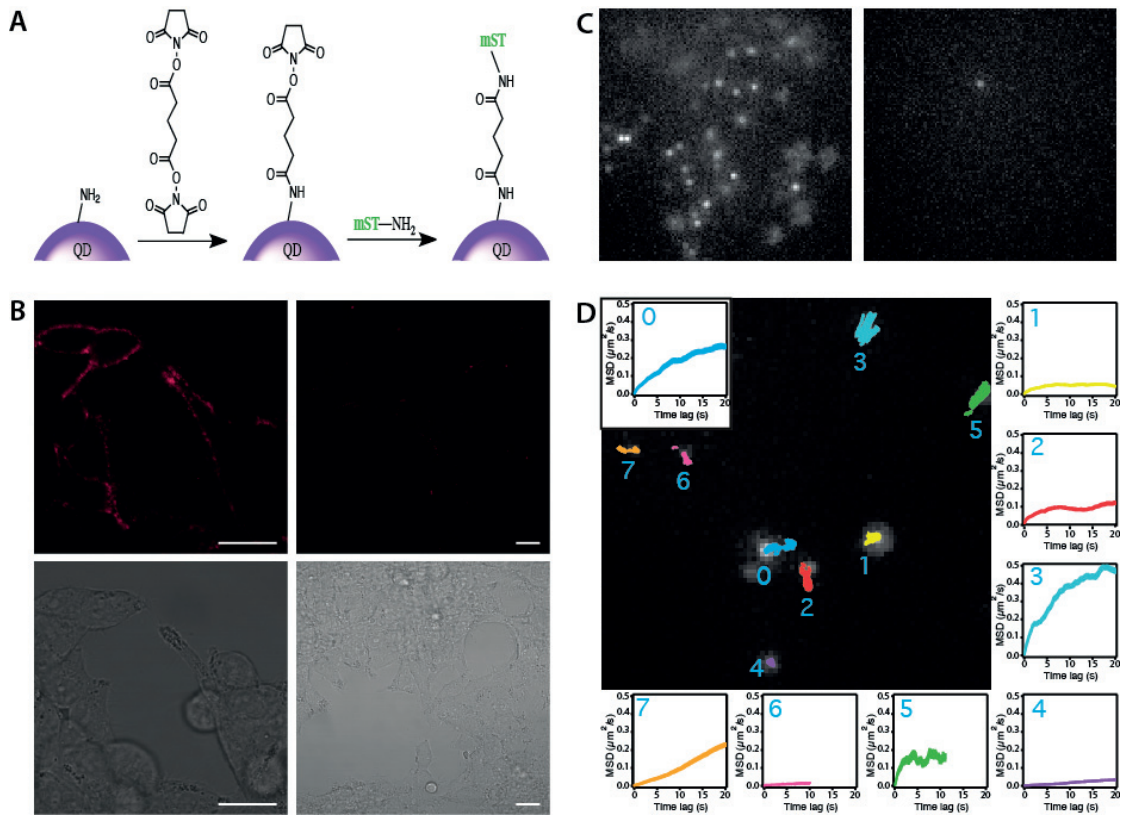


Figure 3.7: **mST-QDot conjugation, characterization and tracking.** (A) Functionalization of QDot with mST using bis[sulfosuccinimidyl] suberate (BS³), an homo-bifunctional amine-to-amine crosslinker. (B) Confocal fluorescence images (top) and the corresponding transmission images (bottom) of living HEK293 cells stably expressing (left) or not expressing (right, negative control) Strep-tagged 5-HT₃R, and labeled with mST-QDots (10 nM). (C) (Left) Wide-field fluorescence image of living HEK293 cells, stably expressing ACP-NK1R, labeled with CoA-biotin and incubated with mST-QDots (100 pM); (right) negative control: HEK293 cells not expressing ACP-NK1R, labeled with CoA-biotin and incubated with mST-QDots (100 pM). (D) Diffusion trajectories of individual biotinylated NK1Rs labeled with mST-QDot in the upper cell membrane of single cell and the corresponding MSD versus t_{lag} plots. The averaged diffusion coefficients range from 0.003 to 0.02 $\mu\text{m}^2/\text{s}$.

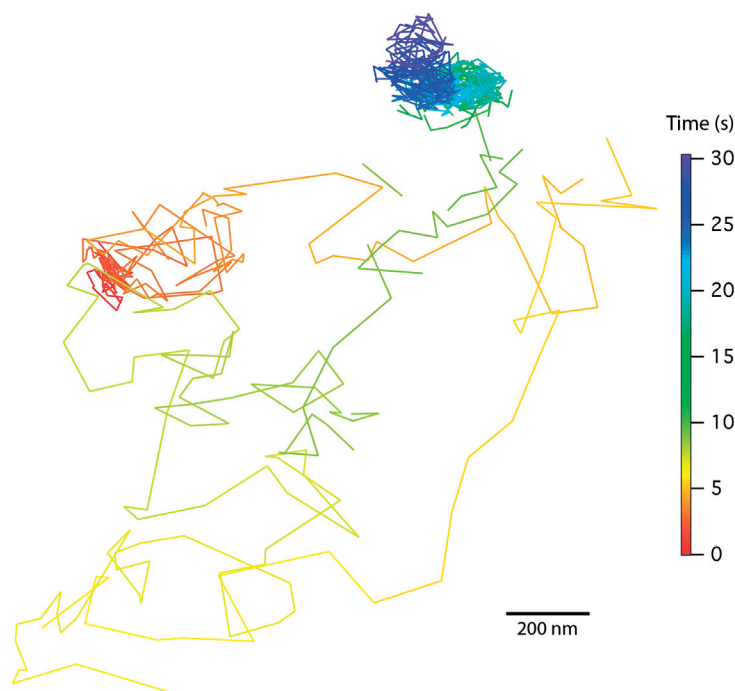


Figure 3.8: **Heterogenous diffusion within a single receptor trajectory.** 1000-frames trajectory (33 Hz) of a single biotinylated NK1R labeled with a single mST-QDot. At the beginning the receptor diffusion is confined, then it becomes Brownian, before it becomes again confined.

used to track biotinylated NK1Rs (chapter 2, p. 39) could induce cross-linking, thus altering the mobility of the receptors. We compared the initial diffusion coefficients (D_{1-10}) and the Hurst parameters (S_{MSS}) obtained with SA-QDots and mST-QDots and found no significant difference (Figure 3.9). These results suggest that, in the present case, NK1R cross-linking by SA-QDots is negligible. However this does not mean that SA-QDots cannot cause receptor cross-linking. Parameters such as expression level and oligomerization state of the receptor have to be taken into account. In the present case, the fact that the NK1R is monomeric [196] and expressed at moderate level ($\sim 25,000$ receptors per cell [196]) are conditions that tend to minimize the risk of cross-linking.

3.5 Conclusion

mST allows direct, one step labeling of Strep-tagged membrane proteins, without risk of cross-linking. The use of the genetically-encoded Strep-Tag II allows to bypass the enzymatic biotinylation step, providing a certain superiority over the streptavidin-biotin system in terms of simplicity, rapidity and specificity. However for single molecule applications, the micromolar affinity of StrepTactin for Strep-Tag II cannot compete with its femtomolar affinity for biotin, and constitutes the major limitation of system.

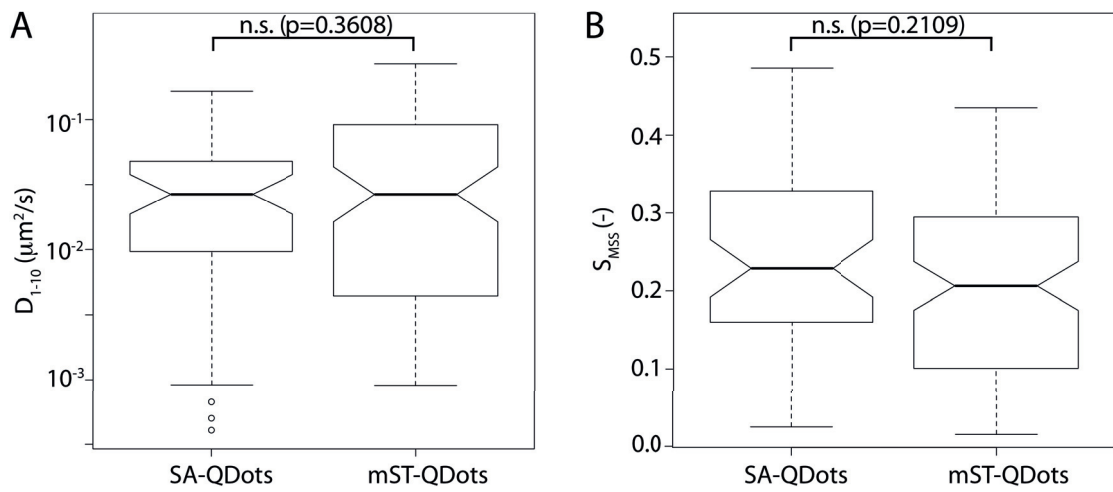


Figure 3.9: **Comparison of SA-QDots and mST-QDots diffusion.** (A) Boxplots of the diffusion coefficient D_{1-10} of biotinylated NK1Rs labeled with SA-QDots (right, $n=53$) or mST-QDots (left, $n=95$). (B) Boxplots of the Hurst parameter S_{MSS} for the same trajectories than in A. The median is drawn as a horizontal line. Notches indicate the 95% confidence interval of the median. Boxes represent the interquartile ranges of the distribution. P-values are from a Wilcoxon rank sum test, testing the null hypothesis H_0 : SA-QDots population is not different from mST-QDots population.

4 Tracking 5-HT₃ receptor dynamics using a fluorescent nanobody

4.1 Abstract

Diffusion of cell surface receptors is of critical importance for correct localization and regulation of receptor activity. In this context, single-molecule fluorescence techniques that allow to follow the motion of individual receptors are particularly attractive as they reveal the full distribution of molecule behaviors and circumvent the averaging inherent in traditional ensemble measurements. Here, we used a fluorescent nanobody (VHH15-CF640R) to track the 5-HT₃ receptor in the plasma membrane of living neuronal cells. This novel high-affinity label which is small, monovalent and highly photostable enabled long-term tracking of individual 5-HT₃Rs and revealed a surprising and intriguing diffusional behavior of some receptors.

4.2 Introduction

Single-molecule tracking (SMT) fluorescence microscopy offers a unique way to directly observe individual molecules at work in living cells. By overcoming averaging intrinsic to ensemble measurements, SMT yields critical information for elucidating the molecular basis of dynamic events taking place in a complex and heterogeneous environment such as the plasma membrane. SMT not only probes the dynamic behavior of the investigated molecules but also provides fundamental insights into the organization of the surrounding membrane and the molecular interactions between membrane components [251, 170].

In order to detect single biomolecules optically, they have to be labeled specifically with an optical probe. For fluorescence microscopy the ideal probe should (i) bind the target molecule with high affinity and specificity, (ii) be highly photostable (for long-term observations), (iii) be extremely bright (for precise localization), (iv) be monovalent (to avoid cross-linking), (v) not perturb the dynamics and functions of the target molecule, and (vi) be as small as possible (to access narrow spaces). Although this perfect probe is still a biophysicist's dream, the past few

Chapter 4. Tracking 5-HT₃ receptor dynamics using a fluorescent nanobody

years have seen the semiconductor quantum dots become ever smaller [252] and the organic dyes ever more stable [146], making these two fluorophores still more attractive. Here we used CF640R, a novel rhodamine-based far-red dye. Its excellent fluorescence quantum yield and exceptional photostability, combined with its remarkable low non-specific binding to cells, make it a prime candidate for single-molecule imaging [253, 254]. The ligand used to attach the fluorophore to the target biomolecule plays also a key role in this quest of the perfect probe. Commonly used streptavidin and conventional antibodies are large and multivalent, abolishing the benefits of the newly developed small photostable fluorophores. Small probes are not only less likely to interfere with the dynamics and function of the target molecule, but also minimize the linkage error caused by the displacement of the fluorophore. This last point is of particular importance for super-resolution localization microscopy [255].

Here we took advantage of the recently developed single-domain antibodies. Camelids such as llamas produce antibodies which naturally lack light chains. The antigen binding fragment of these heavy-chain-only antibodies, termed nanobody or VHH, consists of a single monomeric variable domain which can be easily expressed recombinantly [256]. The small size, monovalency, robustness, and ease of production of nanobodies have made them a promising and versatile tool for molecular imaging and therapeutic purposes [257, 258, 259]. In structural biology, the use of nanobodies as crystallization chaperones led to the elucidation of the X-ray structure of major membrane receptors such as the β 2 adrenergic-Gs protein complex [260] or the mouse 5-HT₃R [96].

For single-molecule tracking experiments, the employment of nanobody-based probes is still in its infancy. The few single-molecule studies dealing with nanobodies have mostly used nanobodies targeting fluorescent proteins fused to the protein of interest [255, 261, 262, 263, 264].

In this paper, we designed VHH15-CF640R, a fluorescent nanobody that binds directly, and with high affinity to the 5-hydroxytryptamine type 3 receptor (5-HT₃R) [96]. This cationic ligand-gated ion channel, belonging to the pentameric Cys-loop receptor superfamily [91], is present in the central and peripheral nervous systems where it mediates and modulates fast excitatory responses to serotonin (5-HT). It is the target of potent drugs used to treat and prevent nausea and vomiting triggered by chemotherapy [265]; 5-HT₃R antagonists may also be used in personalized medicine for treating complex psychiatric disorders such as anxiety, depression or psychosis [108].

Single-molecule investigations on the mobility of other members of the Cys-loop receptor superfamily, such as the glycine [266], GABA [209] and AMPA [267] receptors have highlighted the importance of the dynamic movements of these receptors in the regulation of synaptic transmission [251, 268].

The diffusional behavior of the 5-HT₃R has not been extensively studied and our understanding of the principles underlying its organization in the cellular plasma membrane is extremely limited. Herein, we demonstrate the potential of VHH15-CF640R for direct labeling and track-

ing of individual native 5-HT₃R_s and resolve the influence of the cytoskeleton on the complex mobility pattern of this particular serotonin receptor.

4.3 Materials and methods

4.3.1 Materials

Materials for cell culture like DMEM:F-12 with GlutaMAX, newborn calf serum (NBCS), trypsin-EDTA, Dulbecco's PBS, and blasticidin were from Invitrogen. Hygromycin was from Roche. Tetracycline and laminin (from mouse Engelbreth-Holm-Swarm sarcoma) were from Sigma-Aldrich. Poly-D-lysine was from EMD Millipore. Complete neurobasal growth medium was kindly provided by Lillian Glauser (Laboratory of Prof. Johannes Gräff, EPFL). VHH15 [96] with a single C-terminal cysteine was a gift from Ghérici Hassaine (Theranyx, Marseille). CF640R-maleimide, Tris(2-carboxyethyl)phosphine hydrochloride (TCEP·HCl), bovine serum albumine (BSA), latrunculin A and nocodazole were purchased from Sigma-Aldrich.

4.3.2 Cell culture

T-REx-293 cell line stably expressing the mouse wild-type 5-HT_{3A} receptor [247] and neuroblastoma x glioma hybrid NG108-15 cells (Sigma-Aldrich) were cultured at 37°C under a humidified 5% CO₂ atmosphere in tissue culture-treated flasks (TPP) containing DMEM/F12 medium and 10% v/v NBCS. T-REx-293 stable cells were kept under selective pressure by the presence of 100 µg/ml hygromycin and 5 µg/ml blasticidin. When cells reached 80-100% confluence they were detached from the surface by trypsinization or DPBS (without calcium or magnesium), and reseeded by a 5-50 fold dilution into fresh medium. NG108-15 cells were seeded 24-48 h before microscopy experiments in 8-well chambered glass slides (Nunc). T-REx stable cells were grown in absence of antibiotics on 8-well chambered glass slides and 5-HT₃R expression was induced by adding 5 µg/ml tetracycline 24 h after seeding and 48 h before measuring.

Newborn mouse primary cortical neurons were obtained from Lillian Glauser. The cells were grown in 8-well chambered glass slides pre-coated with mouse laminin (32 µg/ml) and poly-D-lysine (200 µg/ml) in neurobasal medium supplemented with B27 (2% v/v), L-glutamine (500 µM) and penicillin/streptomycin (100 U/ml). Experiments were performed on cultures grown for ~14 days.

4.3.3 Synthesis of VHH15-CF640R

VHH-15 (133 µg) containing a single C-terminal cysteine residue were reduced by incubation with 100 mM TCEP in DPBS for 20 min at room temperature under argon. CF640R-maleimide was added in 10-fold molar excess and incubated with rocking for 2 h at room temperature, protected from light. Labeled nanobodies were separated from free CF640R-maleimide by gel

filtration using a Sephadex G-25 column (GE-healthcare).

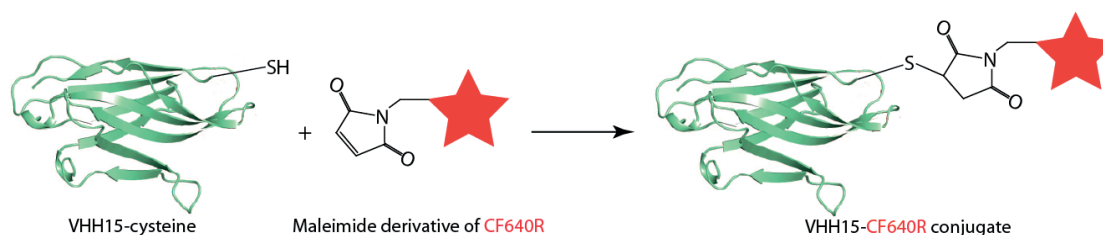


Figure 4.1: Reaction conjugation of VHH15 with CF640R-maleimide at cysteine residue.

4.3.4 5-HT₃R labeling

Prior to labeling, cells were washed 1x with warm (34 °C) serum-free, phenol red-free DMEM supplemented with 1% BSA. For confocal microscopy, cells were incubated with 200 nM VHH15-CF640R for 45 min at 37°C. For SMT experiments, NG108-15 cells were incubated with 100 pM VHH15-CF640R for 30 min at 37°C. For T-REx stable cells and primary cortical neurons, VHH15-CF640R concentrations of 10 pM and 200 nM were used, respectively. Imaging was performed in serum-free, phenol red-free medium supplemented with 1% BSA.

4.3.5 Drug treatments

Latrunculin A and nocodazole were dissolved in DMSO. The treatment of cells with cytoskeleton-disrupting drugs was done by incubating the cells in serum-free, phenol red-free DMEM supplemented with 1% BSA, and containing either 1 μ M latrunculin A (0.01% DMSO) or 10 μ M nocodazole (0.05% DMSO) at 37 °C. SMT measurements were performed 5 min or 10 min after latrunculin A or nocodazole addition respectively, and carried out only during the first 20 minutes after addition of the drug without washing.

4.3.6 Confocal microscopy

Confocal micrographs were taken using a LSM510 Meta laser scanning microscope (Zeiss) equipped with a 63X/1.2NA water-immersion objective using the red HeNE laser (633 nm) and appropriate excitation and emission filters. Fluorescence was detected using photomultiplier tubes (PMT).

4.3.7 SMT experiments

Measurements were performed on the basal plasma membrane of the cell body using total internal reflection fluorescence (TIRF) microscopy. A schematic view of the experimental setup can be found in Appendix A (p. 96). The samples were mounted on an inverted fluorescence microscope (Nikon Eclipse Ti), equipped with a high numerical aperture oil objective (Apo

TIRF 100x, NA 1.49, Nikon). A 640 nm Obis diode laser (Coherent Inc.) was used in combination with an AOTF (acousto-optical tunable filter) to illuminate the sample with 100 ms exposure time and excitation intensity around 0.5 W/cm^2 . Movies of typically 500 frames were recorded at 10 Hz on an EMCCD camera (Ixon 887BV, Andor Technology). The region-of-interest was set to 128 x 128 pixels. The image pixel size was 160 nm.

4.3.8 Data analysis

SMT data analysis was performed using a home-written software in IGOR PRO (WaveMetrics), as detailed elsewhere [269]. Briefly, trajectories were reconstituted by linking fluorescent peaks in successive frames. Trajectories with a minimum of length of 200 frames were then segmented using a sliding window of 100 frames. Each resulting segment was treated as an individual trajectory from which the initial diffusion coefficient (D_{1-10}) and the Hurst parameter (S_{MSS}) were determined. D_{1-10} was evaluated from a linear fit to the first 10 time intervals of a standard means square displacement (MSD) *versus* t_{lag} plot. S_{MSS} , which corresponds to the slope of the moment scaling spectrum (MSS) [157] is a reliable parameter to identify the mode of motions; a S_{MSS} value between and 0.5 indicates sub-diffusion (e.g., confined diffusion) and a value between 0.5 and 1 characterizes super-diffusion (e.g., diffusion resulting from active cellular transport processes); Brownian movements are represented by S_{MSS} values around 0.5. D_{1-10} and S_{MSS} parameters were combined in a color-coded, two-dimensional probability density plot (mobility pattern) using the functions *kde2d()* and *filled.contour()* in R (R Foundation for Statistical Computing). Bandwidths of 0.4 on the x axis, corresponding to $\log_{10}(D_{1-10})$, and 0.11 on the y axis, corresponding to S_{MSS} , were used. Box plots showing the distribution of both parameters were computed using the averaged values of the full-length trajectories (calculated from the segments constituting the trajectory).

4.4 Results

4.4.1 Direct labeling of the 5-HT₃R using a fluorescently labeled VHH

5-HT₃Rs present in the plasma membrane of live cells were labeled with VHH15-CF640R, a single-domain antibody (VHH) against the 5-HT₃R [96] to which a small organic red fluorescent dye (CF640R) has been chemically attached. The ability of VHH15-CF640R to specifically bind to the 5-HT₃R was assessed using confocal microscopy (Figure 4.2). TRex-HEK293 cells stably expressing large amounts of recombinant 5-HT₃R (1-2 million receptors per cell [247]) exhibited high levels of surface labeling (Figure 4.2B). NG108-15 cells, which endogenously expressed modest levels of 5-HT₃R displayed weaker and more punctuate staining at the plasma membrane (Figure 4.2A). No labeling was observed at the membrane of HEK293 which do not express the receptor (negative control, Figure 4.2C), thus demonstrating the probe's specificity.

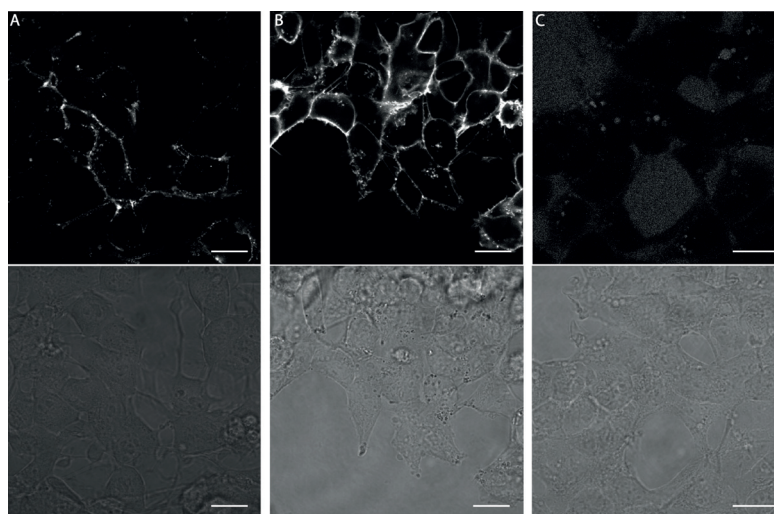


Figure 4.2: Confocal fluorescence micrographs (upper panels) and white light transmission images (lower panels) showing VHH15-CF640R staining of 5-HT₃R in (A) NG108-15 cells, (B) tetracycline-inducible TRex-HEK293 stable cell line expressing the mouse homopentameric 5-HT_{3A} receptor, and (C) TRex-HEK293 parental cells (negative control, without washing). Scale bars correspond to 20 μm .

4.4.2 VHH15-CF640: a perfect probe for tracking individual 5-HT₃Rs

By using VHH15-CF640R concentrations in the picomolar range, about ten receptors per cell were labeled. In addition to being highly specific, the binding of VHH15 to 5-HT₃R is quasi irreversible ($k_{\text{off}} = 4.7 \cdot 10^{-6} \text{ s}^{-1}$ [96], corresponding to $t_{1/2} \approx 41 \text{ h}$). This extreme affinity, combined with the high photostability of CF640R, allowed us to monitor the lateral movements of individual receptors for extended periods of time. The good quantum yield of CF640R, its observation in the red spectral region where cellular autofluorescence is significantly reduced, and the use TIRF microscopy enabled to obtain excellent signal-to-noise ratios (Figure 4.3A-B), improving significantly the tracking precision.

Our SMT experiments revealed an extraordinary diversity of complex trajectories (Figure 4.3C-D), corroborating observations reported in a previous study [270]. Freely diffusing, confined, immobile and directed 5-HT₃Rs were observed, but also receptors exhibiting transitions between these modes of motions. This heterogeneity is reflected in the broad distribution of initial diffusion coefficients (D_{1-10}), ranging from 0.001 to 0.5 $\mu\text{m}^2/\text{s}$, and Hurst parameters (S_{MSS}), ranging from 0 to 0.65 (Figure 4.4).

4.4.3 Comparison of the lateral mobility of heterologously and endogenously expressed receptors

We compared the mobility of the 5-HT₃R in NG108-15 neuroblastoma-glioma cells, which endogenously expressed moderate levels of the receptor, to that in HEK293, which over-

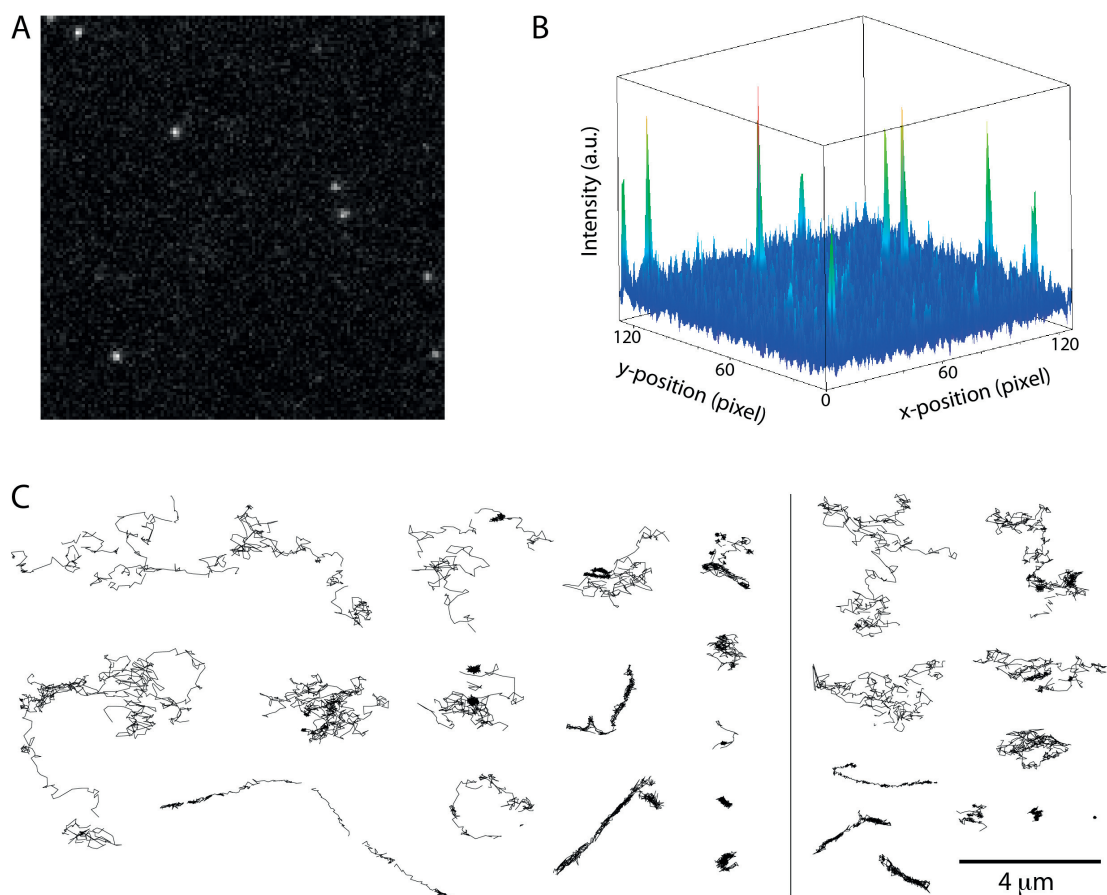


Figure 4.3: **Imaging and tracking of individual 5-HT₃R_s in living cells.** (A) Typical image of single VHH15-CF640R bound to 5-HT₃R in the basal plasma membrane of NG108-15 cells as imaged with TIRF microscopy. (B) 3D plot of the intensities of the single molecules imaged in A. (C) Trajectories of individual 5-HT₃R_s diffusing in the basal plasma membrane of NG108-15 cells (left) or TRex-HEK293 cells (right). The positions of the fluorescent probes were determined with sub-pixel accuracy using 2D Gaussian fitting of the fluorescent peaks. Single-molecule trajectories were reconstructed by linking the positions over time in a series of frames recorded at 10 Hz.

expressed the receptor on the order of millions of receptors per cell [247]. The two resulting mobility patterns display a similar overall shape but with a total redistribution of the mobile and confined fractions (Figure 4.4A-B). Receptors heterologously expressed in HEK293 cells exhibit a much more restricted lateral mobility than those natively expressed in NG108-15 cells; this is reflected by the significantly lower diffusion coefficients and lower Hurst parameters as revealed by the associated box plots (Figure 4.4C-D). The reduced mobility is very likely due to crowding effects related to high protein content in the membrane [271].

4.4.4 A particular diffusional behavior of 5-HT₃R in NG108-15 cells

The diffusion of the 5-HT₃R in NG108-15 showed numerous trajectories with a characteristic elongated shape, as represented on Figure 4.5A. These trajectories are defined by high diffusion coefficients ($> 0.05 \mu\text{m}^2/\text{s}$) and by Hurst parameters ranging from 0.2 to 0.6 (Figure 4.5C). Interestingly, receptors exhibiting such trajectories do not move only in one direction but rather back-and-forth, presumably along a structure underlying the plasma membrane (Figure 4.5B). These trajectories are hence not directed as might be expected, but they are Brownian ($S_{MSS} \approx 0.5$), directed ($S_{MSS} > 0.5$) and confined ($S_{MSS} < 0.5$) at the same time: the receptor exhibits a combination of Brownian diffusion and apparently directed movements, restricted in elongated domains.

4.4.5 Effect of cytoskeleton-disrupting agents on receptor mobility

We investigated whether this diffusion in elongated domains was the result of transport events along cytoskeletal components. We first disrupted the microtubules with 10 μM nocodazole, a microtubule-depolymerizing agent. This resulted in an increase of the fraction of immobile receptors ($D_{1-10} < 0.001 \mu\text{m}^2/\text{s}$, $S_{MSS} < 0.1$), whereas the highly mobile fraction remained unaffected (Figure 4.6B). A specific effect to nocodazole was the disappearance of the peak of intermediate mobility ($0.005 < D_{1-10} < 0.01 \mu\text{m}^2/\text{s}$, $0.15 < S_{MSS} < 0.35$) which is present both in non-treated cells and latrunculin A-treated cells.

We next probed the influence of the actin cytoskeleton on 5-HT₃R diffusion by treating the cells with 1 μM latrunculin A to disrupt the actin filaments. Surprisingly, this resulted in a significant decrease of the overall mobility of the receptor as reflected in the corresponding mobility pattern (Figure 4.6C). This effect was correlated with a decrease of the median short term diffusion coefficient (Figure 4.6D) and an increase of the confinement (lower S_{MSS} values) (Figure 4.6E). Importantly, the population of fast diffusing receptors ($D_{1-10} > 0.05 \mu\text{m}^2/\text{s}$), corresponding in particular to receptors diffusing in elongated domains was reduced (Figure 4.6C). As directed diffusion is characterized by S_{MSS} values > 0.5 , the proportion of directed segments was reduced from 16% to 8% after latrunculin A treatment. Taken together these results suggest that the actin cytoskeleton is involved in the particular diffusional behavior of the 5-HT₃R.

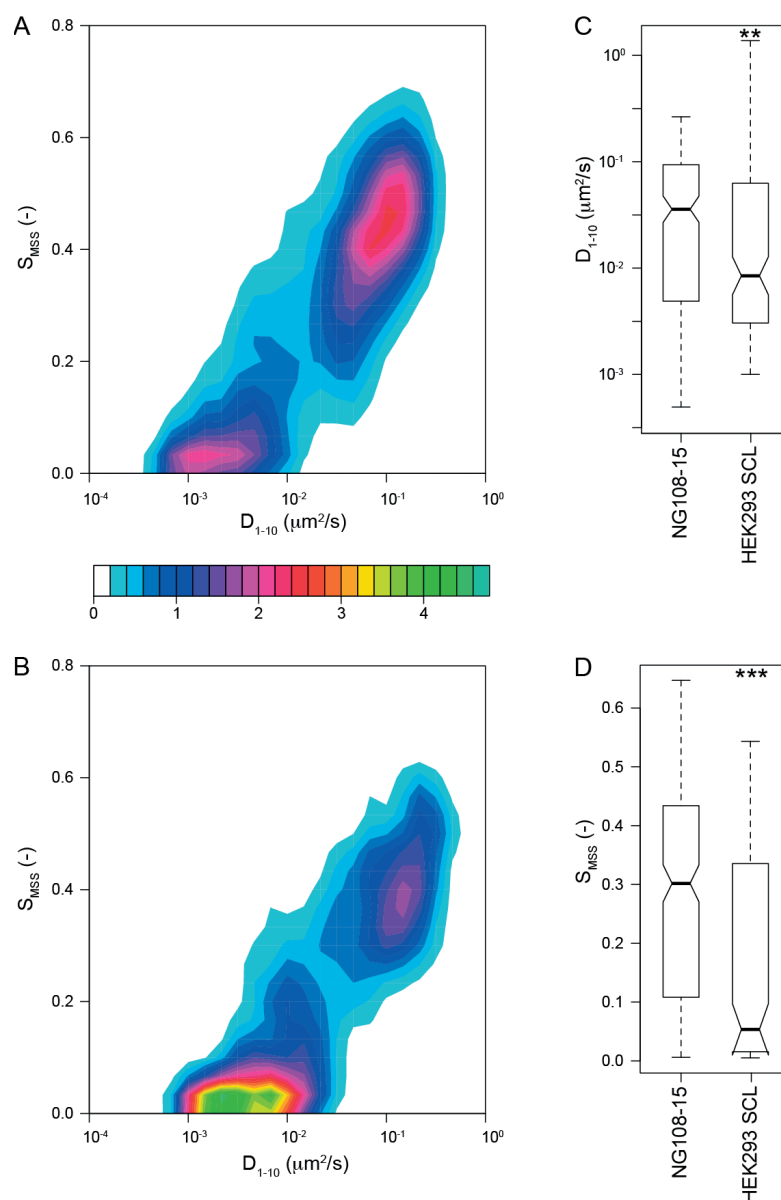


Figure 4.4: **Comparison of 5-HT₃R mobility in high- and low-expressing cells.** (A) Mobility pattern of 5-HT₃R in NG108-15 cells expressing low levels of the receptor (endogenous expression). (B) Mobility pattern of 5-HT₃R in HEK293 stable cell line (SCL) expressing high levels of the receptor. The color code scales with the indicated frequency (arbitrary units) of states. (C) Box plot of the diffusion coefficient D_{1-10} in NG108-15 (n=259) cells and in HEK293 SCL (n=133). (D) Box plot of the Hurst parameter S_{MSS} for the same trajectories as in C. The median is drawn as a horizontal line. Notches indicate the 95% confidence interval of the median. Boxes represent the interquartile ranges of the distribution. p-values were obtained by a Wilcoxon ranking test on the distribution; **p-value <0.01, ***p-value <0.001 with the null hypothesis (H_0) that population A is not different from population B.

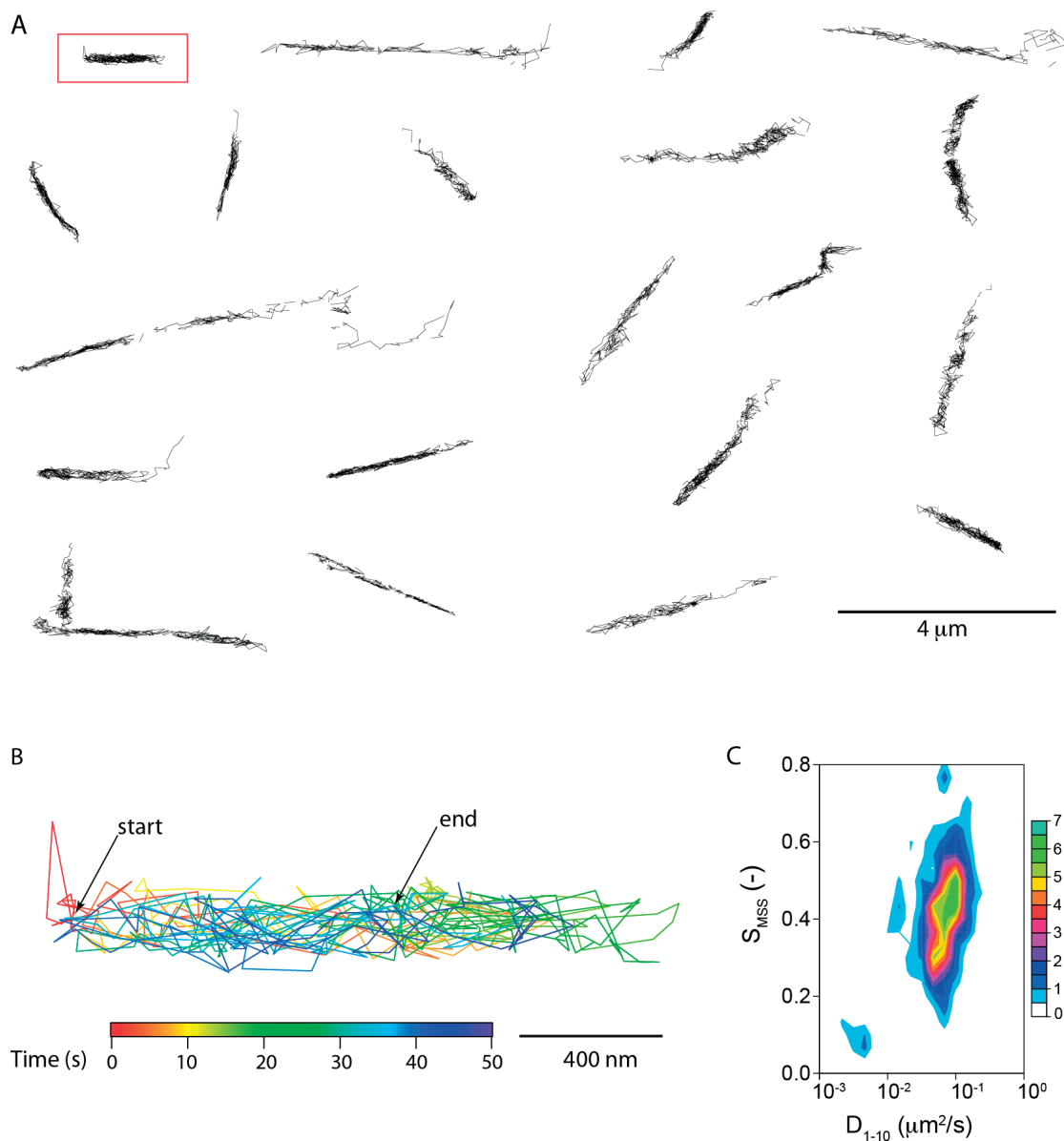


Figure 4.5: **Special diffusion of individual 5-HT₃Rs.** (A) Typical trajectories of 5-HT₃Rs diffusing in elongated domains at the basal plasma membrane of NG108-cells. (B) Trajectory (framed in red in A) colored according to time, highlighting the back-and-forth movements of the receptor. Start (t=0 s) and end (t=46 s) of the trajectory is indicated. (C) Mobility pattern of an arbitrary selection of elongated trajectories (n=21). The color code scales with the indicated frequency (arbitrary units) of states.

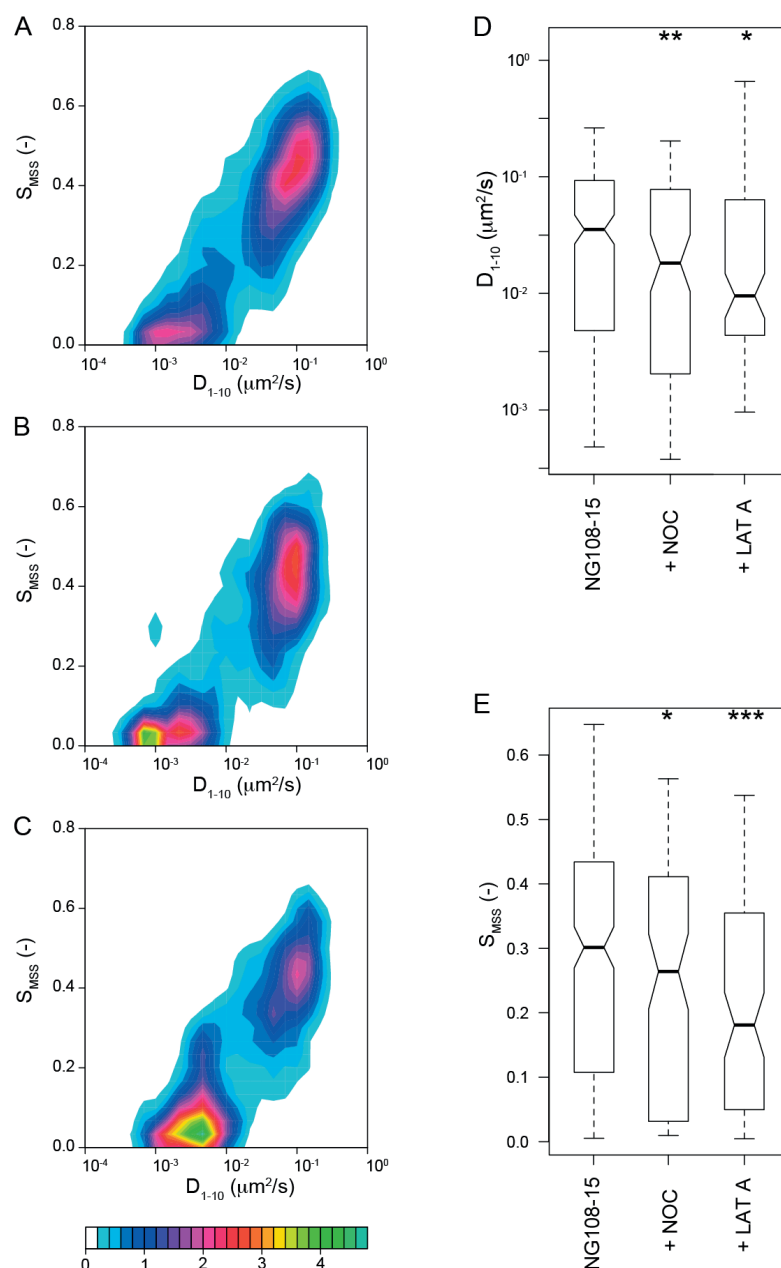


Figure 4.6: **Effect of cytoskeletal disruption on 5-HT₃R mobility in NG108-15 cells.** (A) Mobility pattern of 5-HT₃R in absence of cytoskeleton-disrupting drugs. (B) Mobility pattern in the presence of 10 μM nocodazole. (C) Mobility pattern in the presence of 1 μM latrunculin A. The color code scales with the indicated frequency (arbitrary units) of states. (D) Box plot of the diffusion coefficient D_{1-10} in absence of drugs (n=259), in the presence of nocodazole (NOC) (n=105), and in the presence of latrunculin A (LAT A) (n=90). (E) Box plot of the Hurst parameter S_{MSS} for the same trajectories as in (E). The median is drawn as a horizontal line. Notches indicate the 95% confidence interval of the median. Boxes represent the interquartile ranges of the distribution. p-values were obtained by a Wilcoxon ranking test on the distribution; *p-value <0.05, **p-value <0.01, ***p-value <0.001 with the null hypothesis (H₀) that population A is not different from population B.

SMT in primary neuronal cultures (preliminary results)

A few single-molecule trajectories were obtained on living primary mouse cortical neurons. A selection of trajectories is presented in Figure 4.7.

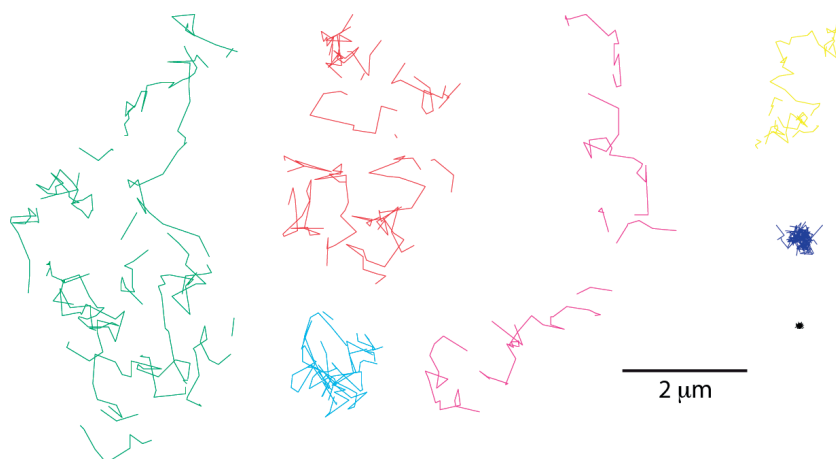


Figure 4.7: **Trajectories of individual 5-HT₃Rs diffusing in the cell body membrane of living neurons.**

4.5 Discussion

Nanobodies constitute a remarkable new tool for direct labeling of membrane proteins *in vivo*. Their small molecular size ($\sim 2 \times 4$ nm) is far less likely to cause interferences with the dynamics and functions of the target protein and allows them to access confined and crowded cellular regions. Moreover their monovalency prevents any risk of cross-linking, unlike streptavidin and conventional antibodies. Combined with a small organic dye having a good photostability, this makes a fluorescent probe with enormous potential for SMT.

Here we used VHH15-CF640R to label individual 5-HT₃Rs in the plasma membrane of living cells. VHH15 binds to the 5-HT₃R with high specificity and high affinity, at the interface between two adjacent A subunits [96]. The fact that up to five VHH15 molecules may bind to the receptor could be problematic for single-molecule imaging; however by using picomolar concentrations of VHH15 in order to label only a few tens of receptors per cell, one can reasonably assume that only mono-labeled receptors will be observed. The choice of the fluorophore is of critical importance for SMT [272]. To fully benefit from the reduced size of the nanobody, the fluorophore has to be small. In this respect, organic fluorescent dyes are the best candidates. Zanetti-Domingues *et al.* have recently evaluated what was the best dye for SMT experiments [253] by analyzing the brightness, photostability and non-specificity adhesion of many different dyes at the single-molecule level. Of the dyes they have examined, CF640R appeared to be the dye of choice for excitation with red light.

VHH15-CF640R enabled us to monitor the lateral diffusion of individual native receptors

with high precision over extended periods of time. Single-molecule trajectories of almost one minute were recorded with 100 ms temporal resolution. Such long trajectories are usually obtained using quantum dots or gold nanoparticles. Our SMT measurement allowed to highlight an intriguing behavior of some 5-HT₃R characterized by high diffusion coefficients and diffusing in a “pseudo-directed manner” in elongated domains with frequent back-and-forth movements. It is tempting to interpret this particular diffusional behavior as the result of a mechanism that would regulate the location of the 5-HT₃R on nerve terminals [273]. However, further experiments should be conducted in primary neurons to confirm this hypothesis.

Previous investigations on the localization of the 5-HT₃R in cell plasma membranes using fluorescence microscopy revealed a strong propensity of the receptor to colocalize with F-actin [274, 275]. Disrupting the actin cytoskeleton with the actin depolymerizing drug latrunculin A resulted in a significant decrease of the receptor mobility, consistent with a diminution of the fraction of receptors diffusing in elongated domains. This result contrast with previous studies on other ionotropic receptors, in which treatment with latrunculin A led generally to a reduction of the confinement and increase of the diffusion coefficient [276, 277, 278]. Emerit *et al.* have shown that treatment of NG108-15 cells with latruncunlin A induced aggregation of 5-HT₃R clusters with residual F-actin [274]. This aggregation phenomenon is very likely responsible for the observed decrease in receptor mobility. In addition to the actin meshwork, microtubules seem also to play a role in the in the dynamic organization of the 5-HT₃R in the cell membrane, albeit to a far lesser extent.

4.6 Conclusion

In conclusion, VHH15-CF640R turned out to be an exceptional fluorescent probe to image single 5-HT₃R in the plasma membrane of living cells. It allowed us to follow the diffusion of endogenous receptors over long time regimes, thus revealing rare trajectories of some individuals performing back-and-forth movements in elongated domains of several micrometers in length. Our data suggest that actin filaments are involved in this peculiar diffusional behavior. Future experiments will aim to figure out the dynamics of the 5-HT₃R in the context of synaptic biology.

Herein we have demonstrated the potential of fluorescent nanobodies for direct labeling and tracking of membrane receptors endogenously expressed in cultured neuronal cells. Because of their small size, fluorescent nanobodies may be of great interest to track the diffusion of individual molecules in narrow and sterically hindered spaces such as the synaptic cleft. Furthermore, as nanobodies can pass the blood-brain barrier [279], they could be used for observing the properties of individual receptors directly in the brain of living animals.

General conclusion and outlook

No one has ever seen or handled a single molecule. Molecular science, therefore, is one of those branches of study which deal with things invisible and imperceptible by our senses, and which cannot be subjected to direct experiment — James Clerk-Maxwell, Nature (1873).

What was once a scientist's dream has become a reality. The 2014 Nobel Prize in Chemistry was awarded to Eric Betzig, Stefan W. Hell, and William E. Moerner “for the development of superresolved fluorescence microscopy”. The first great breakthrough that led to this Nobel Prize was achieved in 1989, when Moerner demonstrated the possibility to optically detect a single molecule in a crystal at cryogenic temperatures [148]. Previously, single molecules were thought to be optically undetectable [280]. This thesis aimed to exploit the recent advances in experimental instrumentation that have made the detection of single molecules possible in order to increase our understating of fundamental biological processes. In particular, we used single-molecule fluorescence tracking microscopy to investigate the diffusional behavior of individual receptors embedded in the plasma membrane of living cells. Tracking of membrane proteins is a unique way to gain insights not only into the dynamics and biological functions of the tracked molecules, but also into the organization of the surrounding plasma membrane and the molecular interactions taking place in this highly heterogenous environment.

Observing single molecules in living cells is not a trivial task. The specific labeling of a small number of molecules of interest with a bright and photostable fluorescent probe is a critical prerequisite for a successful single-molecule tracking experiment. Thanks to the ultra-high affinity of the streptavidin-biotin couple and to the exceptional optical properties of QDots, we were able follow the diffusion of individual NK1 receptors with both high spatial and temporal resolution over long time periods. Thousands of single-molecule trajectories were recorded, revealing a pronounced heterogeneity in the mobility of this prototypical GPCR. In order to take into consideration potential changes in diffusion modes and to increase the amount of information that can be extracted from a single trajectory, we applied a segmentation algorithm, which sequentially cuts the original trajectory into shorter sub-trajectories. Each segment was then analyzed as an independent trajectory. For visualizing the huge amount of diffusional data thus generated, we used two-dimensional density plots of the initial diffusion coefficients versus the Hurst parameter which is associated to the mode of motion of the receptor. This novel way to represent single-molecule mobility, that we called “mobility pattern”, has proven to be an excellent tool to resolve highly heterogenous receptor populations, follow their

General conclusion and outlook

evolution over time and compare results obtained under different experimental conditions. Our results revealed the central importance of clathrin in regulation of NK1R mobility. We showed that the fraction of confined receptors at the basal state depends on the quantity of membrane-associated clathrin and that receptor confinement is correlated to a decrease of the canonical pathway activity of the receptor. These findings suggest the existence of a new clathrin-based mechanism for regulation of NK1 receptor activity and further support the critical role of membrane organization for regulation of GPCR signaling.

A major drawback of the widely used streptavidin-biotin couple is the risk of cross-linking (i.e. one QDot binds several receptors), which could affect the diffusion and biological functions of the target protein. Therefore we have generated a monovalent StrepTactin which can bind to biotinylated but also to Strep-tagged receptors with high affinity and virtually no risk of cross-linking. Fluorescent derivatives were used for direct one-step labeling of Strep-tagged receptors, bypassing the requirement of an initial biotinylation step. Single-particle tracking of biotinylated NK1Rs using monovalent StrepTactin-conjugated QDots yielded very similar diffusion coefficients to those obtained with streptavidin QDots. This allowed us to exclude cross-linking artifacts in the measured NK1R mobility.

Single domain antigen-binding fragments known as “nanobodies” have recently emerged as a powerful alternative to traditional antibodies, and might be the new magic bullet of medicine [281, 257]. In structural biology, nanobodies have been successfully used as crystallization chaperones to decipher the structure of challenging targets such as membrane proteins [282]. Here we used a fluorescent nanobody (VHH15-CF640R) to track endogenous 5-HT₃ receptors in neuronal cells. To our knowledge this is the first time that a fluorescent nanobody is used to perform single-molecule tracking on a native membrane receptor. The long trajectories recorded using VHH15-CF640R uncovered an extraordinary diversity of diffusional behaviors. In particular, receptors exhibiting back-and-forth movements in elongated domains of several micrometers in length have been observed, underlying a hypothetical mechanism for the regulation of 5-HT₃ receptor on nerve terminals. The small size and monovalency of nanobodies will be of great benefit for future studies in narrow or sterically hindered spaces such as the synaptic cleft. Furthermore, as nanobodies can pass the blood-brain barrier [279], they could be used for observing the properties of individual receptors directly in the brain of living animals. To sum up, we are convinced that the potential of nanobody-based probes for biophysical and biomedical research is huge and that fluorescent nanobodies such as the one presented in this thesis will allow to elucidate number of unknown cellular mechanisms in a near future.

Our recent ability to observe and manipulate single molecules in living cells has revolutionized our understanding of numerous biological processes. However, Maxwell is there to remind us that science is constantly evolving and our knowledge is transient and never complete.

Appendix

A Single-molecule microscopy setups (Wide-field/TIRF)

In this thesis, a homebuilt wide-field fluorescence microscopy setup with single-molecule sensitivity was used (Figure A.1) [153]. During the thesis, the system has been upgraded to perform total internal reflection fluorescence (TIRF) imaging (Figure A.2).

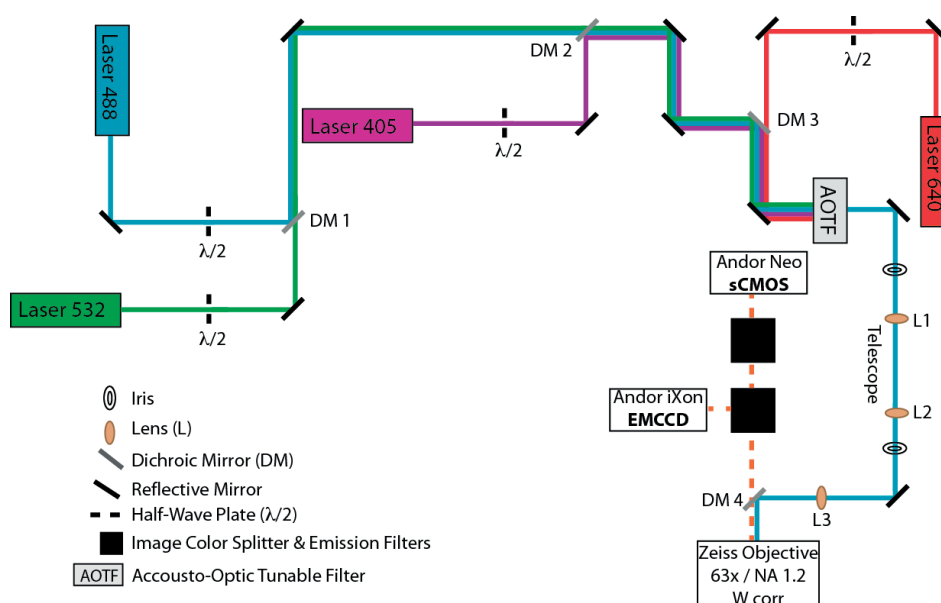


Figure A.1: **Wide-field fluorescence microscopy setup for single-molecule imaging.** The setup is composed of three distinct parts: a laser based excitation system, a microscope, and a detection system. Each laser beam passes a half-wave plate and two mirrors, with one of them being eventually a dichroic (DM1-3). The acousto-optic tunable filter (AOTF) controls and modulates the laser power transmitted from each laser. The telescopic lens pair (L1-2) expands the illumination beam to overfill the back aperture of the microscope objective via a wide-field lens (L3) and an dichroic mirror (DM4). The beam is collimated by the objective and illuminates a wide region (wide-field) of the sample. The emitted fluorescence is collected through the same objective, filtered using appropriate filters, and directed either towards an electron multiplying charge coupled device (EMCCD) or a complementary metal-oxide-semiconductor (CMOS) camera.

General conclusion and outlook

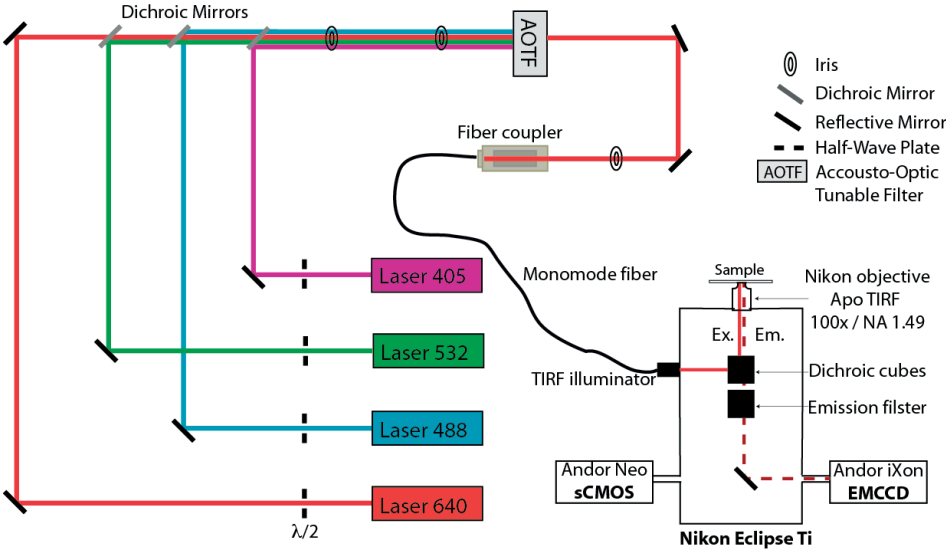


Figure A.2: TIRF microscopy setup for single-molecule imaging.

Bibliography

- [1] Brown, A. G. *Nerve Cells and Nervous Systems*. An Introduction to Neuroscience (Springer Science & Business Media), 2012.
- [2] van Meer, G., D. R. Voelker, and G. W. Feigenson. Membrane lipids: where they are and how they behave. *Nat Rev Mol Cell Biol*, 9(2):112–124, 2008.
- [3] Almén, M. S., K. J. V. Nordström, R. Fredriksson, and H. B. Schiöth. Mapping the human membrane proteome: a majority of the human membrane proteins can be classified according to function and evolutionary origin. *BMC Biology*, 7:50, 2009.
- [4] Dupuy, A. D. and D. M. Engelman. Protein area occupancy at the center of the red blood cell membrane. *Proc Natl Acad Sci USA*, 105(8):2848–2852, 2008.
- [5] Danielli, J. and H. Davson. A contribution to the theory of permeability of thin films. *J Cell Compar Physl*, 5(4):495–508, 1935.
- [6] Singer, S. J. and G. L. Nicolson. The fluid mosaic model of the structure of cell membranes. *Science*, 175(4023):720–731, 1972.
- [7] Lommerse, P. H. M., H. P. Spaink, and T. Schmidt. In vivo plasma membrane organization: results of biophysical approaches. *Biochim. Biophys. Acta*, 1664(2):119–131, 2004.
- [8] Saffman, P. G. and M. Delbrück. Brownian motion in biological membranes. *Proc Natl Acad Sci USA*, 72(8):3111–3113, 1975.
- [9] Murase, K. K., T. T. Fujiwara, A. A. Kusumi, and 10. Ultrafine membrane compartments for molecular diffusion as revealed by single molecule techniques. *Biophys. J.*, 86(6):4075–4093, 2004.
- [10] Kusumi, A., C. Nakada, K. Ritchie, K. Murase, K. Suzuki, H. Murakoshi, R. S. Kasai, J. Kondo, and T. Fujiwara. Paradigm shift of the plasma membrane concept from the two-dimensional continuum fluid to the partitioned fluid: high-speed single-molecule tracking of membrane molecules. *Annu Rev Biophys Biomol Struct*, 34:351–378, 2005.
- [11] Fujiwara, T., K. Ritchie, H. Murakoshi, K. Jacobson, and A. Kusumi. Phospholipids undergo hop diffusion in compartmentalized cell membrane. *J Cell Biol*, 157(6):1071–1081, 2002.

Bibliography

- [12] Sheetz, M. P., M. Schindler, and D. E. Koppel. Lateral mobility of integral membrane proteins is increased in spherocytic erythrocytes. *Nature*, 285(5765):510–511, 1980.
- [13] Edidin, M. Lipid microdomains in cell surface membranes. *Curr. Opin. Struct. Biol.*, 7(4):528–532, 1997.
- [14] Hegener, O., L. Prenner, F. Runkel, S. L. Baader, J. Kappler, and H. Häberlein. Dynamics of beta2-adrenergic receptor-ligand complexes on living cells. *Biochemistry*, 43(20):6190–6199, 2004.
- [15] Iino, R., I. Koyama, and A. Kusumi. Single molecule imaging of green fluorescent proteins in living cells: E-cadherin forms oligomers on the free cell surface. *Biophys. J.*, 80(6):2667–2677, 2001.
- [16] Nelson, S., R. D. Horvat, J. Malvey, D. A. Roess, B. G. Barisas, and C. M. Clay. Characterization of an intrinsically fluorescent gonadotropin-releasing hormone receptor and effects of ligand binding on receptor lateral diffusion. *Endocrinology*, 140(2):950–957, 1999.
- [17] Roess, D. A., R. D. Horvat, H. Munnely, and B. G. Barisas. Luteinizing hormone receptors are self-associated in the plasma membrane. *Endocrinology*, 141(12):4518–4523, 2000.
- [18] Suzuki, K., K. Ritchie, E. Kajikawa, T. Fujiwara, and A. Kusumi. Rapid hop diffusion of a G-protein-coupled receptor in the plasma membrane as revealed by single-molecule techniques. *Biophys. J.*, 88(5):3659–3680, 2005.
- [19] Kusumi, A. and Y. Sako. Cell surface organization by the membrane skeleton. *Curr. Opin. Cell Biol.*, 8(4):566–574, 1996.
- [20] Lingwood, D. and K. Simons. Lipid rafts as a membrane-organizing principle. *Science*, 327(5961):46–50, 2010.
- [21] Doherty, G. J. and H. T. McMahon. Mediation, modulation, and consequences of membrane-cytoskeleton interactions. *Annu Rev Biophys*, 37:65–95, 2008.
- [22] Peterson, J. R. and T. J. Mitchison. Small molecules, big impact: a history of chemical inhibitors and the cytoskeleton. *Chem. Biol.*, 9(12):1275–1285, 2002.
- [23] Luna, E. J. and A. L. Hitt. Cytoskeleton–plasma membrane interactions. *Science*, 258(5084):955–964, 1992.
- [24] Morone, N., T. Fujiwara, K. Murase, R. S. Kasai, H. Ike, S. Yuasa, J. Usukura, and A. Kusumi. Three-dimensional reconstruction of the membrane skeleton at the plasma membrane interface by electron tomography. *J Cell Biol*, 174(6):851–862, 2006.
- [25] Kusumi, A., Y. M. Shirai, I. Koyama-Honda, K. G. M. Suzuki, and T. K. Fujiwara. Hierarchical organization of the plasma membrane: investigations by single-molecule tracking vs. fluorescence correlation spectroscopy. *FEBS Letters*, 584(9):1814–1823, 2010.

- [26] Kusumi, A., K. G. N. Suzuki, R. S. Kasai, K. Ritchie, and T. K. Fujiwara. Hierarchical mesoscale domain organization of the plasma membrane. *Trends Biochem Sci*, 36(11):604–615, 2011.
- [27] Kusumi, A., T. K. Fujiwara, R. Chadda, M. Xie, T. A. Tsunoyama, Z. Kalay, R. S. Kasai, and K. G. N. Suzuki. Dynamic organizing principles of the plasma membrane that regulate signal transduction: commemorating the fortieth anniversary of Singer and Nicolson’s fluid-mosaic model. *Annu. Rev. Cell Dev. Biol.*, 28:215–250, 2012.
- [28] Tsuji, A., K. Kawasaki, S. Ohnishi, H. Merkle, and A. Kusumi. Regulation of band 3 mobilities in erythrocyte ghost membranes by protein association and cytoskeletal meshwork. *Biochemistry*, 27(19):7447–7452, 1988.
- [29] Kusumi, A., Y. Sako, and M. Yamamoto. Confined lateral diffusion of membrane receptors as studied by single particle tracking (nanovid microscopy). Effects of calcium-induced differentiation in cultured epithelial cells. *Biophys. J.*, 65(5):2021–2040, 1993.
- [30] Sako, Y. and A. Kusumi. Compartmentalized structure of the plasma membrane for receptor movements as revealed by a nanometer-level motion analysis. *J Cell Biol*, 125(6):1251–1264, 1994.
- [31] Ritchie, K., X.-Y. Shan, J. Kondo, K. Iwasawa, T. Fujiwara, and A. Kusumi. Detection of non-Brownian diffusion in the cell membrane in single molecule tracking. *Biophys. J.*, 88(3):2266–2277, 2005.
- [32] Kusumi, A., H. Murakoshi, and K. Murase. Single-Molecule Imaging of Diffusion, Recruitment, and Activation of Signaling Molecules in Living Cells. *Biophysical aspects of transmembrane signaling, Springer Series in Biophysics*, 8:123–152, 2005.
- [33] Edidin, M. Membrane cholesterol, protein phosphorylation, and lipid rafts. *Sci. STKE*, 2001(67):pe1, 2001.
- [34] Skwarek, M. Recent controversy surrounding lipid rafts. *Arch. Immunol. Ther. Exp. (Warsz.)*, 52(6):427–431, 2004.
- [35] Lagerholm, B. C., G. E. Weinreb, K. Jacobson, and N. L. Thompson. Detecting microdomains in intact cell membranes. *Annu Rev Phys Chem*, 56:309–336, 2005.
- [36] Mueller, V., C. Ringemann, A. Honigmann, G. Schwarzmann, R. Medda, M. Leutenegger, S. Polyakova, V. N. Belov, S. W. Hell, and C. Eggeling. STED nanoscopy reveals molecular details of cholesterol- and cytoskeleton-modulated lipid interactions in living cells. *Biophys. J.*, 101(7):1651–1660, 2011.
- [37] Honigmann, A., V. Mueller, H. Ta, A. Schoenle, E. Sezgin, S. W. Hell, and C. Eggeling. Scanning STED-FCS reveals spatiotemporal heterogeneity of lipid interaction in the plasma membrane of living cells. *Nat Commun*, 5:5412, 2014.

Bibliography

- [38] Sevcsik, E., M. Brameshuber, M. Fölser, J. Weghuber, A. Honigmann, and G. J. Schütz. GPI-anchored proteins do not reside in ordered domains in the live cell plasma membrane. *Nat Commun*, 6:6969, 2015.
- [39] Alberts, B., A. Johnson, J. Lewis, M. Raff, K. Roberts, and P. Walter. *Molecular Biology of the Cell* (Garland Science), 5 edition, 2007.
- [40] Fleming, R. J., K. Purcell, and S. Artavanis-Tsakonas. The NOTCH receptor and its ligands. *Trends Cell Biol.*, 7(11):437–441, 1997.
- [41] Bray, S. J. Notch signalling: a simple pathway becomes complex. *Nat Rev Mol Cell Biol*, 7(9):678–689, 2006.
- [42] Pierce, K. L., R. T. Premont, and R. J. Lefkowitz. Seven-transmembrane receptors. *Nat Rev Mol Cell Biol*, 3(9):639–650, 2002.
- [43] Katritch, V., V. Cherezov, and R. C. Stevens. Structure-function of the G protein-coupled receptor superfamily. *Annu. Rev. Pharmacol. Toxicol.*, 53:531–556, 2013.
- [44] Bockaert, J. and J. P. Pin. Molecular tinkering of G protein-coupled receptors: an evolutionary success. *EMBO J*, 18(7):1723–1729, 1999.
- [45] Overington, J. P., B. Al-Lazikani, and A. L. Hopkins. How many drug targets are there? *Nat Rev Drug Discov*, 5(12):993–996, 2006.
- [46] Heng, B. C., D. Aubel, and M. Fussenegger. An overview of the diverse roles of G-protein coupled receptors (GPCRs) in the pathophysiology of various human diseases. *Biotechnol. Adv.*, 31(8):1676–1694, 2013.
- [47] Hausch, F. and F. Holsboer. *The seven pillars of molecular pharmacology: GPCR research honored with Nobel Prize for chemistry*, volume 51 (Angew. Chem. Int. Ed.), 2012.
- [48] Wedegaertner, P. B., P. T. Wilson, and H. R. Bourne. Lipid modifications of trimeric G proteins. *J Biol Chem*, 270(2):503–506, 1995.
- [49] Stryer, L., J. Berg, and J. Tymoczko. Biochimie, 5e ed. (trad. Serge Weinman). *Flammarion, Médecine-Sciences, Paris*, 2003.
- [50] Wettschureck, N. and S. Offermanns. Mammalian G proteins and their cell type specific functions. *Physiol Rev*, 85(4):1159–1204, 2005.
- [51] Siehler, S. Regulation of RhoGEF proteins by G12/13-coupled receptors. *Br. J. Pharmacol.*, 158(1):41–49, 2009.
- [52] Fackler, O. T. and R. Grosse. Cell motility through plasma membrane blebbing. *The Journal of cell biology*, 181(6):879–884, 2008.

-
- [53] Khan, S. M., R. Sleno, S. Gora, P. Zylbergold, J.-P. Laverdure, J.-C. Labbé, G. J. Miller, and T. E. Hébert. The expanding roles of $G\beta\gamma$ subunits in G protein-coupled receptor signaling and drug action. *Pharmacol Rev*, 65(2):545–577, 2013.
- [54] Gilman, A. G. G proteins: transducers of receptor-generated signals. *Annu. Rev. Biochem.*, 56:615–649, 1987.
- [55] Levitzki, A. and S. Klein. G-protein subunit dissociation is not an integral part of G-protein action. *Chembiochem*, 3(9):815–818, 2002.
- [56] Bünemann, M., M. Frank, and M. J. Lohse. Gi protein activation in intact cells involves subunit rearrangement rather than dissociation. *Proc Natl Acad Sci USA*, 100(26):16077–16082, 2003.
- [57] Digby, G. J., R. M. Lober, P. R. Sethi, and N. A. Lambert. Some G protein heterotrimers physically dissociate in living cells. *Proc Natl Acad Sci USA*, 103(47):17789–17794, 2006.
- [58] Lambert, N. A. Dissociation of heterotrimeric g proteins in cells. *Sci Signal*, 1(25):re5, 2008.
- [59] Hommers, L. G., C. Klenk, C. Dees, and M. Bünemann. G proteins in reverse mode: receptor-mediated GTP release inhibits G protein and effector function. *Journal of Biological Chemistry*, 285(11):8227–8233, 2010.
- [60] Bondar, A. and J. Lazar. Dissociated $G\alpha$ GTP and $G\beta\gamma$ protein subunits are the major activated form of heterotrimeric Gi/o proteins. *Journal of Biological Chemistry*, 289(3):1271–1281, 2014.
- [61] Ferguson, S. S. Evolving concepts in G protein-coupled receptor endocytosis: the role in receptor desensitization and signaling. *Pharmacol Rev*, 53(1):1–24, 2001.
- [62] Pitcher, J. A., N. J. Freedman, and R. J. Lefkowitz. G protein-coupled receptor kinases. *Annu. Rev. Biochem.*, 67:653–692, 1998.
- [63] Tan, C. M., A. E. Brady, H. H. Nickols, Q. Wang, and L. E. Limbird. Membrane trafficking of G protein-coupled receptors. *Annu. Rev. Pharmacol. Toxicol.*, 44:559–609, 2004.
- [64] Moore, C. A. C., S. K. Milano, and J. L. Benovic. Regulation of receptor trafficking by GRKs and arrestins. *Annu Rev Physiol*, 69:451–482, 2007.
- [65] DeWire, S. M., S. Ahn, R. J. Lefkowitz, and S. K. Shenoy. Beta-arrestins and cell signaling. *Annu Rev Physiol*, 69:483–510, 2007.
- [66] Luttrell, L. M. and D. Gesty-Palmer. Beyond desensitization: physiological relevance of arrestin-dependent signaling. *Pharmacol Rev*, 62(2):305–330, 2010.
- [67] DeFea, K. A. Beta-arrestins as regulators of signal termination and transduction: how do they determine what to scaffold? *Cell. Signal.*, 23(4):621–629, 2011.

Bibliography

- [68] Kang, J., Y. Shi, B. Xiang, B. Qu, W. Su, M. Zhu, M. Zhang, G. Bao, F. Wang, X. Zhang, R. Yang, F. Fan, X. Chen, G. Pei, and L. Ma. A nuclear function of beta-arrestin1 in GPCR signaling: regulation of histone acetylation and gene transcription. *Cell*, 123(5):833–847, 2005.
- [69] Shenoy, S. K. and R. J. Lefkowitz. β -arrestin-mediated receptor trafficking and signal transduction. *Trends Pharmacol Sci*, pages 1–13, 2011.
- [70] Irannejad, R., J. C. Tomshine, J. R. Tomshine, M. Chevalier, J. P. Mahoney, J. Steyaert, S. G. F. Rasmussen, R. K. Sunahara, H. El-Samad, B. Huang, and M. Von Zastrow. Conformational biosensors reveal GPCR signalling from endosomes. *Nature*, 495(7442):534–538, 2013.
- [71] Vilardaga, J.-P., F. G. Jean-Alphonse, and T. J. Gardella. Endosomal generation of cAMP in GPCR signaling. *Nat. Chem. Biol.*, 10(9):700–706, 2014.
- [72] Takahashi, K., A. Tanaka, M. Hara, and S. Nakanishi. The primary structure and gene organization of human substance P and neuromedin K receptors. *Eur. J. Biochem.*, 204(3):1025–1033, 1992.
- [73] Quartara, L. and C. A. Maggi. The tachykinin NK1 receptor. Part II: Distribution and pathophysiological roles. *Neuropeptides*, 32(1):1–49, 1998.
- [74] Otsuka, M. and K. Yoshioka. Neurotransmitter functions of mammalian tachykinins. *Physiol Rev*, 73(2):229–308, 1993.
- [75] Muñoz, M. and R. Coveñas. NK-1 Receptor Antagonists: A New Generation of Anticancer Drugs. *Mini Rev Med Chem*, 2012.
- [76] Alvaro, G. and R. Di Fabio. Neurokinin 1 receptor antagonists—current prospects. *Curr Opin Drug Discov Devel*, 10(5):613–621, 2007.
- [77] Quartara, L. and C. A. Maggi. The tachykinin NK1 receptor. Part I: ligands and mechanisms of cellular activation. *Neuropeptides*, 31(6):537–563, 1997.
- [78] Khawaja, A. M. and D. F. Rogers. Tachykinins: receptor to effector. *Int J Biochem Cell Biol*, 28(7):721–738, 1996.
- [79] Meshki, J. Substance P induces rapid and transient membrane blebbing in U373MG cells in a p21-activated kinase-dependent manner. *PLoS One*, 6(9):e25332, 2011.
- [80] Steinhoff, M. S., B. von Mentzer, P. Geppetti, C. Pothoulakis, and N. W. Bunnett. Tachykinins and their receptors: contributions to physiological control and the mechanisms of disease. *Physiol Rev*, 94(1):265–301, 2014.
- [81] Nakajima, Y., K. Tsuchida, M. Negishi, S. Ito, and S. Nakanishi. Direct linkage of three tachykinin receptors to stimulation of both phosphatidylinositol hydrolysis and cyclic AMP cascades in transfected Chinese hamster ovary cells. *J Biol Chem*, 267(4):2437–2442, 1992.

- [82] Laniyonu, A., E. Sliwinski-Lis, and N. Fleming. Different tachykinin receptor subtypes are coupled to the phosphoinositide or cyclic AMP signal transduction pathways in rat submandibular cells. *FEBS Letters*, 240(1-2):186–190, 1988.
- [83] Meshki, J., S. D. Douglas, J.-P. Lai, L. Schwartz, L. E. Kilpatrick, and F. Tuluc. Neurokinin 1 receptor mediates membrane blebbing in HEK293 cells through a Rho/Rho-associated coiled-coil kinase-dependent mechanism. *J Biol Chem*, 284(14):9280–9289, 2009.
- [84] Chen, P., S. D. Douglas, J. Meshki, and F. Tuluc. Neurokinin 1 receptor mediates membrane blebbing and shear stress-induced microparticle formation in HEK293 cells. *PLoS One*, 7(9):e45322, 2012.
- [85] Rosso, M., M. Muñoz, and M. Berger. The role of neurokinin-1 receptor in the microenvironment of inflammation and cancer. *ScientificWorldJournal*, 2012:381434, 2012.
- [86] Muñoz, M. and R. Coveñas. Involvement of substance P and the NK-1 receptor in cancer progression. *Peptides*, 48:1–9, 2013.
- [87] Lang, K., T. L. Drell, A. Lindecke, B. Niggemann, C. Kaltschmidt, K. S. Zaenker, and F. Entschladen. Induction of a metastatogenic tumor cell type by neurotransmitters and its pharmacological inhibition by established drugs. *Int. J. Cancer*, 112(2):231–238, 2004.
- [88] Feng, F., J. Yang, L. Tong, S. Yuan, Y. Tian, L. Hong, W. Wang, and H. Zhang. Substance P immunoreactive nerve fibres are related to gastric cancer differentiation status and could promote proliferation and migration of gastric cancer cells. *Cell Biol. Int.*, 35(6):623–629, 2011.
- [89] Kew, J. N. C. and C. H. Davies. *Ion Channels. From Structure to Function* (Oxford University Press), 2010.
- [90] Sine, S. M. and A. G. Engel. Recent advances in Cys-loop receptor structure and function. *Nature*, 440(7083):448–455, 2006.
- [91] Thompson, A. J., H. A. Lester, and S. C. R. Lummis. The structural basis of function in Cys-loop receptors. *Q. Rev. Biophys.*, 43(4):449–499, 2010.
- [92] daCosta, C. J. B. and J. E. Baenziger. Gating of pentameric ligand-gated ion channels: structural insights and ambiguities. *Structure*, 21(8):1271–1283, 2013.
- [93] Connolly, C. N. Trafficking of 5-HT(3) and GABA(A) receptors (Review). *Mol. Membr. Biol.*, 25(4):293–301, 2008.
- [94] Perán, M., H. Hooper, H. Boulaiz, J. A. Marchal, A. Aránega, and R. Salas. The M3/M4 cytoplasmic loop of the alpha1 subunit restricts GABAARs lateral mobility: a study using fluorescence recovery after photobleaching. *Cell Motil. Cytoskeleton*, 63(12):747–757, 2006.

Bibliography

- [95] Jansen, M., M. Bali, and M. H. Akabas. Modular design of Cys-loop ligand-gated ion channels: functional 5-HT₃ and GABA ρ 1 receptors lacking the large cytoplasmic M3M4 loop. *J. Gen. Physiol.*, 131(2):137–146, 2008.
- [96] Hassaïne, G., C. Deluz, L. Grasso, R. Wyss, M. B. Tol, R. Hovius, A. Graff, H. Stahlberg, T. Tomizaki, A. Desmyter, C. Moreau, X.-D. Li, F. Poitevin, H. Vogel, and H. Nury. X-ray structure of the mouse serotonin 5-HT₃ receptor. *Nature*, 512(7514):276–281, 2014.
- [97] Hibbs, R. E. and E. Gouaux. Principles of activation and permeation in an anion-selective Cys-loop receptor. *Nature*, 474(7349):54–60, 2011.
- [98] Miller, P. S. and A. R. Aricescu. Crystal structure of a human GABA_A receptor. *Nature*, 512(7514):270–275, 2014.
- [99] Maricq, A. V., A. S. Peterson, A. J. Brake, R. M. Myers, and D. Julius. Primary structure and functional expression of the 5HT₃ receptor, a serotonin-gated ion channel. *Science*, 254(5030):432–437, 1991.
- [100] McCorvy, J. D. and B. L. Roth. Structure and function of serotonin G protein-coupled receptors. *Pharmacol Ther*, 150:129–142, 2015.
- [101] Lummis, S. C. R. 5-HT(3) receptors. *Journal of Biological Chemistry*, 287(48):40239–40245, 2012.
- [102] McMahan, L. L. and J. A. Kauer. Hippocampal interneurons are excited via serotonin-gated ion channels. *J Neurophysiol*, 78(5):2493–2502, 1997.
- [103] Engelman, H. S. and A. B. MacDermott. Presynaptic ionotropic receptors and control of transmitter release. *Nature Reviews Neuroscience*, 5(2):135–145, 2004.
- [104] Inoue, A., T. Hashimoto, I. Hide, H. Nishio, and Y. Nakata. 5-Hydroxytryptamine-facilitated release of substance P from rat spinal cord slices is mediated by nitric oxide and cyclic GMP. *Journal of neurochemistry*, 68(1):128–133, 1997.
- [105] Lemoine, D., R. Jiang, A. Taly, T. Chataigneau, A. Specht, and T. Grutter. Ligand-gated ion channels: new insights into neurological disorders and ligand recognition. *Chem. Rev.*, 112(12):6285–6318, 2012.
- [106] Lemke, T. L. and D. A. Williams. *Foye's Principles of Medicinal Chemistry* (Lippincott Williams & Wilkins), 2012.
- [107] Machu, T. K. Therapeutics of 5-HT₃ receptor antagonists: current uses and future directions. *Pharmacol Ther*, 130(3):338–347, 2011.
- [108] Walstab, J., G. Rappold, and B. Niesler. 5-HT(3) receptors: role in disease and target of drugs. *Pharmacol Ther*, 128(1):146–169, 2010.

- [109] Rajkumar, R. and R. Mahesh. The auspicious role of the 5-HT₃ receptor in depression: a probable neuronal target? *J. Psychopharmacol. (Oxford)*, 24(4):455–469, 2010.
- [110] Müller, W., B. L. Fiebich, and T. Stratz. New treatment options using 5-HT₃ receptor antagonists in rheumatic diseases. *Curr Top Med Chem*, 6(18):2035–2042, 2006.
- [111] Coates, A., S. Abraham, S. B. Kaye, T. Sowerbutts, C. Frewin, R. M. Fox, and M. H. Tattersall. On the receiving end—patient perception of the side-effects of cancer chemotherapy. *Eur J Cancer Clin Oncol*, 19(2):203–208, 1983.
- [112] Wilcox, P. M., J. H. Fetting, K. M. Nettesheim, and M. D. Abeloff. Anticipatory vomiting in women receiving cyclophosphamide, methotrexate, and 5-FU (CMF) adjuvant chemotherapy for breast carcinoma. *Cancer Treat Rep*, 66(8):1601–1604, 1982.
- [113] Jordan, K., F. Jahn, and M. Aapro. Recent developments in the prevention of chemotherapy-induced nausea and vomiting (CINV): a comprehensive review. *Ann. Oncol.*, 26(6):1081–1090, 2015.
- [114] Dewan, P., S. Singhal, and D. Harit. Management of chemotherapy-induced nausea and vomiting. *Indian Pediatr*, 47(2):149–155, 2010.
- [115] Darmani, N. A., S. Chebolu, B. Amos, and T. Alkam. Synergistic antiemetic interactions between serotonergic 5-HT₃ and tachykininergic NK₁-receptor antagonists in the least shrew (*Cryptotis parva*). *Pharmacol. Biochem. Behav.*, 99(4):573–579, 2011.
- [116] Rojas, C., M. Raje, T. Tsukamoto, and B. S. Slusher. Molecular mechanisms of 5-HT₃ and NK₁ receptor antagonists in prevention of emesis. *Eur. J. Pharmacol.*, 722:26–37, 2014.
- [117] Wong, E. H., R. Clark, E. Leung, D. Loury, D. W. Bonhaus, L. Jakeman, H. Parnes, R. L. Whiting, and R. M. Eglen. The interaction of RS 25259-197, a potent and selective antagonist, with 5-HT₃ receptors, in vitro. *Br. J. Pharmacol.*, 114(4):851–859, 1995.
- [118] Hu, W.-P., X.-H. You, B.-C. Guan, L.-Q. Ru, J.-G. Chen, and Z.-W. Li. Substance P potentiates 5-HT₃ receptor-mediated current in rat trigeminal ganglion neurons. *Neurosci. Lett.*, 365(2):147–152, 2004.
- [119] Sun, H., X.-Q. Hu, E. M. Moradel, F. F. Weight, and L. Zhang. Modulation of 5-HT₃ receptor-mediated response and trafficking by activation of protein kinase C. *J Biol Chem*, 278(36):34150–34157, 2003.
- [120] Greenwood-Van Meerveld, B., E. Mohammadi, K. Tyler, C. Pietra, L. A. Bee, and A. Dickenson. Synergistic effect of 5-hydroxytryptamine 3 and neurokinin 1 receptor antagonism in rodent models of somatic and visceral pain. *J. Pharmacol. Exp. Ther.*, 351(1):146–152, 2014.
- [121] Saxton, M. J. and K. Jacobson. Single-particle tracking: applications to membrane dynamics. *Annu Rev Biophys Biomol Struct*, 26:373–399, 1997.

Bibliography

- [122] SHERA, E. B., N. K. SEITZINGER, L. M. DAVIS, R. A. KELLER, and S. A. SOPER. Detection of Single Fluorescent Molecules. *Chemical Physics Letters*, 174(6):553–557, 1990.
- [123] Tsien, R. Y. The green fluorescent protein. *Annu. Rev. Biochem.*, 67:509–544, 1998.
- [124] Zimmer, M. GFP: from jellyfish to the Nobel prize and beyond. *Chem. Soc. Rev.*, 38(10):2823–2832, 2009.
- [125] Müller-Taubenberger, A. Application of fluorescent protein tags as reporters in live-cell imaging studies. *Methods Mol Biol*, 346:229–246, 2006.
- [126] Michalet, X. Quantum Dots for Live Cells, in Vivo Imaging, and Diagnostics. *Science*, 307(5709):538–544, 2005.
- [127] Resch-Genger, U., M. Grabolle, S. Cavaliere-Jaricot, R. Nitschke, and T. Nann. Quantum dots versus organic dyes as fluorescent labels. *Nat. Methods*, 5(9):763–775, 2008.
- [128] Walling, M. A., J. A. Novak, and J. R. E. Shepard. Quantum dots for live cell and in vivo imaging. *Int J Mol Sci*, 10(2):441–491, 2009.
- [129] Pinaud, F., S. Clarke, A. Sittner, and M. Dahan. Probing cellular events, one quantum dot at a time. *Nat. Methods*, 7(4):275–285, 2010.
- [130] Chan, W. C. W., D. J. Maxwell, X. Gao, R. E. Bailey, M. Han, and S. Nie. Luminescent quantum dots for multiplexed biological detection and imaging. *Curr. Opin. Biotechnol.*, 13(1):40–46, 2002.
- [131] Jaiswal, J. K., H. Mattoussi, J. M. Mauro, and S. M. Simon. Long-term multiple color imaging of live cells using quantum dot bioconjugates. *Nat. Biotechnol.*, 21(1):47–51, 2003.
- [132] Arnspang, E. C., J. R. Brewer, and B. C. Lagerholm. Multi-color single particle tracking with quantum dots. *PLoS One*, 7(11):e48521, 2012.
- [133] Knopp, D., D. Tang, and R. Niessner. Review: bioanalytical applications of biomolecule-functionalized nanometer-sized doped silica particles. *Anal. Chim. Acta*, 647(1):14–30, 2009.
- [134] Medintz, I. L., H. T. Uyeda, E. R. Goldman, and H. Mattoussi. Quantum dot bioconjugates for imaging, labelling and sensing. *Nat Mater*, 4(6):435–446, 2005.
- [135] Choquet, D. and A. Triller. The role of receptor diffusion in the organization of the postsynaptic membrane. *Nature Reviews Neuroscience*, 4(4):251–265, 2003.
- [136] Nirmal, M., B. O. Dabbousi, M. G. Bawendi, J. J. Macklin, J. K. Trautman, T. D. Harris, and L. E. Brus. Fluorescence intermittency in single cadmium selenide nanocrystals. *Nature*, 383(6603):802–804, 1996.

- [137] Bannai, H., S. Lévi, C. Schweizer, M. Dahan, and A. Triller. Imaging the lateral diffusion of membrane molecules with quantum dots. *Nature protocols*, 1(6):2628–2634, 2006.
- [138] Saxton, M. J. Single-particle tracking: connecting the dots. *Nat. Methods*, 5(8):671–672, 2008.
- [139] Jaqaman, K., D. Loerke, M. Mettlen, H. Kuwata, S. Grinstein, S. L. Schmid, and G. Danuser. Robust single-particle tracking in live-cell time-lapse sequences. *Nat. Methods*, 5(8):695–702, 2008.
- [140] Sergé, A., N. Bertaux, H. Rigneault, and D. Marguet. Dynamic multiple-target tracing to probe spatiotemporal cartography of cell membranes. *Nat. Methods*, 5(8):687–694, 2008.
- [141] Wang, X., X. Ren, K. Kahen, M. A. Hahn, M. Rajeswaran, S. Maccagnano-Zacher, J. Silcox, G. E. Cragg, A. L. Efros, and T. D. Krauss. Non-blinking semiconductor nanocrystals. *Nature*, 459(7247):686–689, 2009.
- [142] Dertinger, T., R. Colyer, G. Iyer, S. Weiss, and J. Enderlein. Fast, background-free, 3D super-resolution optical fluctuation imaging (SOFI). *Proc Natl Acad Sci USA*, 106(52):22287–22292, 2009.
- [143] Wegner, K. D. and N. Hildebrandt. Quantum dots: bright and versatile in vitro and in vivo fluorescence imaging biosensors. *Chem. Soc. Rev.*, 44(14):4792–4834, 2015.
- [144] Fernández-Suárez, M. and A. Y. Ting. Fluorescent probes for super-resolution imaging in living cells. *Nat Rev Mol Cell Biol*, 9(12):929–943, 2008.
- [145] Zheng, Q., M. F. Juetten, S. Jockusch, M. R. Wasserman, Z. Zhou, R. B. Altman, and S. C. Blanchard. Ultra-stable organic fluorophores for single-molecule research. *Chem. Soc. Rev.*, 43(4):1044–1056, 2014.
- [146] Marx, V. Probes: paths to photostability. *Nat. Methods*, 12(3):187–190, 2015.
- [147] Lippincott-Schwartz, J., E. Snapp, and A. Kenworthy. Studying protein dynamics in living cells. *Nat Rev Mol Cell Biol*, 2(6):444–456, 2001.
- [148] Moerner, W. and L. Kador. Optical detection and spectroscopy of single molecules in a solid. *Phys. Rev. Lett.*, 62(21):2535–2538, 1989.
- [149] Jacobson, K., A. Ishihara, and R. Inman. Lateral diffusion of proteins in membranes. *Annu Rev Physiol*, 49:163–175, 1987.
- [150] Schwille, P., J. Korfach, and W. W. Webb. Fluorescence correlation spectroscopy with single-molecule sensitivity on cell and model membranes. *Cytometry*, 36(3):176–182, 1999.

Bibliography

- [151] Mach, E. *The Principles of Physical Optics*. An Historical and Philosophical Treatment (Courier Corporation), 2013.
- [152] Cognet, L., B. Lounis, and D. Choquet. Tracking receptors by imaging single molecules. *CSH Protoc*, 2008:pdb.top25, 2008.
- [153] Piguet, J. Advanced Fluorescence Microscopy to Study Plasma Membrane Protein Dynamics. *EPFL Thesis (doi:10.5075/epfl-thesis-4869)*, 2010.
- [154] Feder, T. J., I. Brust-Mascher, J. P. Slattery, B. Baird, and W. W. Webb. Constrained diffusion or immobile fraction on cell surfaces: a new interpretation. *Biophys. J.*, 70(6):2767–2773, 1996.
- [155] Bormuth, V., V. Varga, J. Howard, and E. Schäffer. Protein friction limits diffusive and directed movements of kinesin motors on microtubules. *Science*, 325(5942):870–873, 2009.
- [156] Ferrari, R., A. J. Manfroi, and W. R. Young. Strongly and weakly self-similar diffusion. *Physica D*, 154(1-2):111–137, 2001.
- [157] Ewers, H., A. E. Smith, I. F. Sbalzarini, H. Lilie, P. Koumoutsakos, and A. Helenius. Single-particle tracking of murine polyoma virus-like particles on live cells and artificial membranes. *Proc Natl Acad Sci USA*, 102(42):15110–15115, 2005.
- [158] Yano, Y. and K. Matsuzaki. Tag-probe labeling methods for live-cell imaging of membrane proteins. *Biochim. Biophys. Acta*, 1788(10):2124–2131, 2009.
- [159] George, N., H. Pick, H. Vogel, N. Johnsson, and K. Johnsson. Specific labeling of cell surface proteins with chemically diverse compounds. *J. Am. Chem. Soc.*, 126(29):8896–8897, 2004.
- [160] Sunbul, M., M. Yen, Y. Zou, and J. Yin. Enzyme catalyzed site-specific protein labeling and cell imaging with quantum dots. *Chem. Commun. (Camb.)*, (45):5927–5929, 2008.
- [161] Zelman-Femiak, M., K. Wang, K. V. Gromova, P. Knaus, and G. S. Harms. Covalent quantum dot receptor linkage via the acyl carrier protein for single-molecule tracking, internalization, and trafficking studies. *BioTechniques*, 49(2):574–579, 2010.
- [162] Meyer, B. H., K. L. Martinez, J.-M. Segura, P. Pascoal, R. Hovius, N. George, K. Johnsson, and H. Vogel. Covalent labeling of cell-surface proteins for in-vivo FRET studies. *FEBS Letters*, 580(6):1654–1658, 2006.
- [163] Poderys, V., M. Matulionyte, A. Selskis, and R. Rotomskis. Interaction of Water-Soluble CdTe Quantum Dots with Bovine Serum Albumin. *Nanoscale Research Letters*, 6, 2011.
- [164] Meyer, B. Investigation of the neurokinin-1 receptor by fluorescence techniques. EPFL Thesis (doi:10.5075/epfl-thesis-3272), 2005.

- [165] Green, N. M. Avidin and streptavidin. *Methods in enzymology*, 184:51–67, 1990.
- [166] Pinaud, F., X. Michalet, G. Iyer, E. Margeat, H.-P. Moore, and S. Weiss. Dynamic partitioning of a glycosyl-phosphatidylinositol-anchored protein in glycosphingolipid-rich microdomains imaged by single-quantum dot tracking. *Traffic*, 10(6):691–712, 2009.
- [167] Fichter, K. M., M. Flajolet, P. Greengard, and T. Q. Vu. Kinetics of G-protein-coupled receptor endosomal trafficking pathways revealed by single quantum dots. *Proc Natl Acad Sci USA*, 107(43):18658–18663, 2010.
- [168] Adam, G. and M. Delbrück. Reduction of dimensionality in biological diffusion processes. *Structural Chemistry and Molecular Biology*, pages 198–215, 1968.
- [169] Nicolson, G. L. The Fluid-Mosaic Model of Membrane Structure: still relevant to understanding the structure, function and dynamics of biological membranes after more than 40 years. *Biochim. Biophys. Acta*, 1838(6):1451–1466, 2014.
- [170] Kusumi, A., T. A. Tsunoyama, K. M. Hirose, R. S. Kasai, and T. K. Fujiwara. Tracking single molecules at work in living cells. *Nat. Chem. Biol.*, 10(7):524–532, 2014.
- [171] Grecco, H. E., M. Schmick, and P. I. H. Bastiaens. Signaling from the living plasma membrane. *Cell*, 144(6):897–909, 2011.
- [172] Eggeling, C., C. Ringemann, R. Medda, G. Schwarzmann, K. Sandhoff, S. Polyakova, V. N. Belov, B. Hein, C. von Middendorff, A. Schönle, and S. W. Hell. Direct observation of the nanoscale dynamics of membrane lipids in a living cell. *Nature*, 457(7233):1159–1162, 2009.
- [173] Salon, J. A., D. T. Lodowski, and K. Palczewski. The significance of G protein-coupled receptor crystallography for drug discovery. *Pharmacol Rev*, 63(4):901–937, 2011.
- [174] Shoichet, B. K. and B. K. Kobilka. Structure-based drug screening for G-protein-coupled receptors. *Trends Pharmacol Sci*, 33(5):268–272, 2012.
- [175] Venkatakrishnan, A. J., X. Deupi, G. Lebon, C. G. Tate, G. F. Schertler, and M. M. Babu. Molecular signatures of G-protein-coupled receptors. *Nature*, 494(7436):185–194, 2013.
- [176] Hanyaloglu, A. C. and M. Von Zastrow. Regulation of GPCRs by endocytic membrane trafficking and its potential implications. *Annu. Rev. Pharmacol. Toxicol.*, 48:537–568, 2008.
- [177] Valant, C., J. R. Lane, P. M. Sexton, and A. Christopoulos. The Best of Both Worlds? Bitopic Orthosteric/Allosteric Ligands of G Protein-Coupled Receptors. *Annu. Rev. Pharmacol. Toxicol.*, 52:153–178, 2012.
- [178] Urban, J. D., W. P. Clarke, M. Von Zastrow, D. E. Nichols, B. Kobilka, H. Weinstein, J. A. Javitch, B. L. Roth, A. Christopoulos, P. M. Sexton, K. J. Miller, M. Spedding, and R. B. Mailman. Functional selectivity and classical concepts of quantitative pharmacology. *J. Pharmacol. Exp. Ther.*, 320(1):1–13, 2006.

Bibliography

- [179] Reiter, E., S. Ahn, A. K. Shukla, and R. J. Lefkowitz. Molecular mechanism of β -arrestin-biased agonism at seven-transmembrane receptors. *Annu. Rev. Pharmacol. Toxicol.*, 52:179–197, 2012.
- [180] Barak, L. S., K. Warabi, X. Feng, M. G. Caron, and M. M. Kwatra. Real-time visualization of the cellular redistribution of G protein-coupled receptor kinase 2 and beta-arrestin 2 during homologous desensitization of the substance P receptor. *J Biol Chem*, 274(11):7565–7569, 1999.
- [181] Luttrell, L. M. and R. J. Lefkowitz. The role of beta-arrestins in the termination and transduction of G-protein-coupled receptor signals. *Journal of cell science*, 115(Pt 3):455–465, 2002.
- [182] McConalogue, K., O. Déry, M. Lovett, H. Wong, J. H. Walsh, E. F. Grady, and N. W. Bunnnett. Substance P-induced trafficking of beta-arrestins. The role of beta-arrestins in endocytosis of the neurokinin-1 receptor. *J Biol Chem*, 274(23):16257–16268, 1999.
- [183] Garland, A. M., E. F. Grady, D. G. Payan, S. R. Vigna, and N. W. Bunnnett. Agonist-induced internalization of the substance P (NK1) receptor expressed in epithelial cells. *Biochem. J.*, 303 (Pt 1):177–186, 1994.
- [184] Grady, E. F., A. M. Garland, P. D. Gamp, M. Lovett, D. G. Payan, and N. W. Bunnnett. Delineation of the endocytic pathway of substance P and its seven-transmembrane domain NK1 receptor. *Mol. Biol. Cell*, 6(5):509–524, 1995.
- [185] Roosterman, D., G. S. Cottrell, F. Schmidlin, M. Steinhoff, and N. W. Bunnnett. Recycling and resensitization of the neurokinin 1 receptor. Influence of agonist concentration and Rab GTPases. *J Biol Chem*, 279(29):30670–30679, 2004.
- [186] Murphy, J. E., D. Roosterman, G. S. Cottrell, B. E. Padilla, M. Feld, E. Brand, W. J. Cedron, N. W. Bunnnett, and M. Steinhoff. Protein phosphatase 2A mediates resensitization of the neurokinin 1 receptor. *Am. J. Physiol., Cell Physiol.*, 301(4):C780–91, 2011.
- [187] Prummer, M., B. H. Meyer, R. Franzini, J.-M. Segura, N. George, K. Johnsson, and H. Vogel. Post-translational covalent labeling reveals heterogeneous mobility of individual G protein-coupled receptors in living cells. *Chembiochem*, 7(6):908–911, 2006.
- [188] Lill, Y., K. L. Martinez, M. A. Lill, B. H. Meyer, H. Vogel, and B. Hecht. Kinetics of the initial steps of G protein-coupled receptor-mediated cellular signaling revealed by single-molecule imaging. *Chemphyschem*, 6(8):1633–1640, 2005.
- [189] Sbalzarini, I. F. and P. Koumoutsakos. Feature point tracking and trajectory analysis for video imaging in cell biology. *Journal of structural biology*, 151(2):182–195, 2005.
- [190] Piguet, J., C. Schreiter, J.-M. Segura, H. Vogel, and R. Hovius. Acetylcholine receptor organization in membrane domains in muscle cells: evidence for rapsyn-independent and rapsyn-dependent mechanisms. *Journal of Biological Chemistry*, 286(1):363–369, 2011.

-
- [191] Huet, S., E. Karatekin, V. S. Tran, I. Fanget, S. Cribier, and J.-P. Henry. Analysis of transient behavior in complex trajectories: application to secretory vesicle dynamics. *Biophys. J.*, 91(9):3542–3559, 2006.
- [192] Helmuth, J. A., C. J. Burckhardt, P. Koumoutsakos, U. F. Greber, and I. F. Sbalzarini. A novel supervised trajectory segmentation algorithm identifies distinct types of human adenovirus motion in host cells. *Journal of structural biology*, 159(3):347–358, 2007.
- [193] Ganguly, S., R. Saxena, and A. Chattopadhyay. Reorganization of the actin cytoskeleton upon G-protein coupled receptor signaling. *Biochim. Biophys. Acta*, 1808(7):1921–1929, 2011.
- [194] de Keijzer, S., J. Galloway, G. S. Harms, P. N. Devreotes, and P. A. Iglesias. Disrupting microtubule network immobilizes amoeboid chemotactic receptor in the plasma membrane. *Biochim. Biophys. Acta*, 1808(6):1701–1708, 2011.
- [195] Jaqaman, K. and S. Grinstein. Regulation from within: the cytoskeleton in transmembrane signaling. *Trends Cell Biol.*, 22(10):515–526, 2012.
- [196] Meyer, B. H., J.-M. Segura, K. L. Martinez, R. Hovius, N. George, K. Johnsson, and H. Vogel. FRET imaging reveals that functional neurokinin-1 receptors are monomeric and reside in membrane microdomains of live cells. *Proc Natl Acad Sci USA*, 103(7):2138–2143, 2006.
- [197] von Kleist, L., W. Stahlschmidt, H. Bulut, K. Gromova, D. Puchkov, M. J. Robertson, K. A. MacGregor, N. Tomilin, A. Pechstein, N. Chau, M. Chircop, J. Sakoff, J. P. von Kries, W. Saenger, H.-G. Kräusslich, O. Shupliakov, P. J. Robinson, A. McCluskey, and V. Haucke. Role of the Clathrin Terminal Domain in Regulating Coated Pit Dynamics Revealed by Small Molecule Inhibition. *Cell*, 146(3):471–484, 2011.
- [198] Macia, E., M. Ehrlich, R. Massol, E. Boucrot, C. Brunner, and T. Kirchhausen. Dynasore, a cell-permeable inhibitor of dynamin. *Dev Cell*, 10(6):839–850, 2006.
- [199] Harper, C. B., S. Martin, T. H. Nguyen, S. J. Daniels, N. A. Lavidis, M. R. Popoff, G. Hadzic, A. Mariana, N. Chau, A. McCluskey, P. J. Robinson, and F. A. Meunier. Dynamin inhibition blocks botulinum neurotoxin type A endocytosis in neurons and delays botulism. *Journal of Biological Chemistry*, 286(41):35966–35976, 2011.
- [200] Baker, A., A. Saulière, F. Dumas, C. Millot, S. Mazères, A. Lopez, and L. Salomé. Functional membrane diffusion of G-protein coupled receptors. *Eur. Biophys. J.*, 36(8):849–860, 2007.
- [201] Calebiro, D., F. Rieken, J. Wagner, T. Sungkaworn, U. Zabel, A. Borzi, E. Cocucci, A. Zürn, and M. J. Lohse. Single-molecule analysis of fluorescently labeled G-protein-coupled receptors reveals complexes with distinct dynamics and organization. *Proc Natl Acad Sci USA*, 110(2):743–748, 2013.

Bibliography

- [202] Thurner, P., I. Gsandtner, O. Kudlacek, D. Choquet, C. Nanoff, M. Freissmuth, and J. Jezula. A two-state model for the diffusion of the A2A adenosine receptor in hippocampal neurons: agonist-induced switch to slow mobility is modified by synapse-associated protein 102 (SAP102). *Journal of Biological Chemistry*, 289(13):9263–9274, 2014.
- [203] Nicolau, D. V., J. F. Hancock, and K. Burrage. Sources of anomalous diffusion on cell membranes: a Monte Carlo study. *Biophys. J.*, 92(6):1975–1987, 2007.
- [204] Kubale, V., Z. Abramović, A. Pogacnik, A. Heding, M. Sentjurc, and M. Vrecl. Evidence for a role of caveolin-1 in neurokinin-1 receptor plasma-membrane localization, efficient signaling, and interaction with beta-arrestin 2. *Cell Tissue Res.*, 330(2):231–245, 2007.
- [205] Jacquier, V., M. Prummer, J.-M. Segura, H. Pick, and H. Vogel. Visualizing odorant receptor trafficking in living cells down to the single-molecule level. *Proc Natl Acad Sci USA*, 103(39):14325–14330, 2006.
- [206] Vaz, W. L., M. Criado, V. M. Madeira, G. Schoellmann, and T. M. Jovin. Size dependence of the translational diffusion of large integral membrane proteins in liquid-crystalline phase lipid bilayers. A study using fluorescence recovery after photobleaching. *Biochemistry*, 21(22):5608–5612, 1982.
- [207] Jaqaman, K., H. Kuwata, N. Touret, R. Collins, W. S. Trimble, G. Danuser, and S. Grinstein. Cytoskeletal control of CD36 diffusion promotes its receptor and signaling function. *Cell*, 146(4):593–606, 2011.
- [208] Andrews, N. L., K. A. Lidke, J. R. Pfeiffer, A. R. Burns, B. S. Wilson, J. M. Oliver, and D. S. Lidke. Actin restricts FcepsilonRI diffusion and facilitates antigen-induced receptor immobilization. *Nat. Cell Biol.*, 10(8):955–963, 2008.
- [209] Bouzigues, C., M. Morel, A. Triller, and M. Dahan. Asymmetric redistribution of GABA receptors during GABA gradient sensing by nerve growth cones analyzed by single quantum dot imaging. *Proc Natl Acad Sci USA*, 104(27):11251–11256, 2007.
- [210] Destainville, N. and L. Salomé. Quantification and correction of systematic errors due to detector time-averaging in single-molecule tracking experiments. *Biophys. J.*, 90(2):L17–9, 2006.
- [211] Albrecht-Buehler, G. Autonomous movements of cytoplasmic fragments. *Proc Natl Acad Sci USA*, 77(11):6639–6643, 1980.
- [212] Pick, H., E. L. Schmid, A.-P. Tairi, E. Ilegems, R. Hovius, and H. Vogel. Investigating cellular signaling reactions in single attoliter vesicles. *J. Am. Chem. Soc.*, 127(9):2908–2912, 2005.
- [213] Grasso, L., R. Wyss, J. Piguet, M. Werner, G. Hassaïne, R. Hovius, and H. Vogel. Down-scaling the analysis of complex transmembrane signaling cascades to closed attoliter volumes. *PLoS One*, 8(8):e70929, 2013.

- [214] Bauer, B., M. Davidson, and O. Orwar. Proteomic analysis of plasma membrane vesicles. *Angew Chem Int Ed Engl*, 48(9):1656–1659, 2009.
- [215] Wang, X. and J. C. G. Marvizón. Time-course of the internalization and recycling of neurokinin 1 receptors in rat dorsal horn neurons. *Brain Res.*, 944(1-2):239–247, 2002.
- [216] Pelayo, J.-C., D. P. Poole, M. Steinhoff, G. S. Cottrell, and N. W. Bunnett. Endothelin-converting enzyme-1 regulates trafficking and signalling of the neurokinin 1 receptor in endosomes of myenteric neurones. *J. Physiol. (Lond.)*, 589(Pt 21):5213–5230, 2011.
- [217] Weigel, A. V., M. M. Tamkun, and D. Krapf. Quantifying the dynamic interactions between a clathrin-coated pit and cargo molecules. *Proc Natl Acad Sci USA*, 110(48):E4591–600, 2013.
- [218] Grove, J., D. J. Metcalf, A. E. Knight, S. T. Wavre-Shapton, T. Sun, E. D. Protonotarios, L. D. Griffin, J. Lippincott-Schwartz, and M. Marsh. Flat clathrin lattices: stable features of the plasma membrane. *Mol. Biol. Cell*, 25(22):3581–3594, 2014.
- [219] Howes, M. T., M. Kirkham, J. Riches, K. Cortese, P. J. Walser, F. Simpson, M. M. Hill, A. Jones, R. Lundmark, M. R. Lindsay, D. J. Hernandez-Deviez, G. Hadzic, A. McCluskey, R. Bashir, L. Liu, P. Pilch, H. McMahon, P. J. Robinson, J. F. Hancock, S. Mayor, and R. G. Parton. Clathrin-independent carriers form a high capacity endocytic sorting system at the leading edge of migrating cells. *The Journal of cell biology*, 190(4):675–691, 2010.
- [220] Bellve, K. D., D. Leonard, C. Standley, L. M. Lifshitz, R. A. Tuft, A. Hayakawa, S. Corvera, and K. E. Fogarty. Plasma membrane domains specialized for clathrin-mediated endocytosis in primary cells. *J Biol Chem*, 281(23):16139–16146, 2006.
- [221] Lin, H. C., M. S. Moore, D. A. Sanan, and R. G. Anderson. Reconstitution of clathrin-coated pit budding from plasma membranes. *J Cell Biol*, 114(5):881–891, 1991.
- [222] Miller, K., M. Shipman, I. S. Trowbridge, and C. R. Hopkins. Transferrin receptors promote the formation of clathrin lattices. *Cell*, 65(4):621–632, 1991.
- [223] Sandvig, K., S. Pust, T. Skotland, and B. van Deurs. Clathrin-independent endocytosis: mechanisms and function. *Curr. Opin. Cell Biol.*, 23(4):413–420, 2011.
- [224] Cézanne, L. L., S. S. Lecat, B. B. Lagane, C. C. Millot, J.-Y. J. Vollmer, H. H. Matthes, J.-L. J. Galzi, and A. A. Lopez. Dynamic confinement of NK2 receptors in the plasma membrane. Improved FRAP analysis and biological relevance. *J Biol Chem*, 279(43):45057–45067, 2004.
- [225] Ehrlich, M., W. Boll, A. Van Oijen, R. Hariharan, K. Chandran, M. L. Nibert, and T. Kirchhausen. Endocytosis by Random Initiation and Stabilization of Clathrin-Coated Pits. *Cell*, 118(5):591–605, 2004.
- [226] den Otter, W. K. and W. J. Briels. The generation of curved clathrin coats from flat plaques. *Traffic*, 12(10):1407–1416, 2011.

Bibliography

- [227] Cocucci, E., F. Aguet, S. Boulant, and T. Kirchhausen. The first five seconds in the life of a clathrin-coated pit. *Cell*, 150(3):495–507, 2012.
- [228] Zhou, H.-X. Crowding effects of membrane proteins. *J Phys Chem B*, 113(23):7995–8005, 2009.
- [229] Subtil, A. and A. Dautry-Varsat. Microtubule depolymerization inhibits clathrin coated-pit internalization in non-adherent cell lines while interleukin 2 endocytosis is not affected. *Journal of cell science*, 110 (Pt 19):2441–2447, 1997.
- [230] Tank, D. W., E. S. Wu, and W. W. Webb. Enhanced molecular diffusibility in muscle membrane blebs: release of lateral constraints. *J Cell Biol*, 92(1):207–212, 1982.
- [231] CHAIET, L. and F. J. WOLF. The properties of streptavidin, a biotin-binding protein produced by *Streptomyces*. *Arch. Biochem. Biophys.*, 106:1–5, 1964.
- [232] Bayer, E. A. and M. Wilchek. The use of the avidin-biotin complex as a tool in molecular biology. *Methods Biochem Anal*, 26:1–45, 1980.
- [233] Diamandis, E. P. and T. K. Christopoulos. The biotin-(strept)avidin system: principles and applications in biotechnology. *Clin. Chem.*, 37(5):625–636, 1991.
- [234] Dundas, C. M., D. Demonte, and S. Park. Streptavidin-biotin technology: improvements and innovations in chemical and biological applications. *Appl. Microbiol. Biotechnol.*, 97(21):9343–9353, 2013.
- [235] Hermanson, G. T. *Bioconjugate Techniques* (Academic Press), 2013.
- [236] Chen, I., M. Howarth, W. Lin, and A. Y. Ting. Site-specific labeling of cell surface proteins with biophysical probes using biotin ligase. *Nat. Methods*, 2(2):99–104, 2005.
- [237] Wu, S.-C. and S.-L. Wong. Engineering soluble monomeric streptavidin with reversible biotin binding capability. *J Biol Chem*, 280(24):23225–23231, 2005.
- [238] Lim, K. H., H. Huang, A. Pralle, and S. Park. Engineered streptavidin monomer and dimer with improved stability and function. *Biochemistry*, 50(40):8682–8691, 2011.
- [239] Howarth, M., D. J.-F. Chinnapen, K. Gerrow, P. C. Dorrestein, M. R. Grandy, N. L. Kelleher, A. El-Husseini, and A. Y. Ting. A monovalent streptavidin with a single femtomolar biotin binding site. *Nat. Methods*, 3(4):267–273, 2006.
- [240] Howarth, M., W. Liu, S. Puthenveetil, Y. Zheng, L. F. Marshall, M. M. Schmidt, K. D. Wittrup, M. G. Bawendi, and A. Y. Ting. Monovalent, reduced-size quantum dots for imaging receptors on living cells. *Nat. Methods*, 5(5):397–399, 2008.
- [241] Skerra, A. and T. G. Schmidt. Use of the Strep-Tag and streptavidin for detection and purification of recombinant proteins. *Methods in enzymology*, 326:271–304, 2000.

- [242] Knabel, M., T. J. Franz, M. Schiemann, A. Wulf, B. Villmow, B. Schmidt, H. Bernhard, H. Wagner, and D. H. Busch. Reversible MHC multimer staining for functional isolation of T-cell populations and effective adoptive transfer. *Nat. Med.*, 8(6):631–637, 2002.
- [243] Schmidt, T. G., J. Koepke, R. Frank, and A. Skerra. Molecular interaction between the Strep-tag affinity peptide and its cognate target, streptavidin. *J. Mol. Biol.*, 255(5):753–766, 1996.
- [244] Voss, S. and A. Skerra. Mutagenesis of a flexible loop in streptavidin leads to higher affinity for the Strep-tag II peptide and improved performance in recombinant protein purification. *Protein Eng.*, 10(8):975–982, 1997.
- [245] Panwar, P., A. Deniaud, and E. Pebay-Peyroula. Contamination from an affinity column: an encounter with a new villain in the world of membrane-protein crystallization. *Acta Crystallogr. D Biol. Crystallogr.*, 68(Pt 10):1272–1277, 2012.
- [246] Kapusta, P. Absolute Diffusion Coefficients: Compilation of Reference Data for FCS Calibration. *Picoquant application note*, 2010.
- [247] Hassaïne, G., C. Deluz, M. B. Tol, X.-D. Li, A. Graff, H. Vogel, and H. Nury. Large scale expression and purification of the mouse 5-HT3 receptor. *Biochim. Biophys. Acta*, 1828(11):2544–2552, 2013.
- [248] Hess, S. T., S. Huang, A. A. Heikal, and W. W. Webb. Biological and chemical applications of fluorescence correlation spectroscopy: a review. *Biochemistry*, 41(3):697–705, 2002.
- [249] Nagata, K. and H. Handa. *Real-Time Analysis of Biomolecular Interactions*. Applications of BIACORE (Springer Science & Business Media), 2013.
- [250] Chang, Y.-P., F. Pinaud, J. Antelman, and S. Weiss. Tracking bio-molecules in live cells using quantum dots. *J. Biophoton.*, 1(4):287–298, 2008.
- [251] Triller, A. and D. Choquet. New concepts in synaptic biology derived from single-molecule imaging. *Neuron*, 59(3):359–374, 2008.
- [252] Cai, E., P. Ge, S. H. Lee, O. Jeyifous, Y. Wang, Y. Liu, K. M. Wilson, S. J. Lim, M. A. Baird, J. E. Stone, K. Y. Lee, M. W. Davidson, H. J. Chung, K. Schulten, A. M. Smith, W. N. Green, and P. R. Selvin. Stable small quantum dots for synaptic receptor tracking on live neurons. *Angew Chem Int Ed Engl*, 53(46):12484–12488, 2014.
- [253] Zanetti-Domingues, L. C., C. J. Tynan, D. J. Rolfe, D. T. Clarke, and M. Martin-Fernandez. Hydrophobic fluorescent probes introduce artifacts into single molecule tracking experiments due to non-specific binding. *PLoS One*, 8(9):e74200, 2013.
- [254] Bosch, P. J., I. R. Corrêa, M. H. Sonntag, J. Ibach, L. Brunsveld, J. S. Kanger, and V. Subramaniam. Evaluation of fluorophores to label SNAP-tag fused proteins for multicolor single-molecule tracking microscopy in live cells. *Biophys. J.*, 107(4):803–814, 2014.

Bibliography

- [255] Ries, J., C. Kaplan, E. Platonova, H. Eghlidi, and H. Ewers. A simple, versatile method for GFP-based super-resolution microscopy via nanobodies. *Nat. Methods*, 9(6):582–584, 2012.
- [256] Muyldermans, S. Nanobodies: natural single-domain antibodies. *Annu. Rev. Biochem.*, 82:775–797, 2013.
- [257] Chakravarty, R., S. Goel, and W. Cai. Nanobody: the "magic bullet" for molecular imaging? *Theranostics*, 4(4):386–398, 2014.
- [258] Hassanzadeh-Ghassabeh, G., N. Devoogdt, P. De Pauw, C. Vincke, and S. Muyldermans. Nanobodies and their potential applications. *Nanomedicine (Lond)*, 8(6):1013–1026, 2013.
- [259] Oliveira, S., R. Heukers, J. Sornkom, R. J. Kok, and P. M. P. van Bergen En Henegouwen. Targeting tumors with nanobodies for cancer imaging and therapy. *J Control Release*, 172(3):607–617, 2013.
- [260] Rasmussen, S. G. F., B. T. DeVree, Y. Zou, A. C. Kruse, K. Y. Chung, T. S. Kobilka, F. S. Thian, P. S. Chae, E. Pardon, D. Calinski, J. M. Mathiesen, S. T. A. Shah, J. A. Lyons, M. Caffrey, S. H. Gellman, J. Steyaert, G. Skiniotis, W. I. Weis, R. K. Sunahara, and B. K. Kobilka. Crystal structure of the $\beta 2$ adrenergic receptor-Gs protein complex. *Nature*, 477(7366):549–555, 2011.
- [261] Leduc, C., S. Si, J. Gautier, M. Soto-Ribeiro, B. Wehrle-Haller, A. Gautreau, G. Giannone, L. Cognet, and B. Lounis. A highly specific gold nanoprobe for live-cell single-molecule imaging. *Nano Lett.*, 13(4):1489–1494, 2013.
- [262] Biermann, B., S. Sokoll, J. Klueva, M. Missler, J. S. Wiegert, J. B. Sibarita, and M. Heine. Imaging of molecular surface dynamics in brain slices using single-particle tracking. *Nat Commun*, 5, 2014.
- [263] Wang, Y., E. Cai, T. Rosenkranz, P. Ge, K. W. Teng, S. J. Lim, A. M. Smith, H. J. Chung, F. Sachs, W. N. Green, P. Gottlieb, and P. R. Selvin. Small quantum dots conjugated to nanobodies as immunofluorescence probes for nanometric microscopy. *Bioconjug. Chem.*, 25(12):2205–2211, 2014.
- [264] Albrecht, D., C. M. Winterflood, and H. Ewers. Dual color single particle tracking via nanobodies. *Methods and Applications in Fluorescence*, 3(2), 2015.
- [265] Smith, H. S., L. R. Cox, and E. J. Smith. 5-HT₃ receptor antagonists for the treatment of nausea/vomiting. *Ann Palliat Med*, 1(2):115–120, 2012.
- [266] Dahan, M., S. Lévi, C. Luccardini, P. Rostaing, B. Riveau, and A. Triller. Diffusion dynamics of glycine receptors revealed by single-quantum dot tracking. *Science*, 302(5644):442–445, 2003.

- [267] Tardin, C., L. Cognet, C. Bats, B. Lounis, and D. Choquet. Direct imaging of lateral movements of AMPA receptors inside synapses. *EMBO J*, 22(18):4656–4665, 2003.
- [268] Choquet, D. and A. Triller. The Dynamic Synapse. *Neuron*, 80(3):691–703, 2013.
- [269] Veya, L., J. Piguet, and H. Vogel. Single Molecule Imaging Deciphers the Relation between Mobility and Signaling of a Prototypical G Protein-coupled Receptor in Living Cells. *Journal of Biological Chemistry*, 290(46):27723–27735, 2015.
- [270] Guignet, E. G., J.-M. Segura, R. Hovius, and H. Vogel. Repetitive reversible labeling of proteins at polyhistidine sequences for single-molecule imaging in live cells. *Chemphyschem*, 8(8):1221–1227, 2007.
- [271] Banks, D. S. and C. Fradin. Anomalous diffusion of proteins due to molecular crowding. *Biophys. J.*, 89(5):2960–2971, 2005.
- [272] Martin-Fernandez, M. L. and D. T. Clarke. Single molecule fluorescence detection and tracking in mammalian cells: the state-of-the-art and future perspectives. *Int J Mol Sci*, 13(11):14742–14765, 2012.
- [273] Kidd, E. J., A. M. Laporte, X. Langlois, C. M. Fattaccini, C. Doyen, M. C. Lombard, H. Gozlan, and M. Hamon. 5-HT₃ receptors in the rat central nervous system are mainly located on nerve fibres and terminals. *Brain Res.*, 612(1-2):289–298, 1993.
- [274] Emerit, M. B., E. Doucet, M. Darmon, and M. Hamon. Native and cloned 5-HT_{3A}(S) receptors are anchored to F-actin in clonal cells and neurons. *Mol. Cell. Neurosci.*, 20(1):110–124, 2002.
- [275] Ilegems, E., H. M. Pick, C. Deluz, S. Kellenberger, and H. Vogel. Noninvasive imaging of 5-HT₃ receptor trafficking in live cells: from biosynthesis to endocytosis. *J Biol Chem*, 279(51):53346–53352, 2004.
- [276] Charrier, C., M.-V. Ehrensperger, M. Dahan, S. Lévi, and A. Triller. Cytoskeleton regulation of glycine receptor number at synapses and diffusion in the plasma membrane. *J Neurosci*, 26(33):8502–8511, 2006.
- [277] Bürli, T., K. Baer, H. Ewers, C. Sidler, C. Fuhrer, and J.-M. Fritschy. Single particle tracking of alpha7 nicotinic AChR in hippocampal neurons reveals regulated confinement at glutamatergic and GABAergic perisynaptic sites. *PLoS One*, 5(7):e11507, 2010.
- [278] Fernandes, C. C., D. K. Berg, and D. Gómez-Varela. Lateral mobility of nicotinic acetylcholine receptors on neurons is determined by receptor composition, local domain, and cell type. *J Neurosci*, 30(26):8841–8851, 2010.
- [279] Li, T., J.-P. Bourgeois, S. Celli, F. Glacial, A.-M. Le Sourd, S. Mecheri, B. Weksler, I. Romero, P.-O. Couraud, F. Rougeon, and P. Lafaye. Cell-penetrating anti-GFAP VHH and corresponding fluorescent fusion protein VHH-GFP spontaneously cross the blood-brain

Bibliography

barrier and specifically recognize astrocytes: application to brain imaging. *FASEB J.*, 26(10):3969–3979, 2012.

[280] Schirber, M. Nobel Prize—Seeing Single Molecules. *Physics*, 7:104, 2014.

[281] Smolarek, D., O. Bertrand, and M. Czerwinski. Variable fragments of heavy chain antibodies (VHHs): a new magic bullet molecule of medicine? *Postepy Hig Med Dosw (Online)*, 66:348–358, 2012.

[282] Desmyter, A., S. Spinelli, A. Roussel, and C. Cambillau. Camelid nanobodies: killing two birds with one stone. *Curr. Opin. Struct. Biol.*, 32:1–8, 2015.

List of abbreviations

5-HT	serotonin
5-HT ₃ R	5-hydroxyptamine type 3 receptor
AC	adenylate cyclase
ACP	acyl carrier protein
AP-2	adapter protein-2
ATP	adenosine triphosphate
β 2AR	β 2-adrenergic receptor
BS ³	bis(sulfosuccinimidyl)suberate
BSA	bovin serum albumin
cAMP	cyclic adenosine monophosphate
CCD	charge-coupled device
CINV	chemotherapy-induced nausea and vomiting
CNS	central nervous system
CoA	co-enzyme A
DAG	diacylglycerol
DMEM	Dulbecco's modified Eagle's medium
DPBS	Dulbecco's phosphate-buffered saline
DRM	detergent resistant membrane
EC ₅₀	half maximal effective concentration
ER	endoplasmic reticulum
FCS	fluorescence correlation spectroscopy

List of abbreviations

FP	fluorescent protein
FRAP	fluorescence recovery after photobleaching
FRET	fluorescence resonance energy transfer
GABA	γ -aminobutyric acid
GDP	guanosine diphosphate
GFP	green fluorescent protein
GPCR	G protein-coupled receptor
GRK	GPCR kinase
GTP	guanosine triphosphate
GuHCl	guanidinium hydrochloride
HEK	human embryonic kidney
ICLR	ion channel-linked receptor
IP₃	inositol 1,4,5-triphosphate
IPTG	isopropyl β -D-1-triogalactopyranoside
LGIC	ligand-gated ion channels
MAP	mitogen-activated protein
MLC	myosin regulatory light chain
MSD	mean square displacement
MSS	moment scaling spectrum
MWCO	molecular mass cut-off
NBCS	newborn calf serum
NHS	N-hydroxysuccinimide
Ni-NTA	nickel-nitrilotriacetic acid
NK1R	neurokinin-1 receptor
NTPase	nucleoside triphosphatase
OD₂₈₀	optical density at 280 nm
OD₆₀₀	optical density at 600 nm

PBS	phosphate buffered saline
PEG	polyethylene glycol
PIP2	phosphatidylinositol 4,5-biphosphate
PKA	protein kinase A
PKC	protein kinase C
PLC	phospholipase C
pLGIC	pentameric ligand-gated ion channel
PNS	peripheral nervous system
PPTase	phosphopantetheine transferase
QDot	quantum dot
Rho-GEF	guanine nucleotide exchange factor
ROCK	rho-associated protein kinase
RTK	receptor tyrosine kinase
SA	streptavidin
SA-QDot	streptavidin-coated quantum dot
SDS-PAGE	sodium dodecyl sulphate-polyacrylamide gel electrophoresis
S_{MSS}	Hurst parameter (MSS slope)
SMT	single molecule tracking
SOFI	super-resolution optical fluctuation imaging
SP	substance P
SPT	single particle tracking
TACR1	tachykinin receptor 1
TIRF	total internal reflection fluorescence

Acknowledgments

La thèse... quelle aventure! Une aventure de longue haleine, un défi personnel qui aura duré presque 5 ans. Je tiens à remercier ici toutes les personnes qui m'ont aidé, soutenu, encouragé et supporté durant toutes ces années et qui ont ainsi contribué à la réalisation de ce travail.

Je remercie en premier lieu mon directeur de thèse, le *Professeur Horst Vogel*, de m'avoir donné l'opportunité d'intégrer la grande famille du LCPPM et de m'avoir fait confiance. Grâce à vous j'ai pu explorer le fascinant domaine de la biophysique avec une grande liberté, et ce, dans un environnement de travail en tout point exceptionnel. Merci encore pour votre disponibilité, vos nombreux conseils et pour m'avoir fait voyager aux quatre coins du monde.

J'adresse mes plus sincères remerciements aux membres de mon jury de thèse qui ont accepté de consacrer une partie de leur temps à l'évaluation de mon travail: *Professeure Sandrine Gerber, Professeur Kai Johnsson, Professeur Jerker Widengren, Docteur Johannes le Coutre et Docteur Gerardo Turcatti*, merci!

J'aimerais également chaleureusement remercier *Madame Tabet* pour sa précieuse aide et sa formidable efficacité sur la plan administratif, mais aussi pour sa gentillesse et son sourire au quotidien. Mais que ferait-on sans vous?

Un énorme merci à tous mes collègues et amis du LCPPM: *Romain, Luigi, Thamani, Loïc, Marc, Catarina, Joachim, Olivia, Cédric, Samuel, Ruud, Horst Pick, Wolf, Micha, Ghérici, Hugues, Sophie, Shuguang, Menno, Davor et Enrico*. Merci *Jo* pour l'aide considérable que tu m'as apporté tout au long de ma thèse, merci pour ta patience, ta disponibilité et ton incroyable enthousiasme. Merci pour tout ce que tu m'as appris! Merci *Romain* pour le FCS. Merci *Luigi* pour le Biacore. Mais surtout merci à vous deux pour avoir été présents à TOUTES les pauses cafés. Que de bons souvenirs à refaire le monde! Merci *Ruud* pour ton soutien, tes conseils, les réponses à mes nombreuses questions et pour avoir accepté de relire une partie de ma thèse. Merci *Horst* pour la publication, ce fût un réel plaisir de collaborer avec toi. Merci *Olivia* de m'avoir fait découvrir le fabuleux monde des récepteurs olfactifs et de m'avoir inculqué ton sens de l'organisation. Merci *Ghérici* pour les VHHs et ta bonne humeur. Merci à tous ceux qui ont partagé mon bureau: *Olivia, Cédric, Wolf et Loïc*, merci pour votre aide au quotidien et les moments de franche rigolade. Merci à tous les membres de la grande famille LCPPM pour tous ces merveilleux moments que nous avons passés ensemble, au labo, autour d'un

Acknowledgments

café, d'une bière, d'une raclette ou d'un barbecue. Merci!

J'aimerais encore remercier mes deux étudiants *Louise* et *Juan* qui m'ont énormément aidé sur le projet de la StrepTactin. Merci *Juan* d'avoir relu le chapitre en question.

I would like to express my deepest gratitude to *Professor Shimon Weiss* and to *Xavier Michalet* who welcomed me to UCLA and made me discover the magic world of quantum dots. I extend my thanks to all my *UCLA colleagues* for their kindness and warm welcome. This was an unforgettable experience!

I would also like to thank *Professor Thorsten Wohland* who welcomed me into his research group at National University of Singapore, where I had the wonderful opportunity to learn novel fluorescence imaging techniques. Many thanks to all lab members for making my stay a very pleasant one.

Merci à mes *coéquipiers du LUC hockey* et mes *amis grimpeurs du Cube* pour ces moments de défoulement entre midi et une heure qui font un bien fou au corps et à l'esprit. Merci à *Yannick* mon ancien coloc et à tous *mes amis jurassiens* pour tous les bons moments, autant sportifs que festifs, qui m'ont permis de me détendre les neurones.

Merci du fond du coeur à mes parents, *Cathy et Jean-Marc*, à qui je dédie cette thèse. Je suis tellement reconnaissant pour tout ce que vous avez fait pour moi. Je suis devenu ce que je suis grâce à vous! Merci aussi à *Florent et Cyrille*. Je suis tellement chanceux de vous avoir comme frères!

Enfin j'aimerais remercier celle qui partage ma vie depuis le début de cette aventure et qui m'apporte tant de bonheur. Merci *Naïc* pour ton soutien inconditionnel, merci pour tout ce que tu me donnes et tout ce que tu es... Je t'aime!

MERCI!

Lausanne, le 14 décembre 2015

L. V.

Curriculum vitae

Luc Veya

Born on October 8, 1986 in Saignelégier (JU), Switzerland.

- 2011-2015 PhD thesis under the supervision of Prof. Horst Vogel, Swiss Federal Institute of Technology Lausanne (EPFL).
- 2014 Visiting PhD student, Host: Prof. Thorsten Wohland, Biophysical Fluorescence Laboratory, National University of Singapore (NUS).
- 2011 Visiting PhD student, Host: Prof. Shimon Weiss, Department of Chemistry and Biochemistry, University of California Los Angeles (UCLA).
- 2009-2011 Master in Molecular and Biological Chemistry, EPFL.
- 2005-2009 Bachelor in Chemistry, EPFL.
- 2002-2005 Swiss Maturity (Biology-Chemistry), Lycée Blaise-Cendrars, La Chaux-de-Fonds, Switzerland.